AD-A142 399 AIR FORCE ACADEMY AERONAUTICS DIGEST(U) AIR FORCE ACADEMY CO J DEJONGH ET AL. MAR 84 USAFA-TR-84-5 1/2

UNCLASSIFIED F/G 20/4 NL

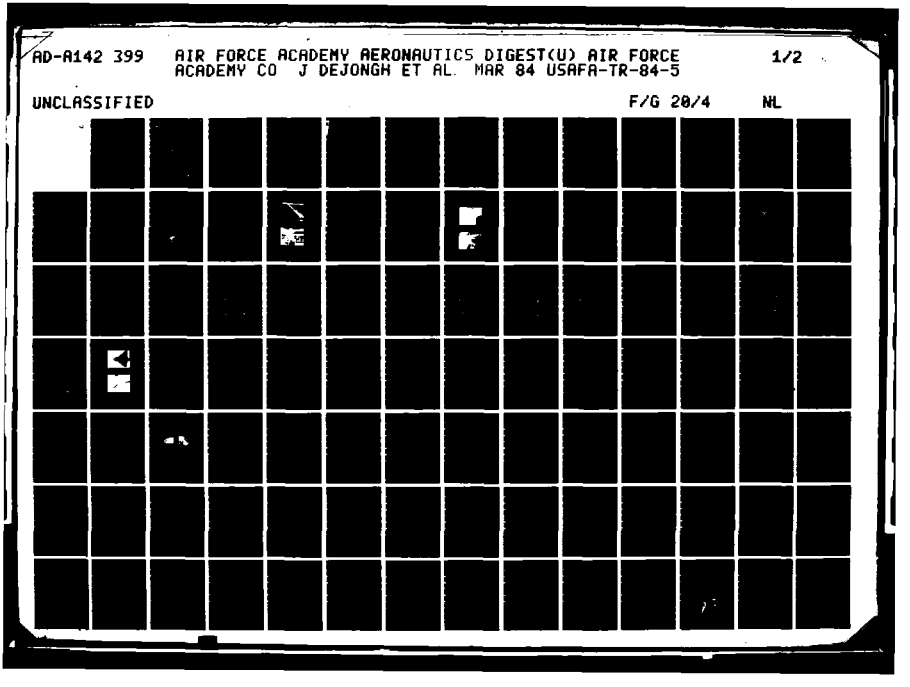

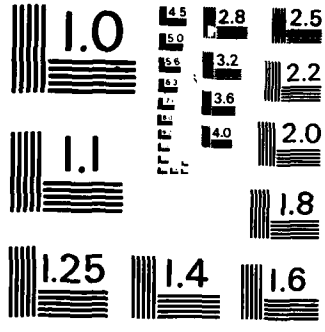

MICROCOPY RESOLUTION TEST CHART
NATIONAL BUREAU OF STANDARDS - 1963 - A

(12)

USAFA-TR-84-5

AIR FORCE ACADEMY
Aeronautics Digest

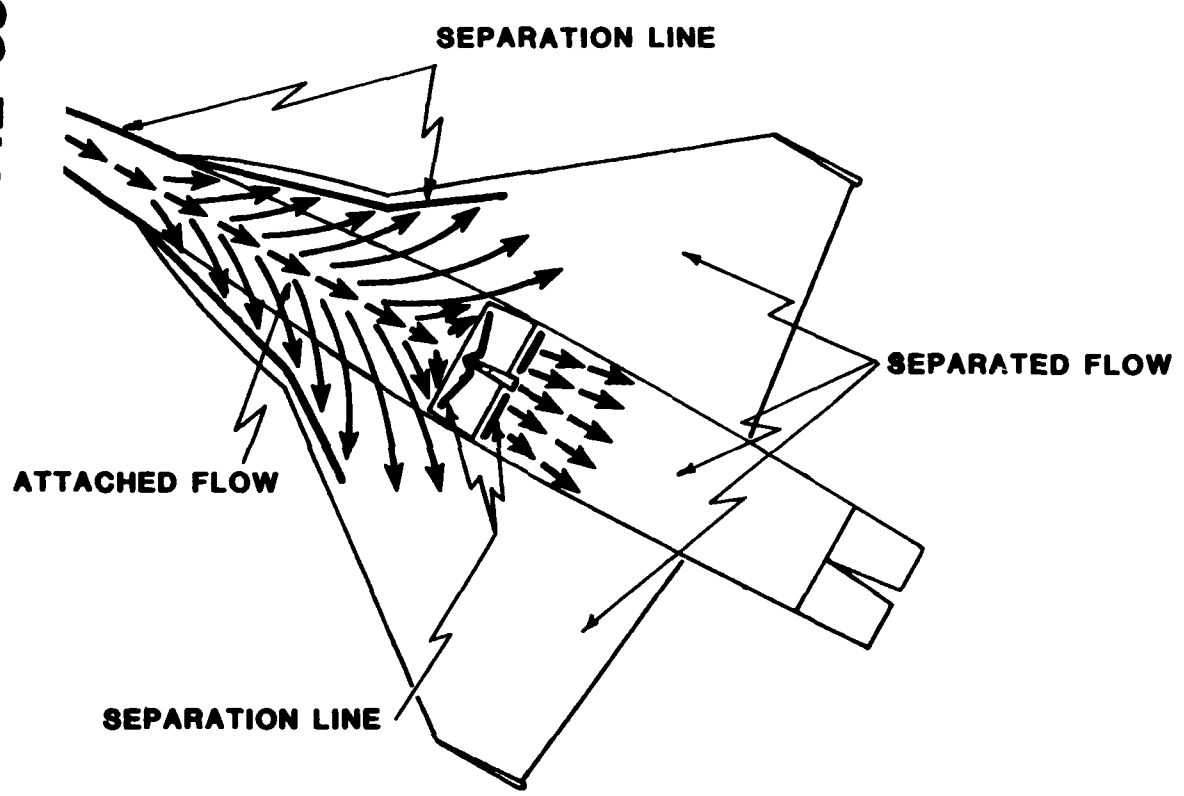

MARCH 1984
Final Report

APPROVED FOR PUBLIC RELEASE: DISTRIBUTION UNLIMITED

Department of Aeronautics
Dean of the Faculty
United States Air Force Academy
Colorado 80840

USAFA-TR-84-5

COVER:
The cover shows a drawing of the results of a surface oil flow test conducted in the USAF Academy's 2 ft. x 3 ft. subsonic wind tunnel. The model tested is the Northrop top-mounted inlet vertical assisted takeoff and landing (VATOL) configuration. The model was mounted at a 45-degree angle of attack in a freestream of 100 ft/sec. Additional results for this configuration are given in Major Jonas's article in this issue of the Aeronautics Digest.

Editorial Review by Maj Robert M. Hogge, Department of English
USAF Academy, Colorado Springs, Colorado 80840

This document is presented as a compilation of monographs worthy of publication. The United States Air Force Academy vouches for the quality of research, without necessarily endorsing the opinions and conclusions of the authors.

This Digest has been cleared for open publication and/or public release by the appropriate Office of Information in accordance with AFR 190-1 and DODD 5230.9. There is no objection to unlimited distribution of the Digest to the public at large, or by DTIC to the National Technical Information Service.

This Digest has been reviewed and is approved for publication.

Thomas E. McCann, Lt. Colonel, USAF
Director of Research, Studies, and Analysis

UNCLASSIFIED

SECURITY CLASSIFICATION OF THIS PAGE

REPORT DOCUMENTATION PAGE

1a. REPORT SECURITY CLASSIFICATION UNCLASSIFIED	1b. RESTRICTIVE MARKINGS
2a. SECURITY CLASSIFICATION AUTHORITY	3. DISTRIBUTION/AVAILABILITY OF REPORT Approved for public release Distribution unlimited.
2b. DECLASSIFICATION/DOWNGRADING SCHEDULE	
4. PERFORMING ORGANIZATION REPORT NUMBER(S) USAFA-TR-84-5	5. MONITORING ORGANIZATION REPORT NUMBER(S)
6a. NAME OF PERFORMING ORGANIZATION Department of Aeronautics 6b. OFFICE SYMBOL (If applicable)	7a. NAME OF MONITORING ORGANIZATION
6c. ADDRESS (City, State and ZIP Code) U. S. Air Force Academy Colorado Springs, CO. 80840	7b. ADDRESS (City, State and ZIP Code)
8a. NAME OF FUNDING/SPONSORING ORGANIZATION 8b. OFFICE SYMBOL (If applicable)	9. PROCUREMENT INSTRUMENT IDENTIFICATION NUMBER
8c. ADDRESS (City, State and ZIP Code)	10. SOURCE OF FUNDING NOS PROGRAM ELEMENT NO. / PROJECT NO. / TASK NO. / WORK UNIT NO
11. TITLE (Include Security Classification) Air Force Academy Aeronautics Digest	
12. PERSONAL AUTHOR(S) Editors: DeJongh, J., Heiser, W., Hogge, R.	
13a. TYPE OF REPORT Final Report 13b. TIME COVERED FROM _____ TO _____	14. DATE OF REPORT (Yr., Mo., Day) March, 1984 15. PAGE COUNT 171
16. SUPPLEMENTARY NOTATION	
17. COSATI CODES FIELD / GROUP / SUB. GR.	18. SUBJECT TERMS (Continue on reverse if necessary and identify by block number) Aerodynamics Engineering Education, Aeronautical history, wave equation, uncertainity analysis, wake measurements, seven hole probe insturmentation, wake vorticity.

19. ABSTRACT (Continue on reverse if necessary and identify by block number)

This Digest covers unclassified research in aeronautics performed by individuals assigned to or associated with the United States Air Force Academy. This report includes technical papers in the specific areas of aerodynamics, propulsion, aeronautical history, and engineering education.

20. DISTRIBUTION/AVAILABILITY OF ABSTRACT UNCLASSIFIED/UNLIMITED ☒ SAME AS RPT ☐ DTIC USERS ☐	21 ABSTRACT SECURITY CLASSIFICATION UNCLASSIFIED
22a. NAME OF RESPONSIBLE INDIVIDUAL Major Jay E. DeJongh	22b TELEPHONE NUMBER (Include Area Code) 303-472-4010 22c OFFICE SYMBOL DFAN

DD FORM 1473, 83 APR EDITION OF 1 JAN 73 IS OBSOLETE

UNCLASSIFIED

SECURITY CLASSIFICATION OF THIS PAGE

PREFACE

This report is the eleventh issue of the Air Force Academy Aeronautics Digest*. Our policy is to print articles which represent recent scholarly work by students and faculty of the Department of Aeronautics, members of other departments of the Academy and the Frank J. Seiler Research Laboratory, researchers directly or indirectly involved with USAFA-sponsored projects, and authors in fields of interest to the USAFA.

In addition to complete papers, the Digest includes, when appropriate, abstracts of lengthier reports and articles published in other formats. The editors will consider for publication contributions in the general field of Aeronautics, including:

- Aeronautical Engineering
  - Aerodynamics
  - Flight Mechanics
  - Propulsion
  - Structures
  - Instrumentation
- Fluid Dynamics
- Thermodynamics and Heat Transfer
- Biomechanics
- Engineering Education
- Aeronautical History

Papers on other topics will be considered on an individual basis. Contributions should be sent to:

Editor, Aeronautics Digest
DFAN
US Air Force Academy
Colorado Springs, CO 80840

The Aeronautics Digest is edited at present by Maj Jay E. DeJongh, PhD; William H. Heiser, PhD; and Maj Robert M. Hogge, PhD, who provided the final editorial review. Our thanks also to Contract Technical Services, Inc. for editing and illustration services.

*Previous issues of the Digest can be ordered from the Defense Technical Information Center (DTIC), Cameron Station, Alexandria, VA 22324.

CONTENTS

SECTION I

Aerodynamics

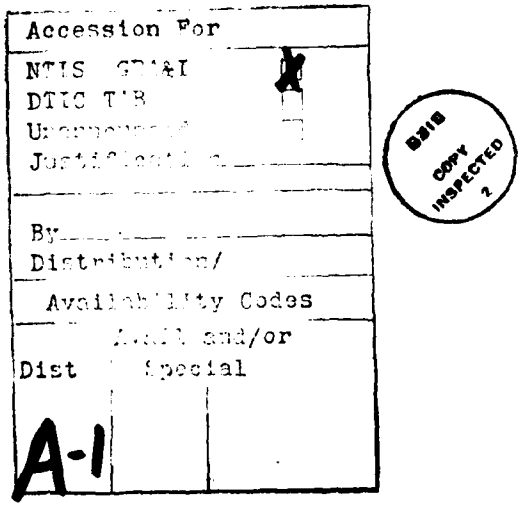

EXTERNAL FLOW-FIELD MEASUREMENTS ON A TOP-MOUNTED, INLET-VATOL CONFIGURATION AT HIGH ANGLES OF ATTACK

Frederick M. Jonas*

Abstract

This paper presents the results of a research effort conducted for the NASA Ames Research Center in which a seven-hole pressure probe was used to map an unknown flow field. Also included in this effort are results that define the probe's measurement capabilities. Using a seven-hole pressure probe, external flow-field measurements were made on a 1/40th-scale, top-mounted inlet model of the Northrop VATOL (vertical assisted takeoff and landing) configuration. The tests were conducted in the USAF Academy's 2 ft. x 3 ft. Subsonic Wind Tunnel. The model was mounted at a fixed 45-degree angle of attack and the test-section velocity was nominally 100 ft/sec for all subject tests. External flow-field measurements were made over most of the upper surface of the wing and fuselage. The results show the presence of two counter-rotating vortices produced by the wings' leading-edge extensions. These vortices help keep the flow over the wing and fuselage upper surfaces attached. Vortex disintegration appeared to occur just aft of the leading edge of the inlet compression ramp.

I. Introduction

This research effort was conducted to accomplish two objectives: first, to measure the external flow field in and around the top-mounted inlets on a 1/40th scale model of the Northrop VATOL at a fixed 45-degree angle of attack using the seven-hole pressure probe and second, to determine the measurement capabilities of the seven-hole pressure probe in high and low shear flow environments. All tests were conducted in the USAF Academy's Aeronautics Laboratory's 2 ft. x 3 ft. Subsonic Wind Tunnel at a nominal test section velocity of 100 fps.

The Northrop VATOL configuration is a top-mounted inlet fighter aircraft with a delta-wing planform and wing leading-edge extensions (LEX). Since this configuration was designed to operate at high angles of attack, an examination of the interactions of the LEX vortices with the top-mounted inlets during these conditions of flight is valuable. The seven-hole pressure probe was used to map the external flow field on the upper surface of the wing and fuselage,

*Major, USAF, Associate Professor of Aeronautics, DFAN

starting just forward of the wing LEX and extending over the entire body. Both qualitative and quantitative information on these interactions was obtained. Crossflow velocities and local total pressures are presented in graphical form for the data planes investigated (Figures 12 and 14). Surface oil flow results for this test condition are also presented (Figure 15).

In addition, as part of this research effort, the measurement capabilities of the seven-hole pressure probe in high and low shear flows were determined. It should be noted that this test was part of an ongoing research effort at the USAF Academy to establish the capabilities and limitations of the seven-hole pressure probe in mapping unknown flow fields. The results of our research show this probe to be a valuable and reliable instrument in making these kinds of investigations. For this test, seven-hole pressure probe measurements were compared to hot-wire anemometer results in the wake flow behind an airfoil (low shear flow). Next, seven-hole pressure probe measurements of local total pressure at a point in the vortex wake (high shear flow) created by the wing LEX of the Northrop VATOL model were compared to measurements of local total pressure obtained using a total pressure probe. For this last effort the total pressure probe was aligned first with the freestream flow and then with the local flow.

The results of these investigations appear in Section V. A review of the basic flow characteristics, in terms of velocity and pressure in viscous wake phenomena, appears in the Theory section below. This section serves as a review of what one should expect to see when measuring these wake phenomena. In the following section, the apparatus and procedure used in the conduct of this investigation are described. The paper closes with a description and summary of the

results of the investigation.

II. Theory

In the measurement of wake phenomena, one has certain expectations regarding pressures and velocities. For example, in the measurement of an airfoil wake in a steady incompressible viscous flow, one expects the velocity profile through the wake to appear as shown in Figure 1.

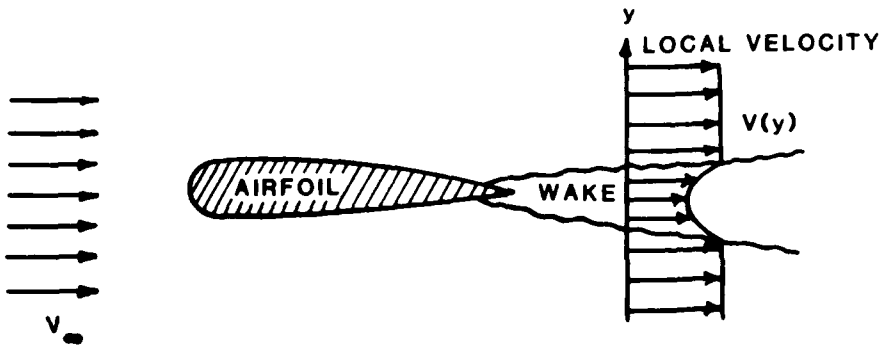

Figure 1. Velocity Profile Through an Airfoil Wake

Depending on how far behind the airfoil's trailing edge measurements are made, one may or may not see any variation in the local static pressures through the wake. In fact, beyond a distance of less than one chord length behind the trailing edge, changes in the local static pressure through the wake are negligible. On the other hand, the local total pressure deficit through the wake is expected to have the same shape as the velocity profile regardless of distance behind the trailing edge. The local total pressure deficit, like the velocity profile, would then diffuse or decay slowly as one moves farther away from the airfoil's trailing edge, since the local total pressure at

any point is a measure of both local velocity and static pressure. At any point in a steady incompressible flow

$$P_{0_L} = P_L + \tfrac{1}{2}\rho V_L^2 \tag{1}$$

The variation of P_{0_L} through the wake is, of course, caused by viscous effects.

We would expect to see similar trends in a simple, two-dimensional viscous vortex. These trends are easily verified by using a model: a vortex filament that dissolves with time because of fluid friction (Ref. 1).

Using a two-dimensional, time-dependent viscous vortex to model the characteristics of a three-dimensional, viscous-vortex filament in steady flow may at first seem confusing, since we will be measuring the latter. The decay of a three-dimensional viscous vortex with downstream distance in a steady flow, however, can be related to the decay of a two-dimensional vortex with time according to the relation that distance equals velocity times time, or

$$t = d/V_\infty \quad \text{or} \quad d = V_\infty t \tag{2}$$

Thus, in the discussion that follows, for the two-dimensional vortex, time can be replaced with distance along the three-dimensional vortex filament. The change in the properties with time described for the two-dimensional vortex thus corresponds to the change in properties for the vortex filament as the vortex proceeds downstream along its length. The variation in the circumferential velocity component with respect to time is described by

$$U_\theta (r,t) = \frac{\Gamma_1}{2\pi r}\left(1-e^{-r^2/4\nu t}\right) \tag{3}$$

where Γ_1 is the circulation around an infinitely large circle (Ref.

1). The change in velocity with respect to time is shown in Figure 2.

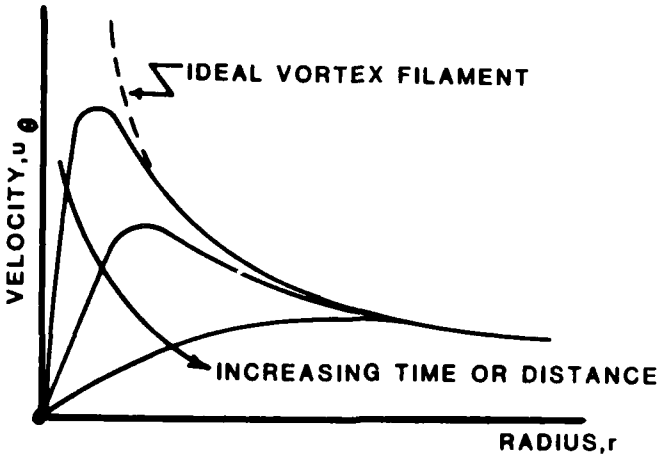

Figure 2. Variation of Velocity with Radius, Viscous Vortex Filament

Note that as the center of the vortex is approached, the velocity approaches 0, and as the radius becomes very large, the velocity again approaches 0. From momentum considerations one can show that

$$\frac{1}{r}\frac{\partial P}{\partial \theta} = 0 \tag{4}$$

$$\frac{\partial P}{\partial r} = \rho\frac{U_\theta^2}{r} = \frac{\rho}{r}\left(\frac{\Gamma_1}{2\pi r}\right)^2 \left(1-e^{-r^2/4\nu t}\right) \tag{5}$$

which describes the variation of local static pressure through the filament. Note that for Eqn. (5)

$$\frac{\partial P}{\partial r} > 0 \;\forall\; r > 0 \tag{6}$$

and

$$\frac{\partial P}{\partial r} \to 0 \quad \text{as} \quad r \to \infty \tag{7}$$

or, that the static pressure increases from some minimum value as one moves away from the vortex center and that the static pressure levels off far away from the vortex center. Finally, if one assumes that at any point in this incompressible viscous flow the local total pressure is the sum of the local static and dynamic pressures, or

$$P_{o_L} = P_L + \tfrac{1}{2}\rho U_\theta^2 \tag{8}$$

then the change in the local total pressure with radius is described by

$$\frac{\partial P_{o_L}}{\partial r} = \frac{\partial P_L}{\partial r} + \rho U_\theta \frac{\partial U_\theta}{\partial r} \tag{9}$$

Substituting Eqn. (5) into this expression for $\partial P/\partial r$ and differentiating Eqn. (3) to obtain $\partial U_\theta/\partial r$ results in the following equation, describing the change in local total pressure through the vortex.

$$\frac{\partial P_{o_L}}{\partial r} = \frac{\rho}{r}\left(\frac{\Gamma_1}{2\pi}\right)^2 \frac{1}{2\nu t} e^{-r^2/4\nu t}\left(1-e^{-r^2/4\nu t}\right) \tag{10}$$

Again, note that

$$\frac{\partial P_{o_L}}{\partial r} > 0 \;\forall\; r > 0 \tag{11}$$

and

$$\frac{\partial P_{o_L}}{\partial r} \to 0 \quad \text{as } r \to \infty \quad \text{and as} \quad r \to 0 \tag{12}$$

or that, as before with the local static pressure, the local total pressure increases from some minimum value as one moves away from the center of the vortex and then levels off. From these descriptions we would expect local total and static pressures to vary through the vortex filament, as shown in Figure 3, at any time, t.

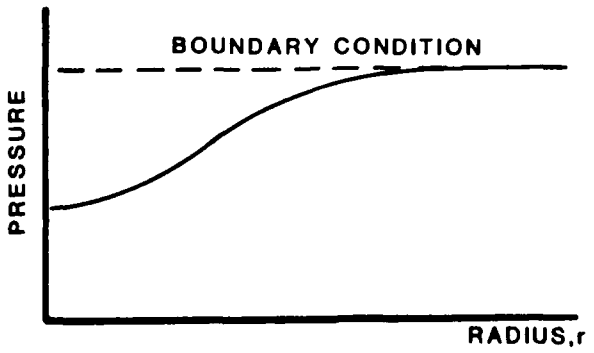

Figure 3. Variation of Pressure with Radius, Viscous Vortex Filament

A three-dimensional vortex in steady incompressible viscous flow, although more complicated, would be expected to exhibit the same local variations in velocity and static and total pressures as the two-dimensional vortex filament would, as previously discussed. The pressure boundary conditions are represented by the freestream inviscid values of P_∞ and P_{O_∞}. At no time would one expect to see the local total pressure in the vortex exceed the freestream values (Ref. 2). Intuition tells one that in any viscous phenomenon, the effects of viscous interactions or fluid friction can be expected to dissipate energy, causing a loss in local total pressure through the wake. These changes in pressures through viscous wakes are why pressure probes can be used to measure wake phenomena (Ref. 2) and map their locations.

III. Apparatus

A. Wind Tunnel

The Subsonic Wind Tunnel in the Aeronautics Laboratory of the USAF Academy is a continuous-flow, closed-circuit wind tunnel operating at atmospheric pressures. The test section is fixed in geometry, nominally 2 ft. high by 3 ft. wide and 70 in. in length;

its sidewalls diverge approximately 1/2 degree with respect to the tunnel centerline. The Mach number range is 0.04 M · 0.35, which corresponds to a speed of 50 to 400 fps. The corresponding Reynolds number per foot is 0.2 (10^6) to 1.3 (10^6) and the dynamic pressure ranges from 1.8 psf to 130 psf. A schematic of the wind tunnel is shown in Figure 4.

B. Model

A 1/40th scale model of the Northrop VATOL configuration (Refs. 3 and 4) was used in this investigation. Flow into the flow-through inlets of the model was adjusted to match conditions typical of 0.9 Mach cruise, Ao/Ac = 0.66, for all tests. The model was strut-mounted at a fixed angle of attack of 45 degrees with respect to the aircraft horizontal reference line (HRL). All tests were conducted at a nominal test-section velocity of 100 fps. A schematic of the model is shown in Figure 5, while a typical installation is shown in Figure 6.

C. Pressure Probes

A 0.109 in OD seven-hole pressure probe (Ref. 5) was used to map the external flow about the model. The probe was aligned with the freestream flow direction for all of the tests, as shown in Figure 6. In subsonic compressible flows, relative flow angles of up to 70 degrees with respect to the probe centerline are measurable to within ±1.6 degrees, while the ratio of local total pressure to local dynamic pressure is measurable to within ±5 percent at 95 percent certainty (Ref. 5). The seven-hole pressure probe data was collected, reduced, and displayed by means of the seven-hole probe data acquisition system (Ref. 5), which uses the PDP 11/45 computer system. The probe traverse, axis system, and nomenclature are shown in Figure 7.

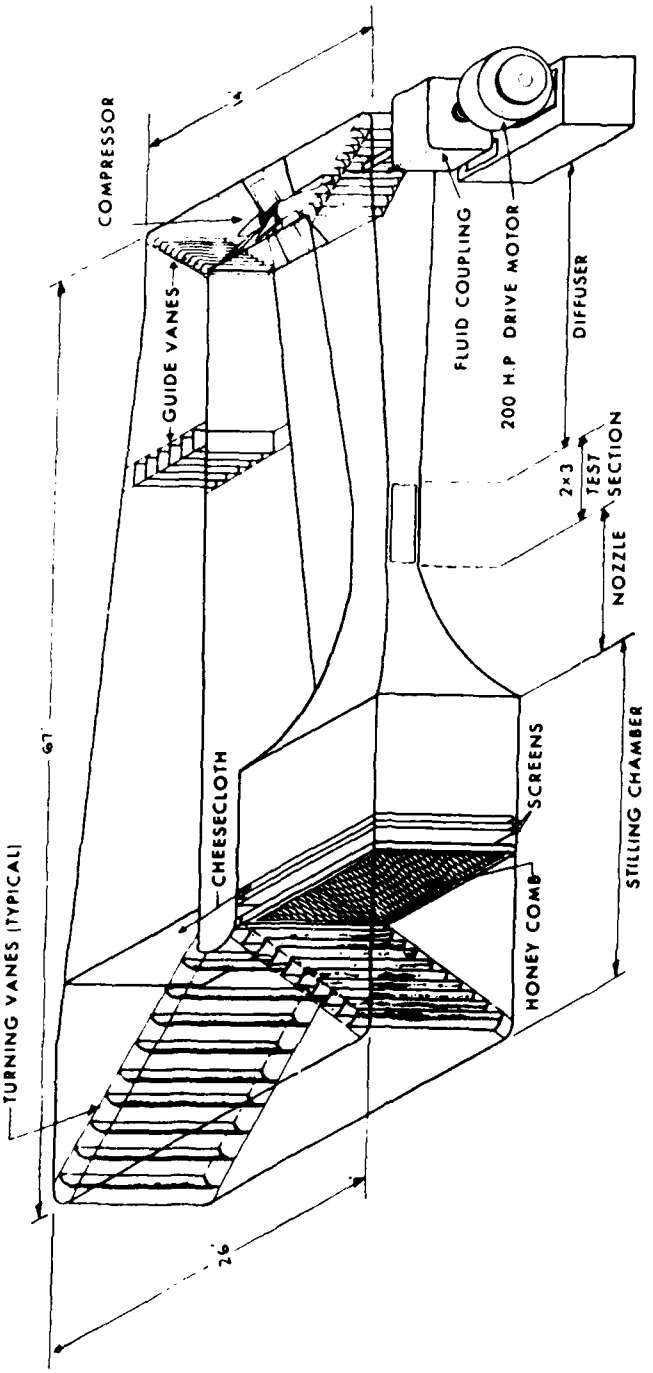

Figure 4. USAFA 2 ft. x 3 ft. Subsonic Wind Tunnel

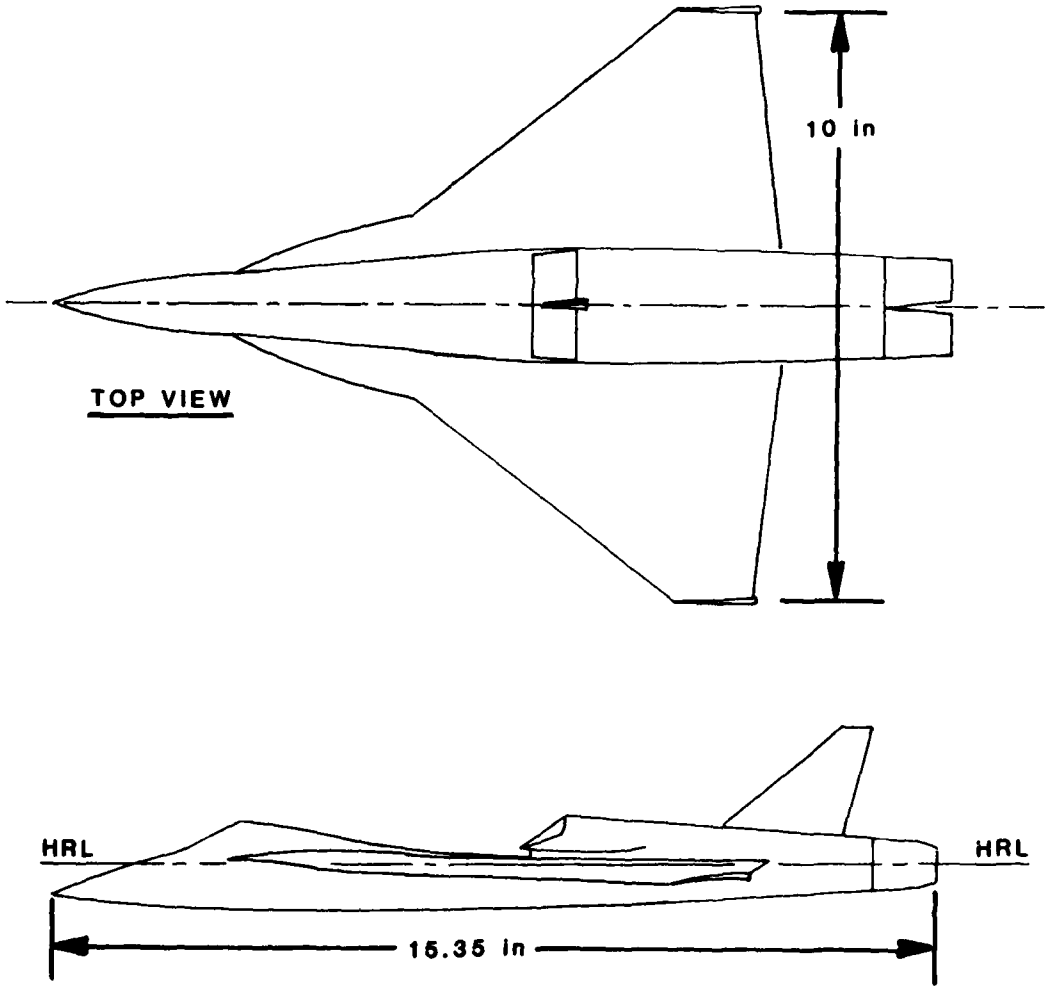

Figure 5. Northrop Top-Mounted Inlet VATOL Concept

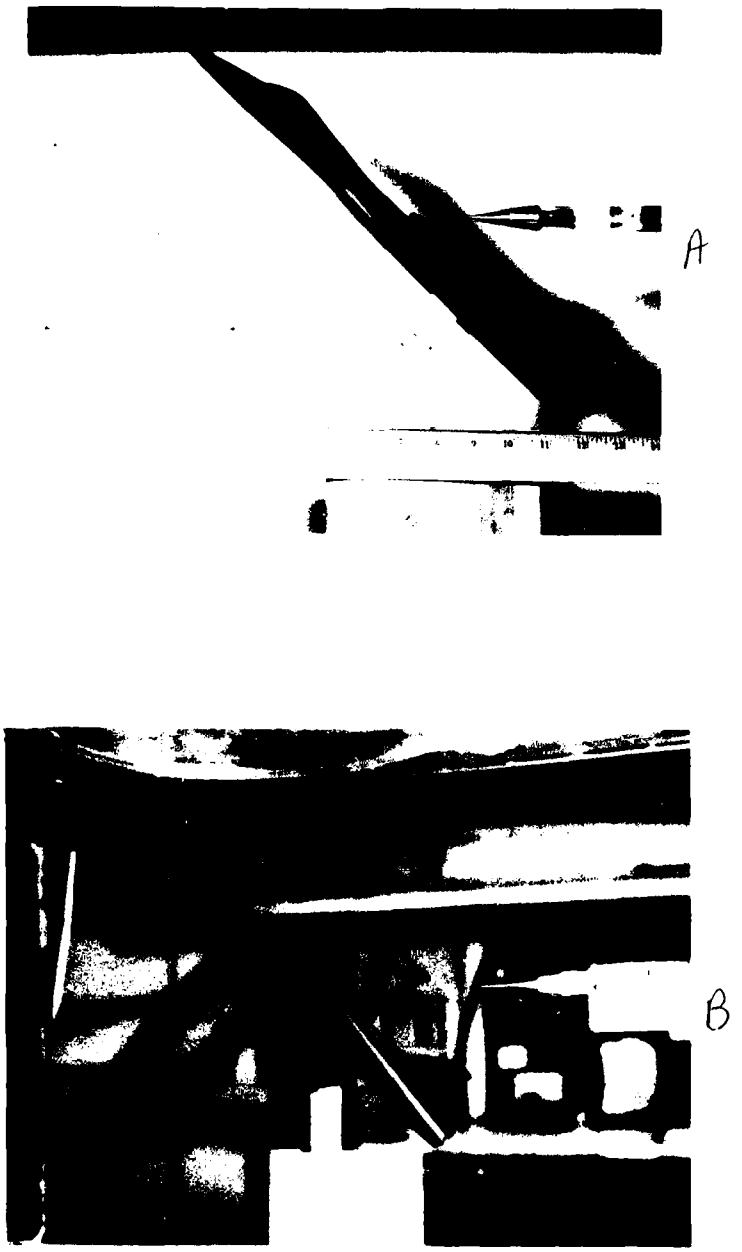

Figure 6. Wind Tunnel Installation, 1/40th-Scale Northrop VATOL Model

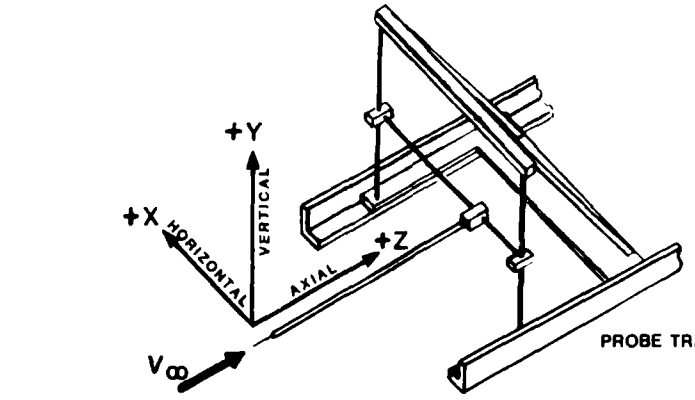

PROBE TRAVERSE & AXIS SYSTEM

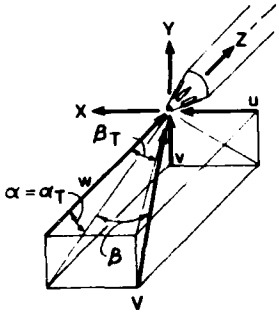

LOW ANGLE REFERENCE SYSTEM

CONVENTIONAL	TANGENT
$w = V \cos\alpha \cos\beta$ $u = V \sin\beta$ $v = V \sin\alpha \cos\beta$	$\alpha_T = \arctan \frac{v}{w}$ $\beta_T = \arctan \frac{u}{w}$

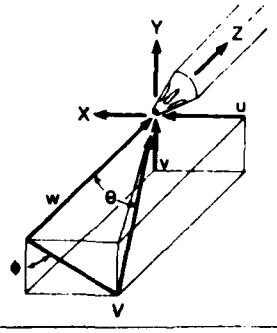

HIGH ANGLE REFERENCE SYSTEM

POLAR	TANGENT
$w = V \cos\theta$ $u = V \sin\theta \sin\phi$ $v = V \sin\theta \cos\phi$	$\alpha_T = \arctan \frac{v}{w}$ $\beta_T = \arctan \frac{u}{w}$

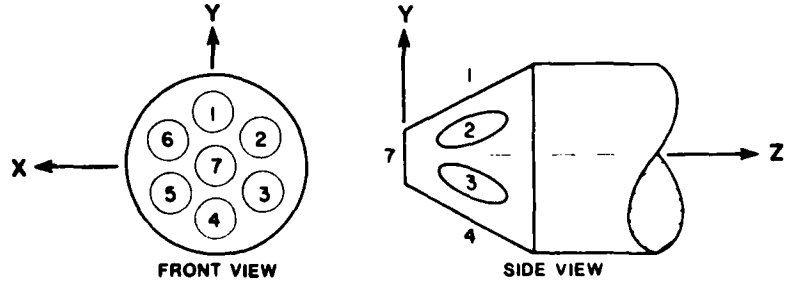

PORT NUMBERING CONVENTION & PRINCIPAL AXES

Figure 7. Seven-Hole Pressure Probe Traverse, Axis System, Nomenclature

Two separate total pressure probes were used to measure local total pressures at specific points above the model for later comparison with the seven-hole pressure probe measurements. The first total pressure probe, shown in Figure 8, is a 0.125 in OD hemispherical-head pitot tube. This probe was aligned with the freestream flow for all tests. The second total pressure probe, consisting of a 0.109 in OD and 0.086 in ID tube, was bent at a 23.8 ± 0.1 degree angle to correspond to the local flow angle (measured using the seven-hole pressure probe) at a specific point above the model. The tunnel installation at this point is shown in Figure 9. Pressure data for both probes was collected using the PDP 11/45 data acquisition system.

D. Airfoil Model

An NACA 0015 airfoil model was used to obtain wake measurement comparisons between the seven-hole pressure probe and the hot-wire anemometer in the subsonic wind tunnel. The airfoil model spanned the wind tunnel, thus representing two-dimensional flow. The model's chord length was 6 in. and spanned the wind tunnel from the top to the bottom walls. The airfoil was set near 0 degrees angle of attack, and tests were conducted at 60 fps and 100 fps.

E. Hot-Wire Anemometer

A constant-temperature, hot-wire anemometry system (Thermo-Systems Model 1050) belonging to the Frank J. Seiler Research Laboratory (an AF Systems Command tenant organization) was used to make airfoil wake velocity measurements. A single-wire sensor probe was employed to measure freestream velocity components through the airfoil's wake. Linearized anemometer signals were processed using

signal conditioning circuits supplied with the system. Data was recorded using a Houston Instrument Model 2000 x-y recorder.

Figure 8. Total Pressure Probe Aligned with Freestream

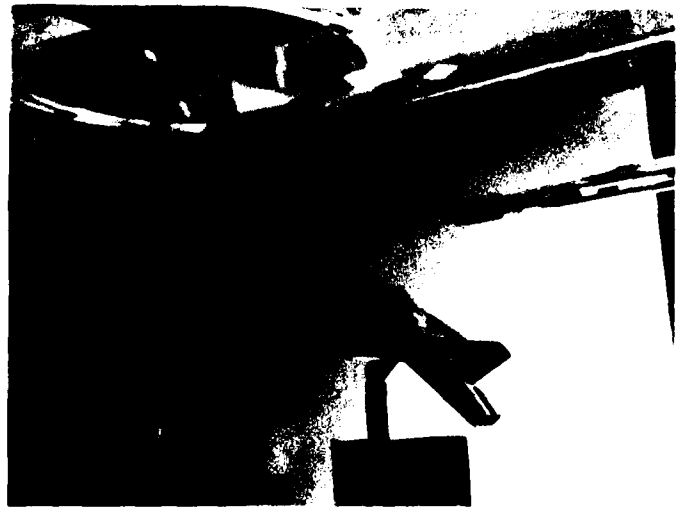

Figure 9. Total Pressure Probe Aligned with Local Flow

IV. Procedure

A. Flow Surveys

1. Seven-Hole Probe/Northrop VATOL Model

The seven-hole pressure probe was used to collect flow field data at 18 data planes chosen to survey flow regions in and around the top-mounted inlets. The probe was parallel to the freestream velocity (α = 0 degrees) for all data planes. Each data plane was defined by a constant value of Z (Figures 7 and 10), and data was collected in each plane normal to the freestream flow (defined by x-y planes). The reference point for all data-grid points (x=0, y=0, z=0) was the centerline top of the inlet lip, as shown in Figure 6 and 10. All data planes consisted of 200 grid or data points for a total of 3600 data points. The nomenclature pertaining to each data plane is defined as follows:

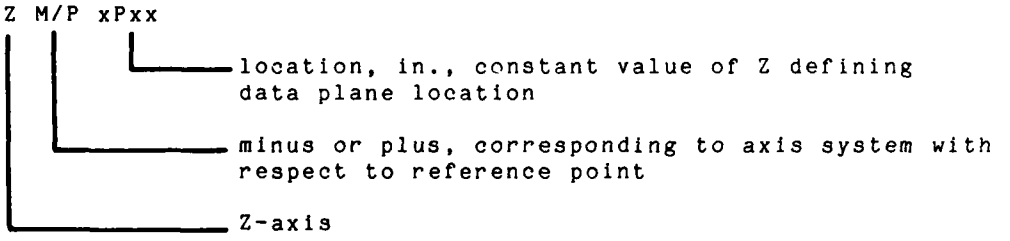

For example, ZM5P25 corresponds to a data plane located at Z = -5.25 in. Data planes are shown in Figure 10 and are listed in Table I.

2. Pressure Probes/Northrop VATOL Model

For the measurement of local total pressures both the seven-hole pressure probe and total pressure probes were used for the purpose of comparison. The measurements were made in the data plane ZMP75. Regions of local total pressure greater than the freestream total pressure were first identified using the seven-hole pressure probe. These regions are shown in Figure 11 and coincide with the

outboard portions and top centerline of the vortices. Data grid points and local flow angles in these regions were then identified for further investigation using the total pressure probes. For the first test, a total pressure probe was aligned with the freestream flow (as was the seven-hole pressure probe) and 10 measurements were made at three identified grid points. For the second test, a total pressure probe was then aligned with the local flow at one selected grid point (Figure 11) to measure the actual local total pressure associated with the total velocity vector. A total of 69 data points was recorded at this grid point. Note that each data point represents an average of 50 samples rather than an instantaneous value.

3. Airfoil Model Test

For the wake investigations of the NACA 0015 airfoil model, both the seven-hole probe and hot-wire anemometer were used. The data was collected 3 chord lengths downstream from the model. Each survey consisted of a data pass through the airfoil wake in a direction normal to the airfoil wake centerline. Both probes were parallel to the freestream velocity, and data was collected at the model midspan to minimize wind-tunnel wall effects.

B. Surface Oil Flow

Surface oil flows were conducted on the Northrop VATOL model mounted at 45 degrees angle of attack. Test section velocity was 100 fps.

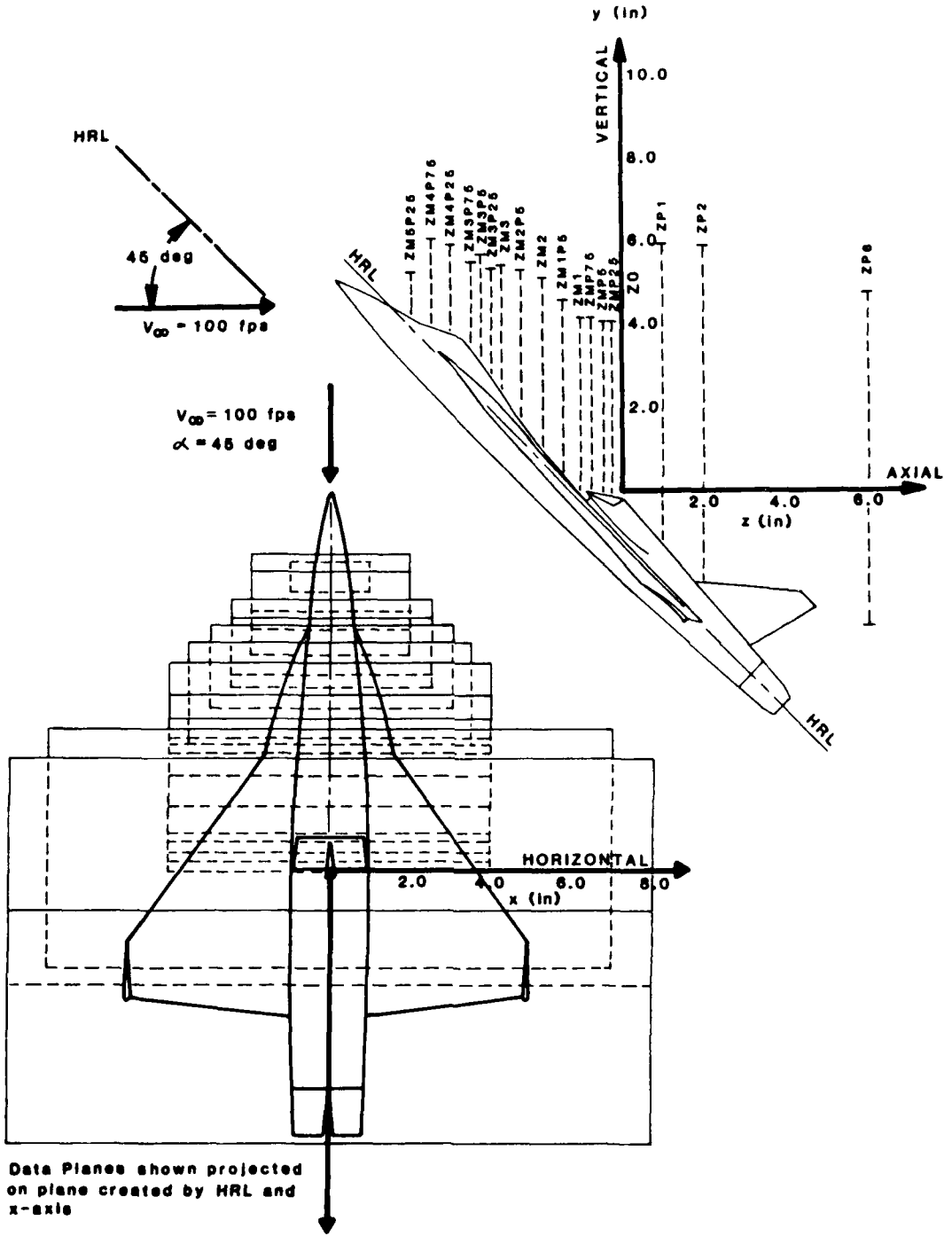

Figure 10. Data Plane Locations, Grid Sizes

Table I
NORTHROP VATOL MODEL, SEVEN-HOLE PROBE DATA PLANES

Data Plane	Grid Size (x by y, inches)	Location
ZP6	16x8	1 inch aft of nozzles
ZP2	16x8	Junction vertical tail LE and fuselage
ZP1	14x7	---
Z0	8x4	Reference plane, top of inlet lip
ZMP25	8x4	---
ZMP5	8x4	---
ZMP75	8x4	LE of lower inlet ramp
ZM1	8x4	---
ZM1P5	8x4	---
ZM2	8x4	Intersection of LEX and wing LE
ZM2P5	7x3.5	---
ZM3	6x3	---
ZM3P25	5x2.5	---
ZM3P5	5x2.5	---
ZM3P75	4x2	---
ZM4P25	4x2	---
ZM4P75	4x2	Approximately where LE of LEX joins fuselage
ZM5P25	2x1	Approximately where canopy LE joins fuselage

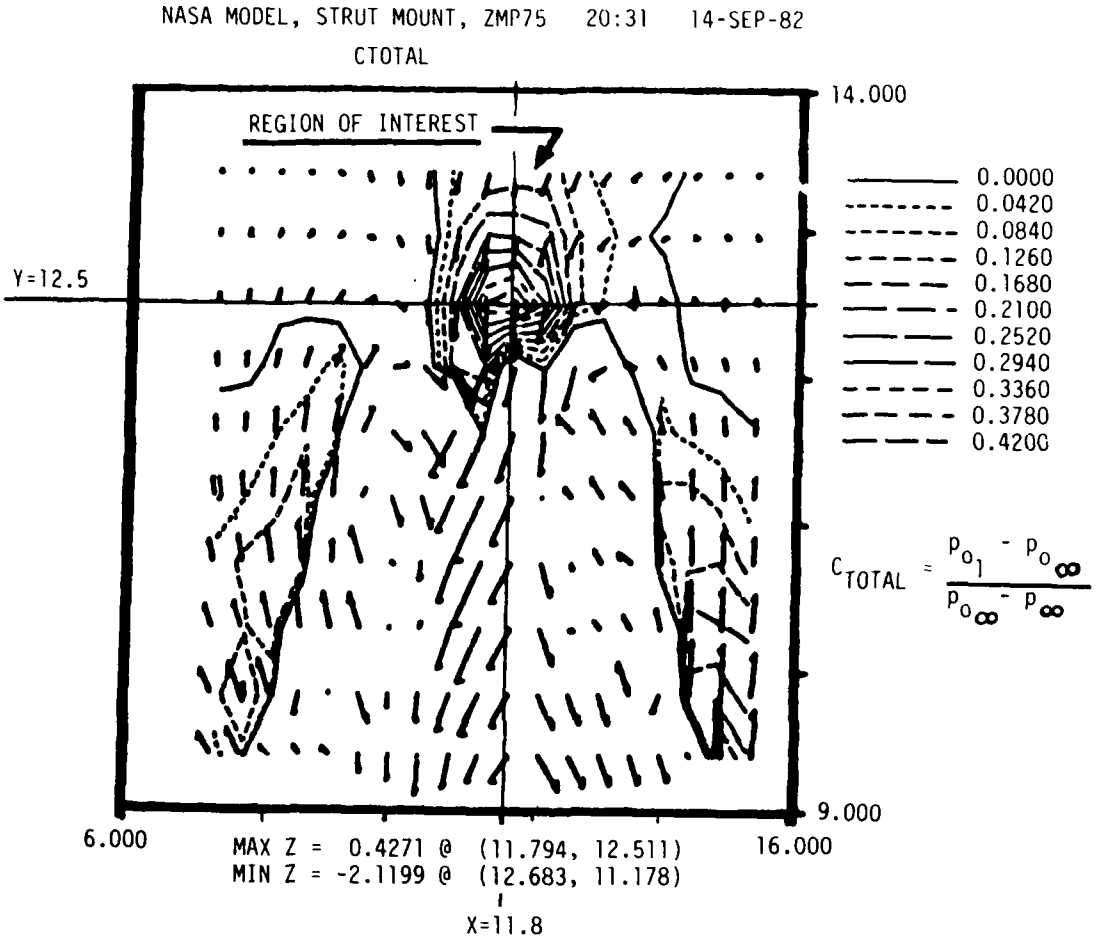

Figure 11. Regions of Positive C_{Total}, Data Plane ZMP75

V. Discussion

In this section, the results of this research effort will be presented and discussed as follows:

A. Seven-hole pressure probe external flow field measurements, 1/40th-scale Northrop VATOL model at 45 degrees angle of attack, test section velocity of 100 ft/sec. Surface oil flow results

will also be presented.

B. Seven-hole pressure probe and hot-wire anemometer measurements of an airfoil wake, NACA 0015 airfoil, at a test section velocity of 60 and 100 ft/sec, nominal angle of attack near 0 degrees.

C. Investigations of local total pressure in a vortex wake using the seven-hole pressure probe, pitot probe aligned with freestream flow, and pitot probe aligned with local flow. Testing was conducted on Northrop VATOL model mounted at 45 degrees angle of attack, test section velocity of 100 ft/sec.

In reporting the results of the pressure probe testing the nondimensional coefficient, C_{Total}, will be presented where

$$C_{Total} = \frac{P_{O_L} - P_{O_\infty}}{P_{O_\infty} - P_\infty} \tag{13}$$

P_{O_L} = local total pressure

P_{O_∞} = freestream total pressure

P_∞ = freestream static pressure

A. Seven-Hole Pressure Probe/Northrop VATOL Model

The results of the external flow field measurements on the Northrop VATOL model mounted at 45 degrees angle of attack at a test section velocity of 100 ft/sec are presented in Figures 12a-i, 13, and 14a-c. Each data plane consists of 200 individual test or grid points.

Figures 12a-i present the crossflow velocities and then contours first for negative and then for positive values of C_{Total}. The data is presented by data plane, starting from the nose of the model and moving downstream. The data planes are viewed looking upstream from behind the model. As seen from the plots of crossflow velocity, there is a slight side-wash or positive sideslip in the flow. This was due to the model mounting in the wind tunnel and not to a flow condition in the test section, as was later verified. In general, the magnitude of this sideslip was negligible and did not appreciably affect the

qualitative results. Clearly identifiable in the crossflow-velocity plots is the circulatory nature of the flow corresponding to the formation of the fuselage/leading edge extension (LEX) vortices. The vortices are counter-rotating with the direction of rotation being counterclockwise for the right vortex and clockwise for the left vortex.

As previously discussed in the Theory section, the vortex wakes are clearly evident in the contour plots of Figure 12 for the negative values of C_{Total}. The contours (constant values of C_{Total}) are generally elliptical in shape. The values of C_{Total} proceed from 0 at the boundaries to a minimum negative value of C_{Total} that should correspond to the vortex core. Note that in these figures both the minimum and maximum values of C_{Total} for each data plane are presented, as well as their location (x,y). The vortex cores do not clearly appear until data plane ZM3P25 (Figure 12c), just aft of the canopy. Their appearance is indicated by the shape of the contours and the maximum negative value of C_{Total}. The vortices then steadily grow in size (or diffuse) as one moves downstream towards the inlets. Multiple low-energy cells first appear at data plane ZM1, as shown by the negative contour values of C_{Total}. This data plane is located just in front of the inlet ramp. The presence of these low-energy cells, as well as their growth and diffusion, is more apparent in data planes ZMP5, ZMP75, Z0, ZP1, ZP2, and ZP6. At this high angle of attack, the vortices have probably burst at or near the LEX wing juncture; thus, what we see in these data planes is the interference and blockage effects of the inlet. These effects are also evident in the crossflow-velocity plots as the vortices lose their definition due to this interference and the mixing of the burst vortex cores with the local freestream air.

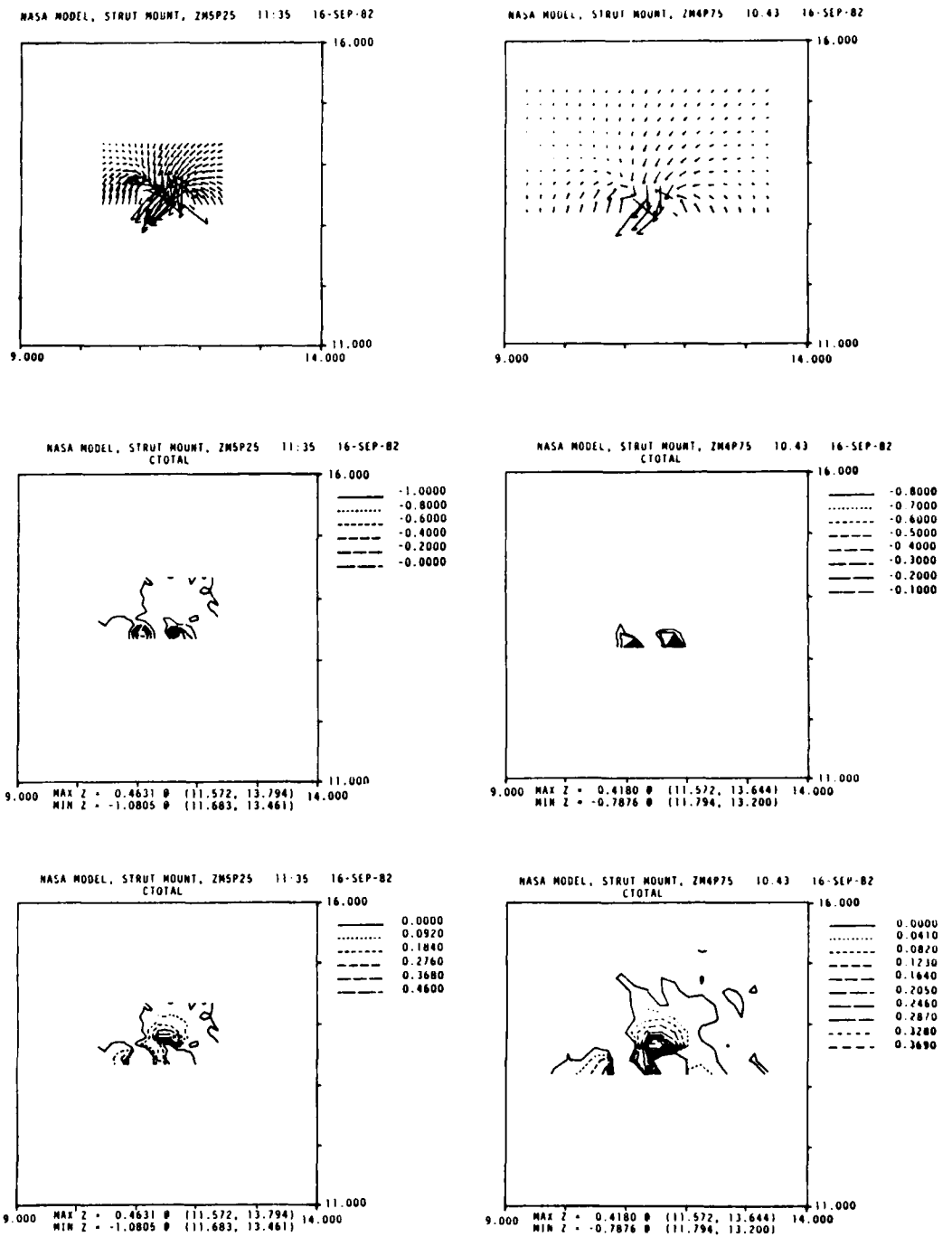

Figure 12a. Seven-Hole Pressure Probe Results, Crossflow Velocity and C_{Total} Contours, Data Planes ZM5P25 and ZM4P75

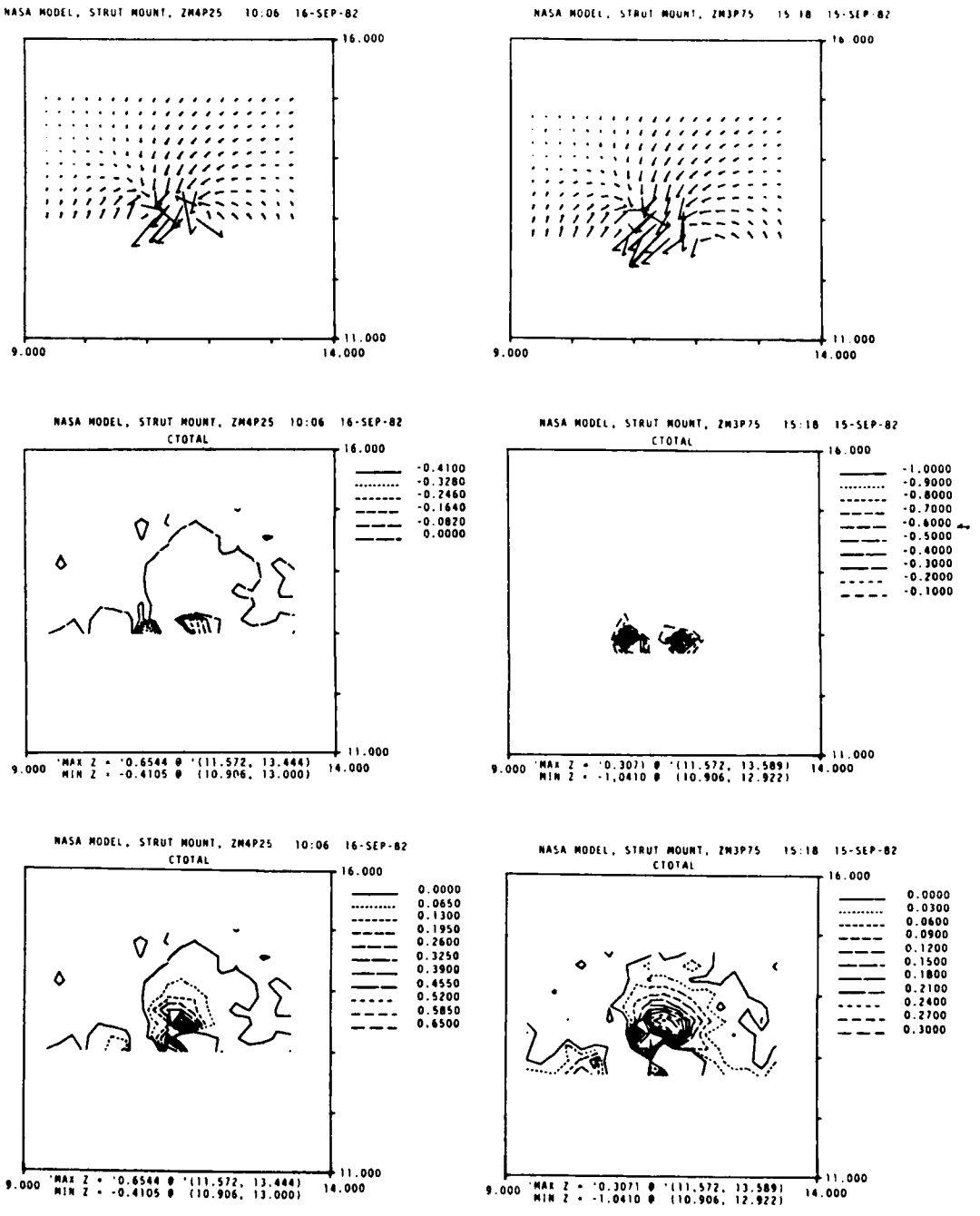

Figure 12b. Seven-Hole Pressure Probe Results, Crossflow Velocity and C_{Total} Contours, Data Planes ZM4P25 and ZM3P75

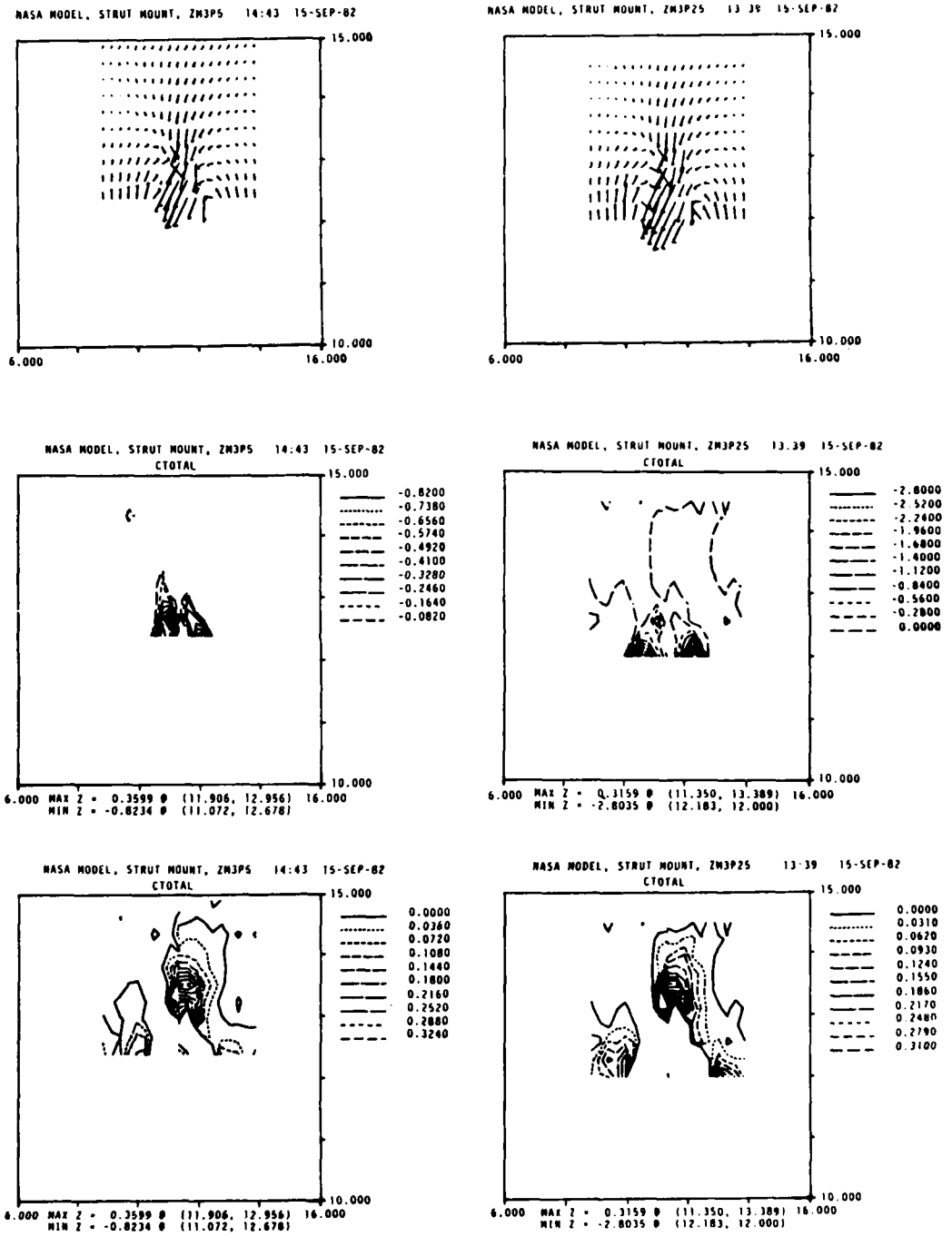

Figure 12c. Seven-Hole Pressure Probe Results, Crossflow Velocity and C_{Total} Contours, Data Planes ZM3P5 and ZM3P25

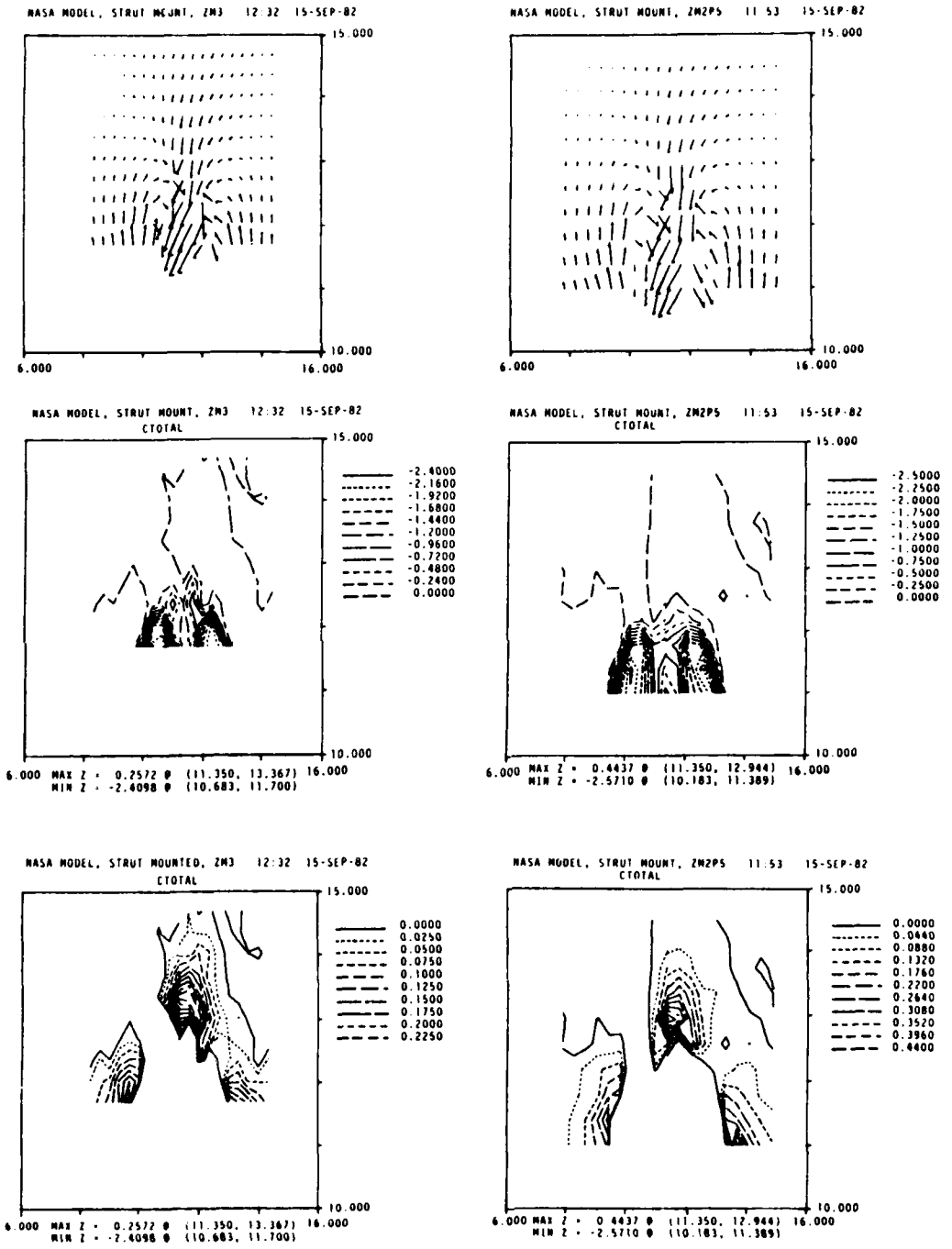

Figure 12d. Seven-Hole Pressure Probe Results, Crossflow Velocity and C_{Total} Contours, Data Planes ZM3 and ZM2P5

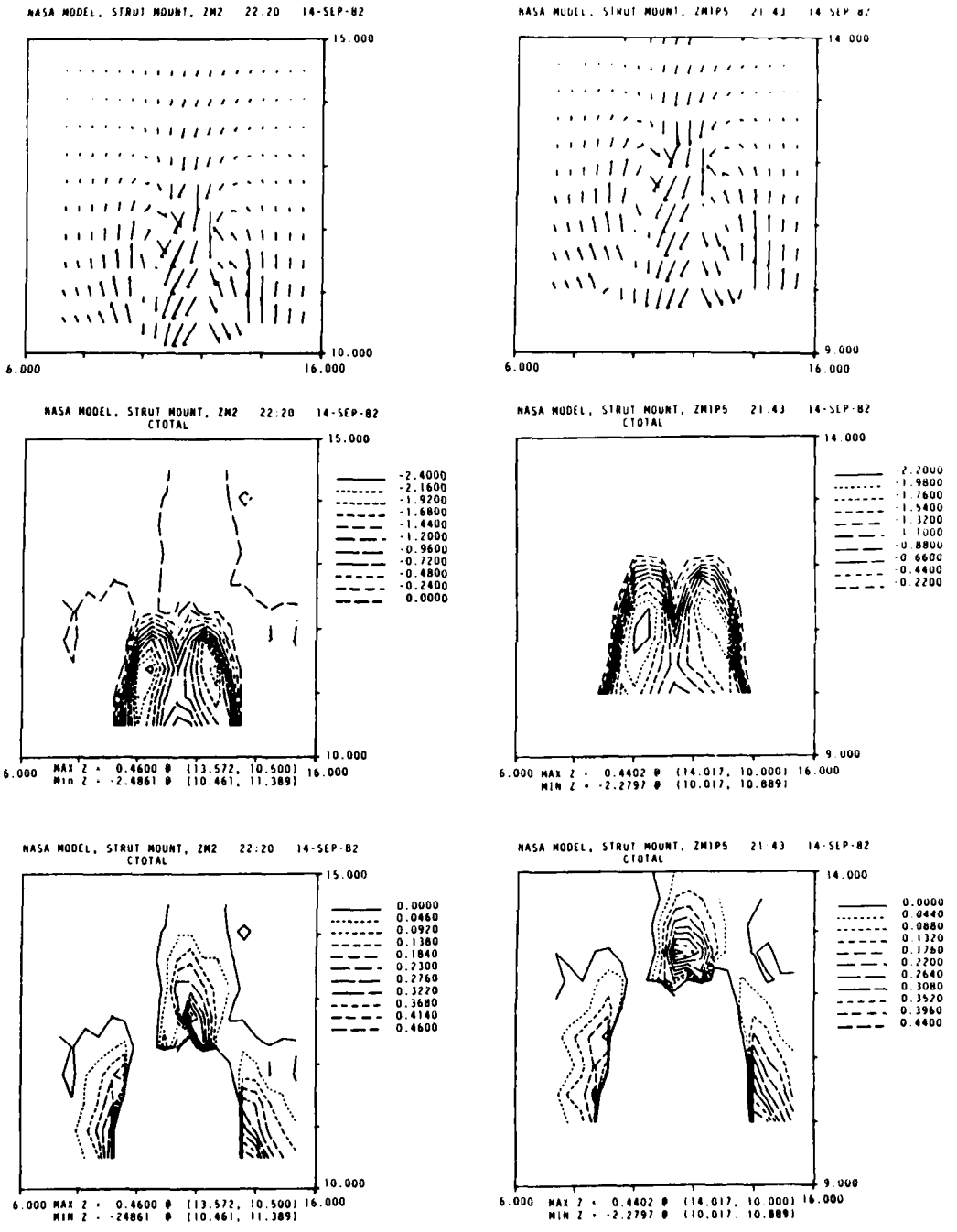

Figure 12e. Seven-Hole Pressure Probe Results, Crossflow Velocity and C_{Total} Contours, Data Planes ZM2 and ZM1P5

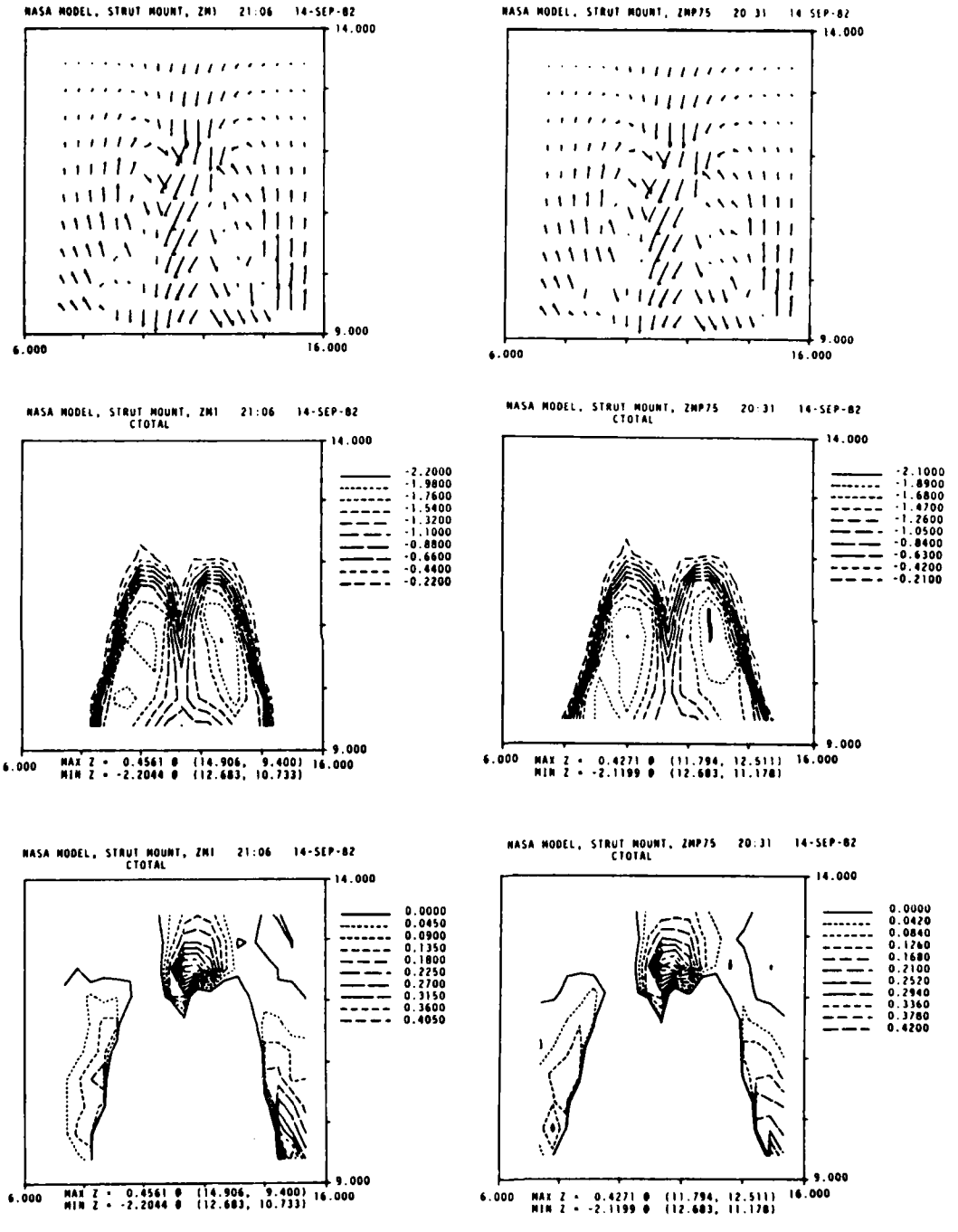

Figure 12f. Seven-Hole Pressure Probe Results, Crossflow Velocity and C_{Total} Contours, Data Planes ZM1 and ZMP75

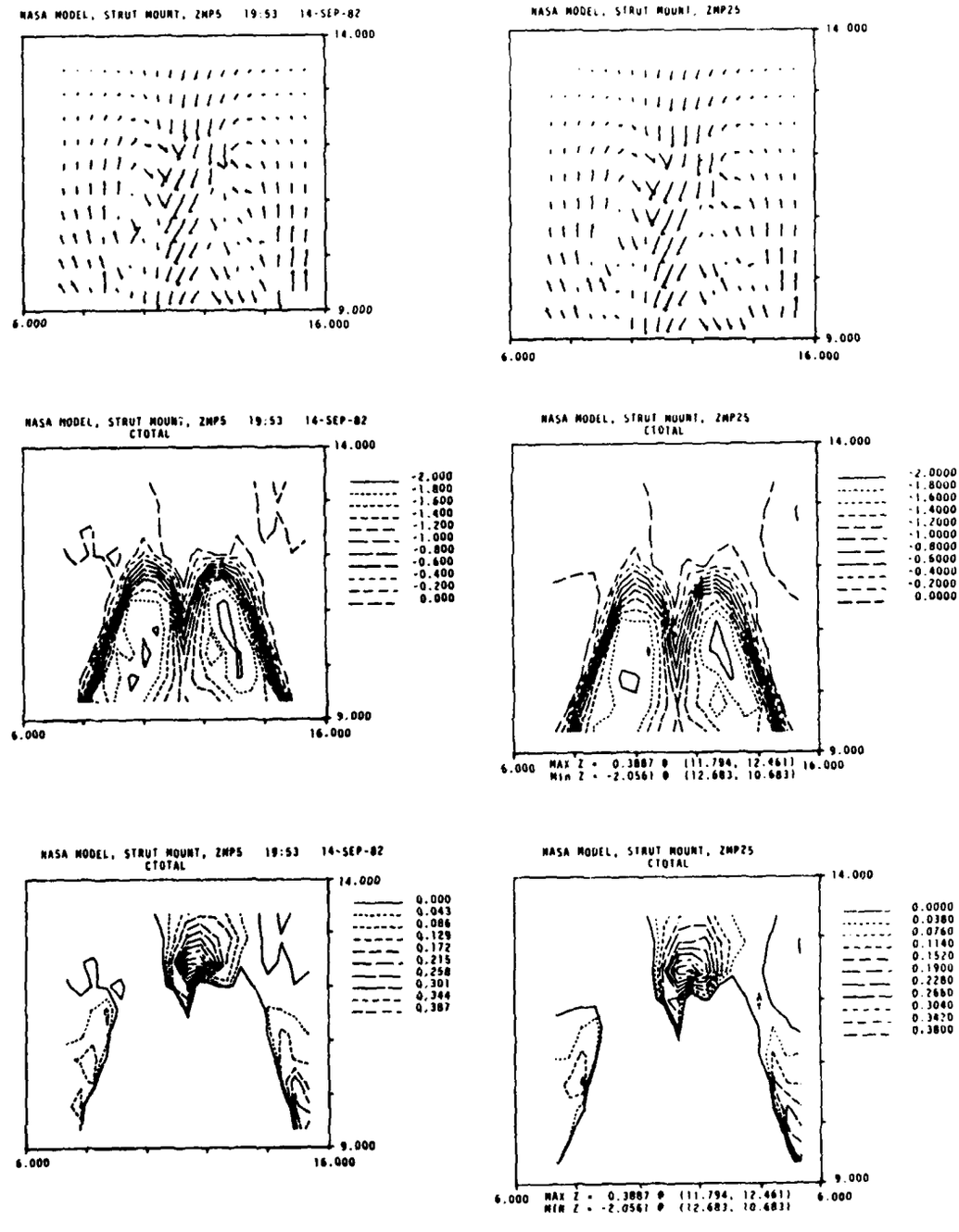

Figure 12g. Seven-Hole Pressure Probe Results, Crossflow Velocity and C_{Total} Contours, Data Planes ZMP5 and ZMP25

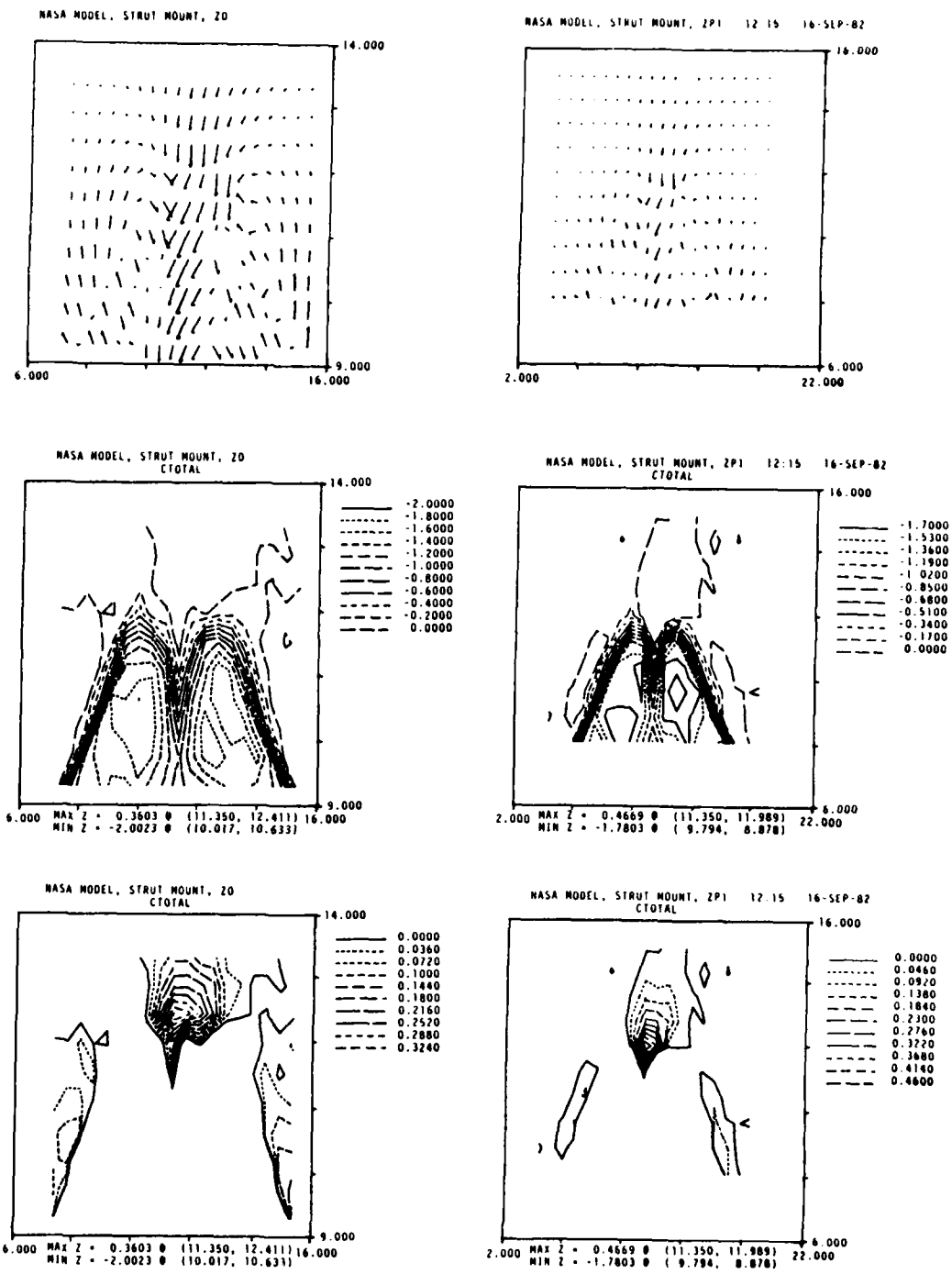

Figure 12h. Seven-Hole Pressure Probe Results, Crossflow Velocity and C_{Total} Contours, Data Planes Z0 and ZP1

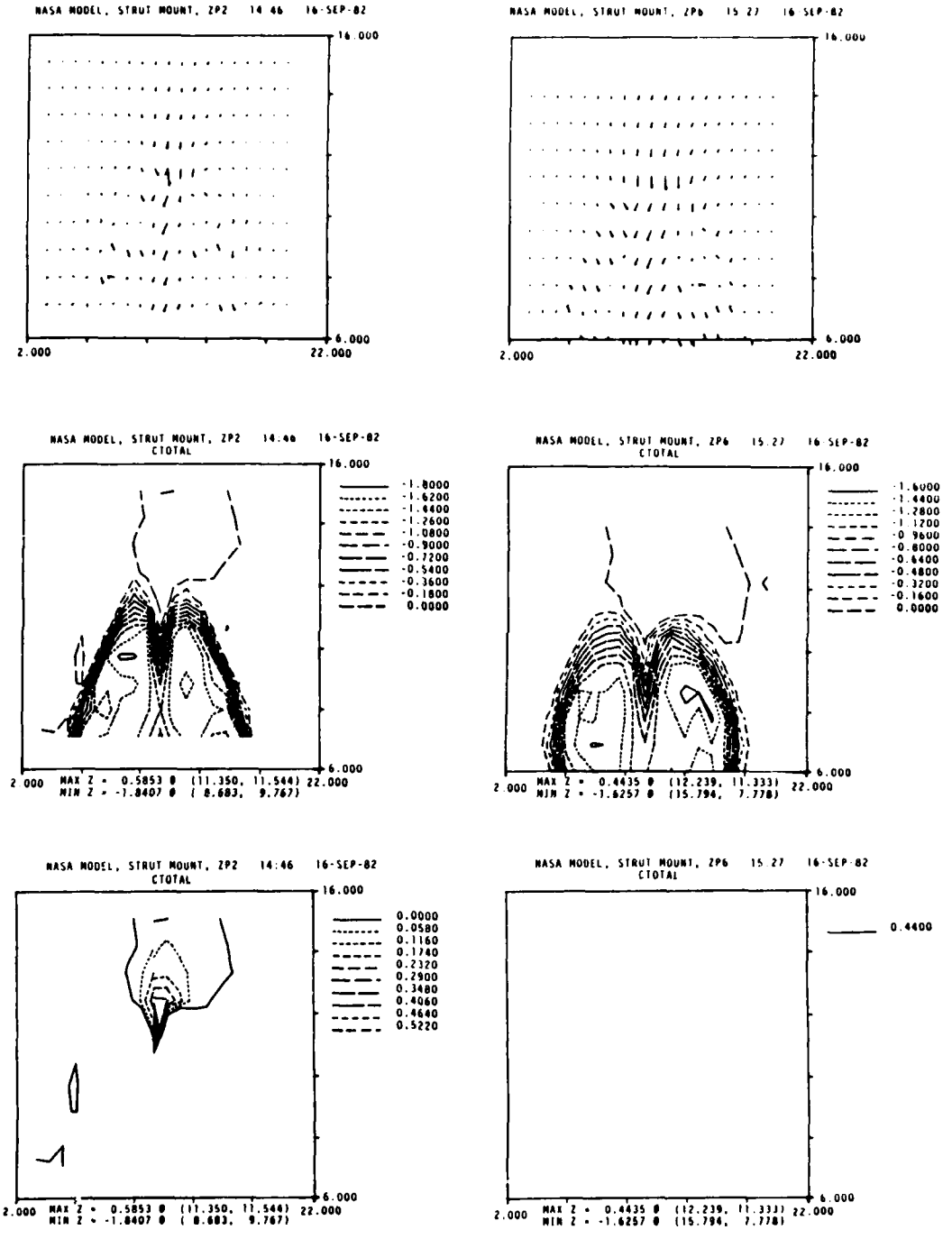

Figure 12i. Seven-Hole Pressure Probe Results, Crossflow Velocity and C_{Total} Contours, Data Planes ZP2 and ZP6

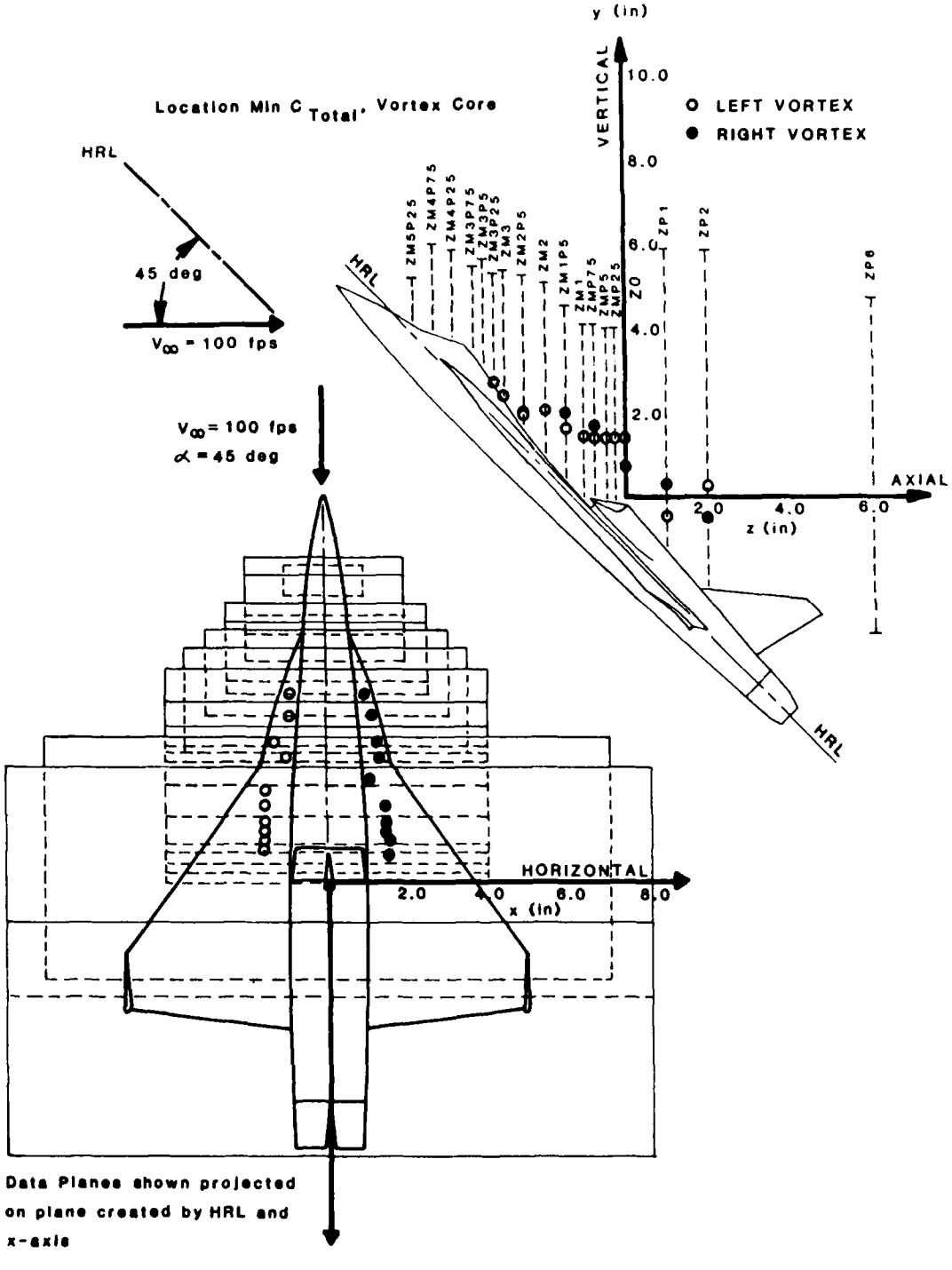

Figure 13. Vortex Core Locations from Minimum Values of C_{Total}

The trace of the vortex cores corresponding to the location of the maximum negative values of C_{Total} is shown in Figure 13 for data planes ZM3P25 to ZP2. As seen in this figure, the vortex cores seem to originate from the point at which the leading edge of the LEX joins the fuselage. The decay in the strength of the vortices as one moves downstream is evidenced by the decreasing absolute magnitude of the value of C_{Total} identified with the vortex core. These values are listed in Table II by data plane with the location of the particular vortex associated with the minimum value of C_{Total} (L being the left vortex and R being the right vortex) given. The approximate location of the vortex cores, in inches, is also presented with respect to the probe axis system for each data plane. The values in parentheses indicate approximate or average locations.

Shown in Figure 14a-c are axonometric or three-dimensional projections of the C_{Total} data for each data plane (note that the order of presentation is reversed). All projections were plotted using the same scale factor, and the growth (diffusion) and decay (dissipation) of the vortices is clearly visible. Further evidence of mixing is the relative flattening of the peaks of the C_{Total} values (negative C_{Total} being up or out of the plane of projection).

Table II
VORTEX CORE LOCATIONS

Data Plane	Maximum Negative C_{Total}	Location (x,y - inches) Left Vortex	Right Vortex
ZM3P25	-2.80R	10.50, 12.00	12.20, 12.00
ZM3	-2.41L	10.60, 11.70	12.40, 11.70
ZM2P5	-2.57L	10.20, 11.40	12.50, 11.30
ZM2	-2.49L	10.45, 11.40	12.60, 11.40
ZM1P5	-2.28L	10.00, 10.90	12.30, 11.30
ZM1	-2.20R	(10.00, 10.70)	12.70, 10.70
ZMP75	-2.12R	(10.00, 10.70)	12.70, 11.00
ZMP5	-2.07R	(10.00, 10.70)	12.70, 10.70
ZMP25	-2.06R	(10.00, 10.70)	(12.70, 10.70)
Z	-2.00L	(10.00, 10.70)	(12.60, 10.00)
ZP1	-1.78L	(9.80, 8.90)	(12.80, 9.60)
ZP2	-1.84L	(8.70, 9.80)	(12.80, 8.90)
ZP6	-1.63R	---	---

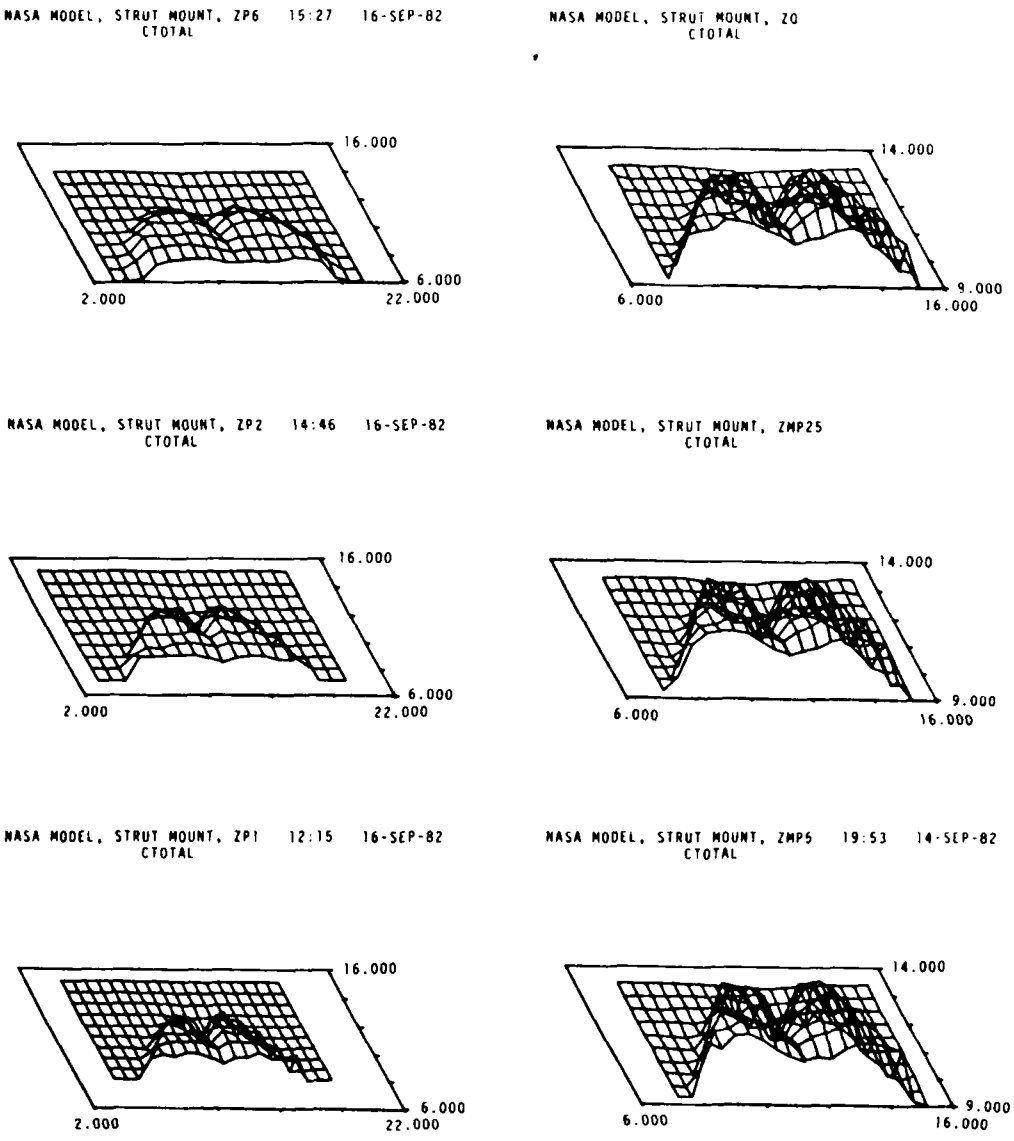

Figure 14a. Axonometric Projections, C_{Total}, Data Planes ZP6 to ZMP5

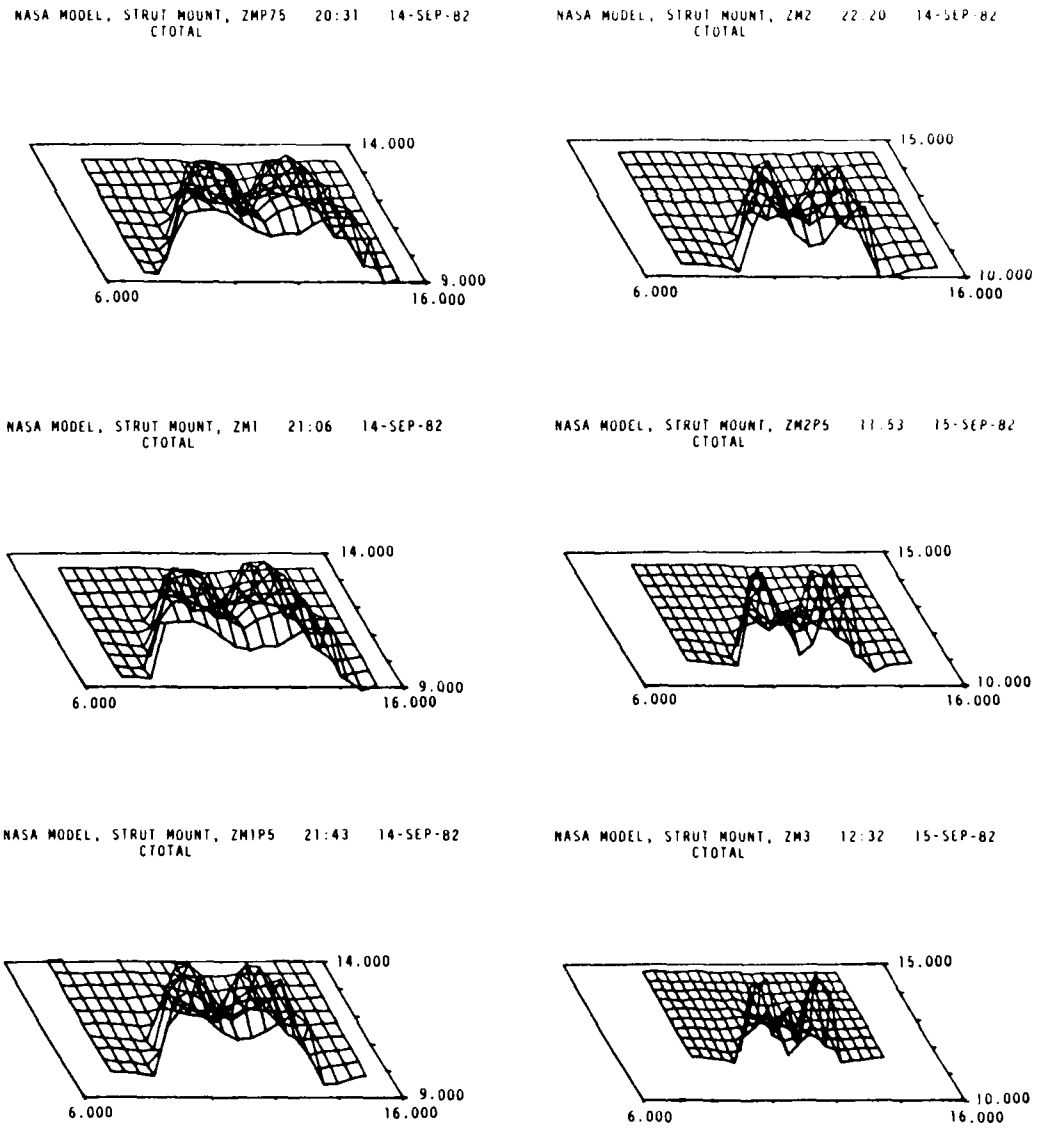

Figure 14b. Axonometric Projections, C_{Total}, Data Planes ZMP75 to ZM3

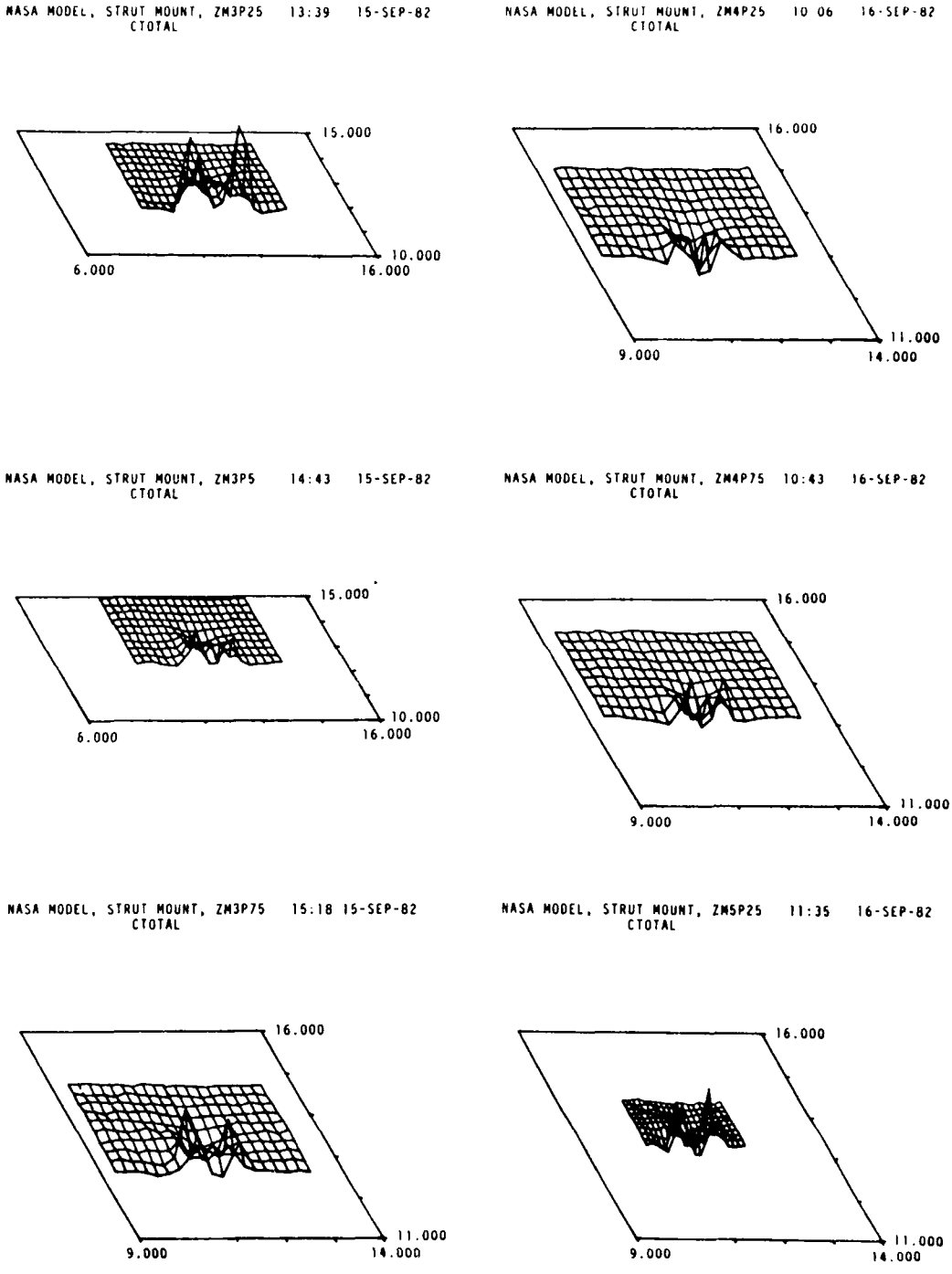

Figure 14c. Axonometric Projections, C_{Total}, Data Planes ZM3P25 to ZM5P25

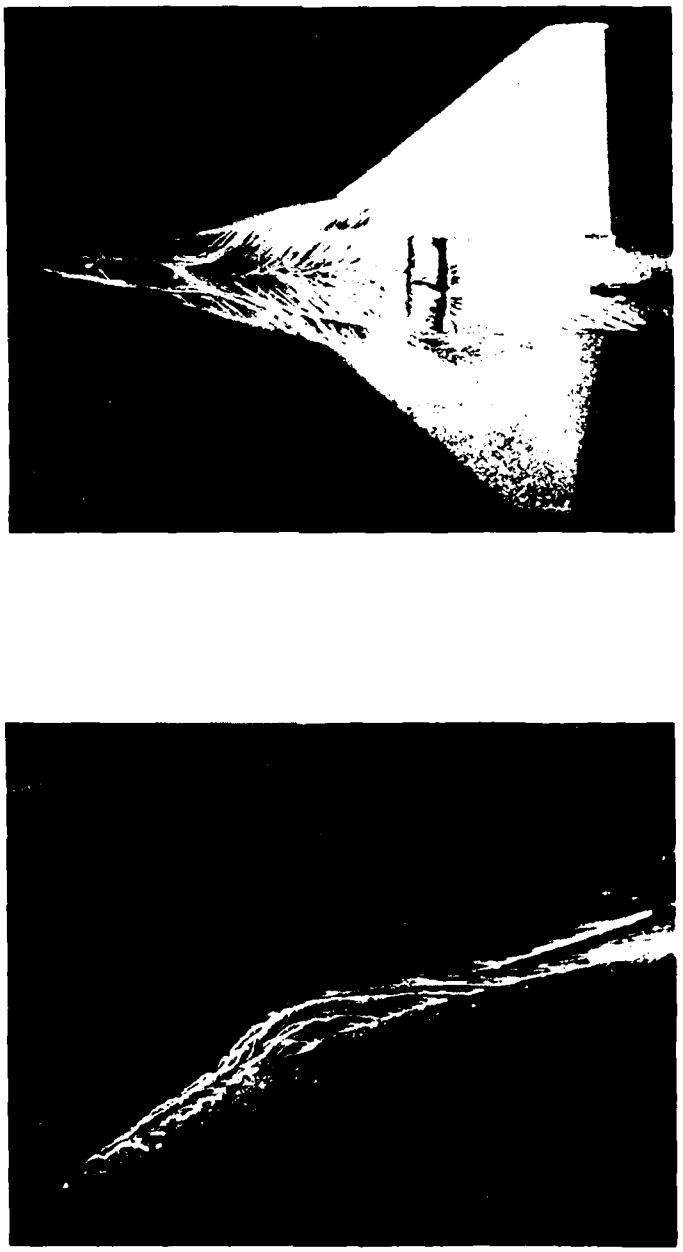

Figure 15. Surface Oil Flow, Northrop VATOL Model at 45 Degree Angle of Attack

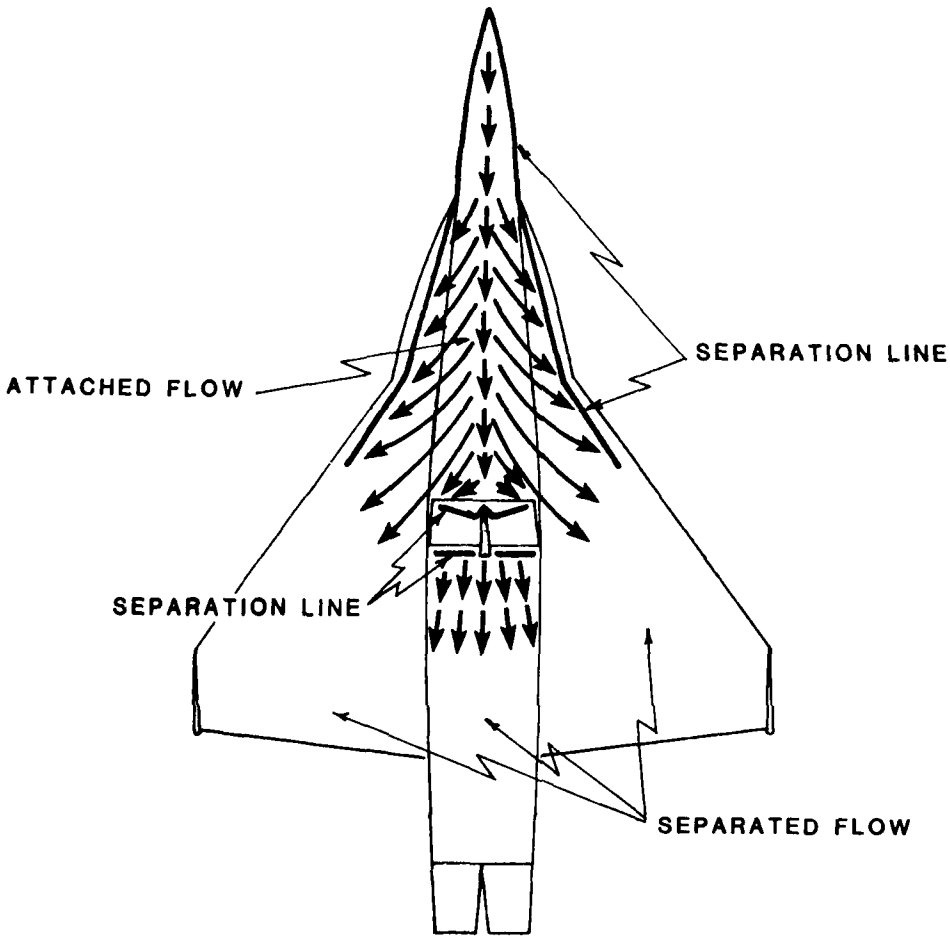

Figure 15. Surface Oil Flow, Northrop VATOL Model at 45 Degree Angle of Attack, Continued

Surface oil flow results at the same test conditions are shown in Figure 15. The traces of the counter-rotating vortices producing an outwash and the separation line near the leading edge of the LEX are clearly visible. The surface oil was applied rather liberally to determine if there were any strong reverse flow patterns near the trailing edge of the wing. As can be seen, the flow has fully separated over the entire aft portion of the wing with no indication of reverse flow. In fact, the main lifting surface shows regions of separated flow except near the inlets. The flow around the inlets

remains attached from the upper surface of the inlet nacelle to approximately the location of the horizontal tail. The flow on the nozzle afterbody has separated. Interestingly, there is a separation line on the fuselage nose that appears to correspond to the separation vortex forming off the nose.

Positive values of C_{Total} are also shown in Figures 12a-i. The location of these regions of positive C_{Total} is consistent from data plane to data plane. These regions of positive C_{Total} correspond to the regions of upwash associated with each vortex and the downwash region where the two vortices meet above the fuselage. The strength and location of these regions (same data planes as identified with the vortex cores) are shown in Table III.

Table III
POSITIVE C_{Total} LOCATIONS

Data Plane	Maximum C_{Total}	Location (x,y - inches)
ZM3P25	0.32	11.35, 13.39 centerline, downwash
ZM3	0.26	11.35, 13.37 " "
ZM2P5	0.44	11.35, 12.94 " "
ZM2	0.46	13.52, 10.50 right vortex, upwash
ZM1P5	0.44	14.01, 10.00 " "
ZM1	0.46	14.91, 9.40 " "
ZMP75	0.43	11.29, 12.51 centerline, downwash
ZMP5	0.43	11.29, 12.46 " "
ZMP25	0.30	11.29, 12.46 " "
Z	0.36	11.35, 12.41 " "
ZP1	0.47	11.35, 11.99 " "
ZP2	0.58	11.35, 11.54 " "
ZP6	0.44	12.24, 11.33 " "

In general, it seems that the maximum positive C_{Total} values first grow and then remain constant until after passing over the inlet lip. A value of 0.45 for C_{Total} corresponds to a local total pressure 0.2 percent higher than the freestream total pressure at the nominal test conditions. This value of C_{Total} has a magnitude greater than the expected data uncertainties at the 95 percent confidence level (Ref.

5). That these readings exist and are consistent from data plane to data plane indicates that they either exist or are the result of an idiosyncrasy of the seven-hole pressure probe. The second alternative appears more likely at this time; that is, the positive C_{Total} readings result from the physical interaction and limitations of the probe in regions of high shear flow. Several studies of the seven-hole pressure probe are being conducted at present to quantify these limitations. The results of two of these efforts -- a correlation of the seven-hole probe measurements with hot-wire anemometer measurements in an airfoil wake or low shear flow and an attempt to measure the actual pressures in these positive regions of C_{Total} using total pressure probes -- appear in Sections B and C below.

B. Airfoil-Wake Measurements

Measurements of the velocity profile through the wake of an NACA 0015 airfoil were made at a location 3 chord lengths aft of the airfoil's trailing edge. The airfoil model was set at a nominal angle of attack near 0 degrees, and the tests were conducted at test-section velocities of 60 ft/sec and 100 ft/sec. Measurements of the velocity profile (velocity deficit) were made using a single-wire, hot-wire anemometer and the seven-hole pressure probe. The wake surveys were made at the centerline spanwise station of the airfoil model. The seven-hole pressure probe data consisted of three passes through the airfoil wake at this location. Each pass through the wake was in the opposite direction from the previous pass. Although the pressure data is not presented, there was no evidence of positive values of C_{Total} through the wake, and the static pressures were very nearly equal to the freestream static pressure at this data plane location. This correlation is to be expected from the theoretical model presented

earlier. As can be seen from Figure 16, the velocity profiles compare very well, especially at the higher velocity (100 ft/sec), as one would expect. The seven-hole pressure probe data is within 3.4 percent at 60 ft/sec and 0.7 percent at 100 ft/sec of the peak velocity deficit measured by the hot-wire anemometer. Both values are within the 95 percent confidence level of uncertainty, based on Mach number, of the seven-hole pressure probe data acquisition system (Ref. 5). There was no evidence of hysteresis in the seven-hole pressure probe measurements based on the direction of the probe's traverse through the wake.

C. Positive C_{Total} Measurements

Measurements of local total pressure, and thus C_{Total}, were made using three different pressure probes at the data plane ZMP75 on the Northrop VATOL model. Regions of positive local total pressure coefficient, C_{Total}, were identified using the seven-hole pressure probe, as shown in Figure 11. At specific points in these regions, two total pressure probes (one aligned with the freestream flow and one aligned with the local flow) were inserted to measure the local total pressure. The results for the point (11.80, 12.50) in the data plane ZMP75 are summarized in Table IV. It should be noted that the local flow angle at this point was determined from the seven-hole pressure probe data to be α = -23.41 degrees with negligible sideslip. The angle of the bent probe was 23.8 degrees, which is within the data uncertainty of the seven-hole pressure probe measurements.

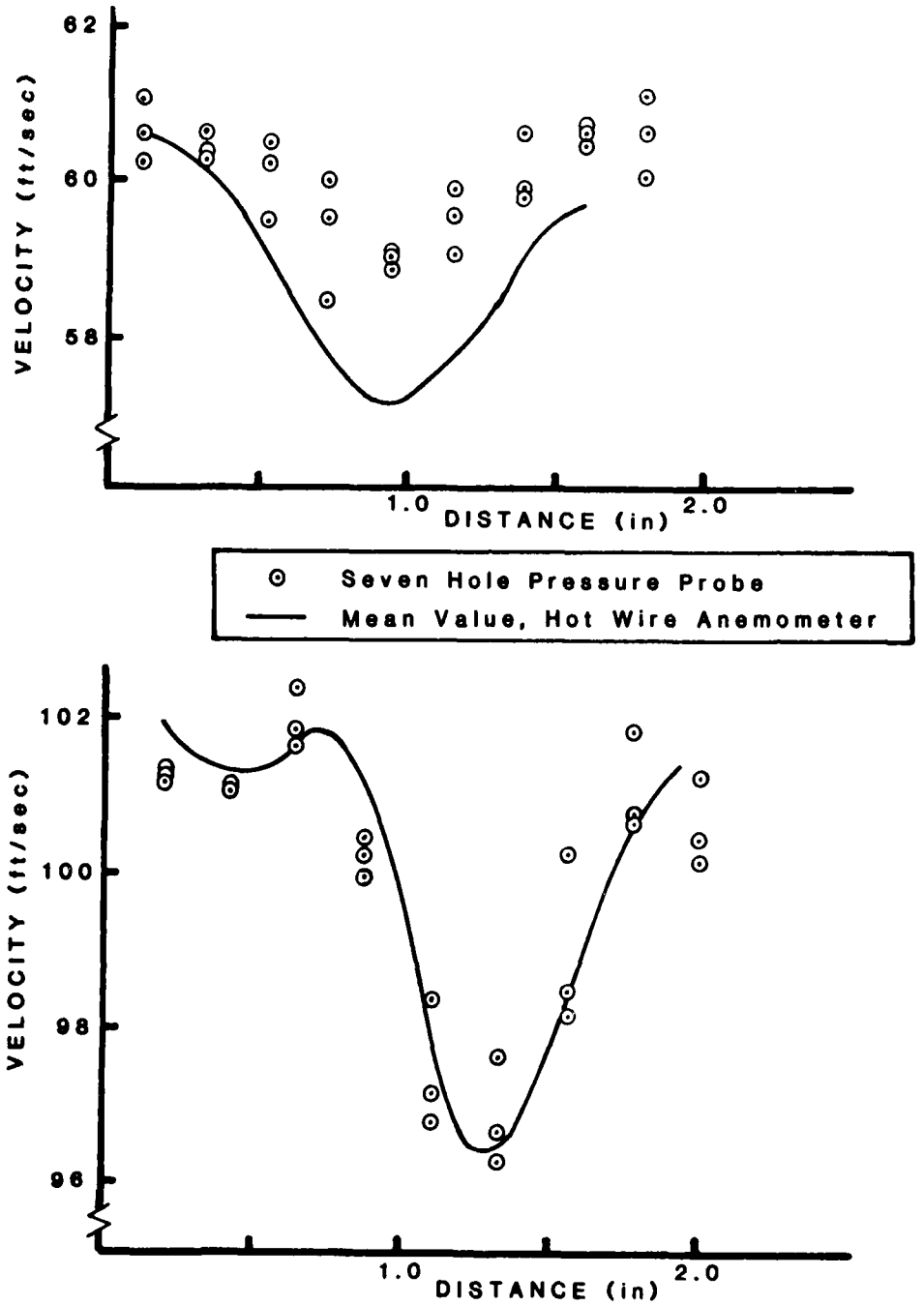

Figure 16. Velocity Profiles through an Airfoil Wake, Seven-Hole Pressure Probe and Hot-Wire Anemometer at Test Section Velocities of 60 and 100 ft/sec

Table IV
LOCAL TOTAL PRESSURE COMPARISONS

	Seven-Hole Pressure Probe	Total Pressure Probe Aligned with Freestream	Total Pressure Probe Aligned with Local Flow
Number of Readings (50 Data Samples Per Reading	1	10	69
Average Value C_{Total}	+0.197	-0.046	-0.013
Standard Deviation, σ	+0.003	+0.0237	+0.023
Maximum Value C_{Total}	---	-0.003	+0.040
Minimum Value C_{Total}	---	-0.067	-0.055
Percentage of Positive C_{Total} Readings	---	0%	26%

As can be seen from the data, the total pressure probe measurements of the positive value of C_{Total} at this point do not agree with the measurements made by the seven-hole pressure probe. For the total pressure probe aligned with the freestream flow, there were no measurements made where C_{Total} was greater than 0. However, due to the flow angularity at this point, the flow has probably separated at the probe tip and does not represent a measure of the true local total pressure.

For the total pressure probe aligned with the local flow, 26 percent of the measurements resulted in a local total pressure greater than that of the freestream value. These measurements, however, are lower than those obtained using the seven-hole probe. It should be kept in mind, however, that this total pressure probe was bent at an angle based on measurements made using the seven-hole pressure probe and that this measurement is being made at a region of high shear

flow. If the shear or velocity gradient at this point is such that holes on opposite sides of the seven-hole pressure probe see significantly different velocities, then the local flow angularity measurement could be in error as well. If this measurement of local flow angle is then substantially in error, the flow around the tip of the total pressure probe supposedly aligned with the local flow could also be separated. Separated flow around the tip would lead to measurements which would not represent the true local total pressure. Nevertheless, the average value for C_{Total} based on these measurements was negative, which corresponds to the theoretical model presented earlier. The maximum positive value of C_{Total} measured with this total pressure probe, +0.040, is within 2.3 standard deviations of the mean value, -0.013, or within the 97.9 percent uncertainty band.

Although these contradictions do not exclude the possibility that the regions of positive C_{Total} measured by the seven-hole pressure probe do exist, they seem to indicate that the readings may be erroneous in regions of high shear flow. It must be recalled that at present the seven-hole probe is calibrated in a uniform flow. The regions where the positive values of C_{Total} have been measured by the seven-hole pressure probe are regions of high shear gradients whose effect may not be properly accounted for in this data reduction and whose limits need to be defined. These results do not imply, however, that the seven-hole pressure probe data is not useful, since it has more than demonstrated its value in mapping hitherto undefined external flow fields.

VI. Summary

The external flow field on a 1/40th-scale model of the Northrop VATOL configuration was mapped using the seven-hole pressure probe

data acquisition system. The model was mounted at 45 degrees angle of attack relative to the horizontal reference line, and the test section velocity was 100 ft/sec. Two counter-rotating vortices produced by the leading edge extensions were mapped, and their growth and decay were observed. Flow interference effects due to the top-mounted inlets were identified by the appearance of multiple pressure contour cells and a low-energy region in the cores of the vortices as they passed over the inlets. Flow is shown to be attached from the upper fuselage to the inlet locations and separated over the majority of the upper surfaces of the aircraft wings.

Comparisons of seven-hole pressure probe measurements with hot-wire anemometer measurements were made in a low shear flow wake 3 chord lengths aft of a two-dimensional airfoil model. The comparisons showed good agreement, with the seven-hole pressure probe measurements of local velocity being within 3.4 percent at a test section velocity of 60 ft/sec and 0.7 percent at a test section velocity of 100 ft/sec of the peak velocity deficit measured by the hot-wire anemometer. The overall signature of the airfoil wake was clearly identified by both measurement systems.

Finally, the measurements of local total pressures made by the seven-hole pressure probe were compared to those made by total pressure probes. Tests were conducted using the 1/40th-scale Northrop VATOL model mounted at 45 degrees angle of attack and a test section velocity of 100 ft/sec. This investigation was made to determine the actual values of local total pressures in flow regions where (according to seven-hole probe measurements) these values are greater than the freestream total pressure. The measurements made using total pressure probes did not confirm the seven-hole pressure probe measurements. To investigate this phenomenon further, research into

seven-hole pressure probe characteristics in regions of high shear flow, such as the flow typically encountered in viscous vortex wakes, is recommended.

Symbols

English Symbols

A	area, inches^2 or feet^2
ALPHAT	angle of attack, degrees
BETAT	angle of sideslip, degrees
C_{Static}	dimensionless coefficient, $P_{\ell} - P_{\infty} / P_{O_{\infty}} - P_{\infty}$
C_{Total}	dimensionless coefficient, $P_{C_{\ell}} - P / P_{O_{\infty}} - P_{\infty}$
d	distance, inches or feet
HRL	horizontal reference line
M	*Mach number*
p	pressure, psi or psf
r	radius, inches or feet
(r,θ)	polar coordinates
t	time, seconds
(U_r, U_θ)	velocity components, polar coordinates, fps
(u,v,w)	velocity components, Cartesian coordinates, fps
V	velocity, fps
(x,y,z)	Cartesian coordinates, inches or feet

Greek Symbols

α, α_T	angle of attack, degrees
β, β_T	angle of sideslip, degrees
Γ	circulation, ft^2/sec
ν	*kinematic viscosity, ft^2/sec*
ρ	density, slug/ft^2

σ	standard deviation

Subscripts

ℓ	local conditions
o	total or stagnation conditions
∞	freestream conditions

References

1. Durand, W.F., Aerodynamic Theory, Vol. III. Div. F-1, Berlin, Julius Springer, 1935.

2. Sisson, G. and R. Crandall, "Canard Wake Measurement and Description," Aeronautics Digest, USAFA-TR-81-4, USAF Academy, May 1981.

3. Nelms, W.P. and D.A. Durston, "Preliminary Aerodynamic Characteristics of Several Advanced VSTOL Fighter/Attack Aircraft Concepts," SAE Paper 801178, SAE Aerospace Congress and Exposition, Los Angeles, California, 13-16 October 1980.

4. Smeltzer, D., W. Nelms, and T. Williams, "Airframe Effects on a Top-Mounted Inlet System for VSTOL Fighter Aircraft," AIAA-81-2631, AIAA/NASA Ames VSTOL Conference, Palo Alto, California, 7-9 December 1981.

5. Gerner, A., G. Sisson, et al., Seven-Hole Probe Data Acquisition System, USAFA-TN-81-8, 18 November 1981.

EXPERIMENTAL MEASUREMENTS OF WAKE CHARACTERISTICS OF LOW ASPECT-RATIO DELTA AND FLAPPED-PLATE PLANFORMS

C.R. Kedzie* and K.E. Griffin**

Abstract

This report documents the characteristics and location of the wakes for two generic lifting-surface planforms. The geometric description locates these wakes as they develop downstream from a low aspect-ratio delta wing and a bent-plate wing. The wakes are depicted graphically at several locations downstream from these wings, with accompanying cross-velocity vector plots to assist in their interpretation. The data used to determine the wake characteristics was obtained by surveying each wing's flow field with a seven-hole pressure probe.

I. Introduction

For this project, we used a seven-hole probe to measure the wakes produced by two simple planform shapes: (1) a low aspect-ratio flat plate with a 50 percent chord flap deployed 20 degrees and (2) a low aspect-ratio delta wing. These planforms were tested at low speeds and moderate angles of attack to study their wake characteristics. In the past, R.H. Wickens worked with these planforms to demonstrate lifting-surface wakes using such flow visualization techniques as the water table and dye methods described in Ref. 1. The following data represents flow visualizations at higher Reynolds numbers (where the vortex systems exhibit the turbulence that is characteristic of an aircraft's lifting surfaces) and also at higher freestream pressure and velocity values. The planforms analyzed here are the same as those used to develop analytical methods (such as those found in Ref. 2) for predicting the effects of lifting-surface wakes. These analytical methods use mathematical functions called singularities to model the wake trailing a lifting surface. Not knowing the location of the wake, however, has limited the usefulness of these methods. The experimental values of pressure and velocity reported here will provide the necessary wake locations and downwash velocity values for correlation with the

*Cadet, USAF Academy
**Captain, USAF Academy, Associate Professor of Aeronautics, DFAN

analytical predictions for these planforms.

The first planform configuration (Figure 1) is a plate bent at the midchord so that the trailing half simulates a trailing flap deflected downward by a 20-degree angle. The angle of attack of this planform is measured with respect to the front half of the plate. This bent plate configuration is interesting because of the effect of the bend on the structure of the tip vortex. The discontinuity in slope at the midchord produces a secondary vortex, which interreacts with the main vortex created at the wing tip. In fact, when we observe experiments with very low Reynolds numbers, we see that this secondary vortex core becomes embedded in the wake wrapped around the core of the wing tip's main vortex. This secondary vortex core, caused by the midchord bend, provides a pressure characteristic, or signature, in the main vortex system that can be observed at downstream locations. The rotation rate of the main vortex can then be determined by observing the change in angular position of this pressure signature in successive locations (planes) downstream of the plate.

The second planform configuration is shown in Figure 2. This highly-swept delta configuration produces a leading edge/tip vortex system similar to that observed around the strakes of modern fighter aircraft. This vortex system builds in strength when moving streamwise along the leading edge. Downstream, it wraps the trailing edge wake up and in towards the centerline of the model. Since modern fighter configurations use this strake vortex to delay flow separation over their primary wings, it is of critical importance to know the location and strength of this type of lifting-surface vortex system.

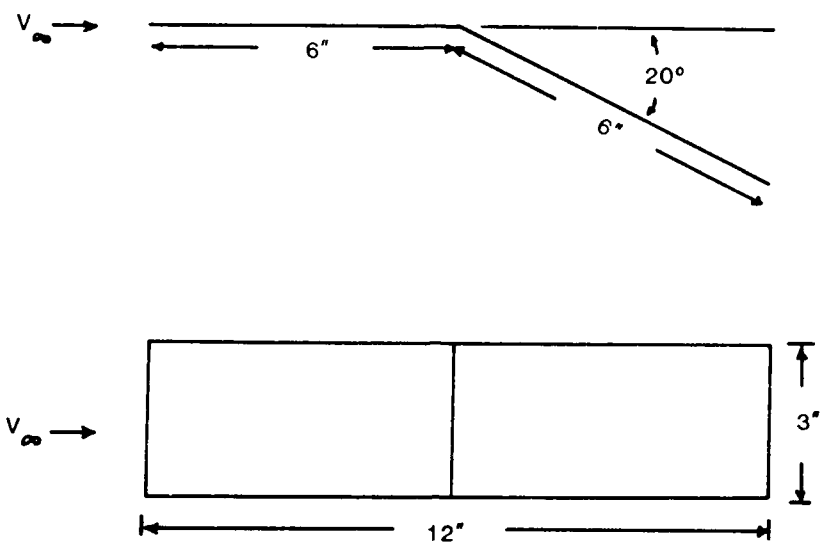

Figure 1. Model Geometry for Bent Plane

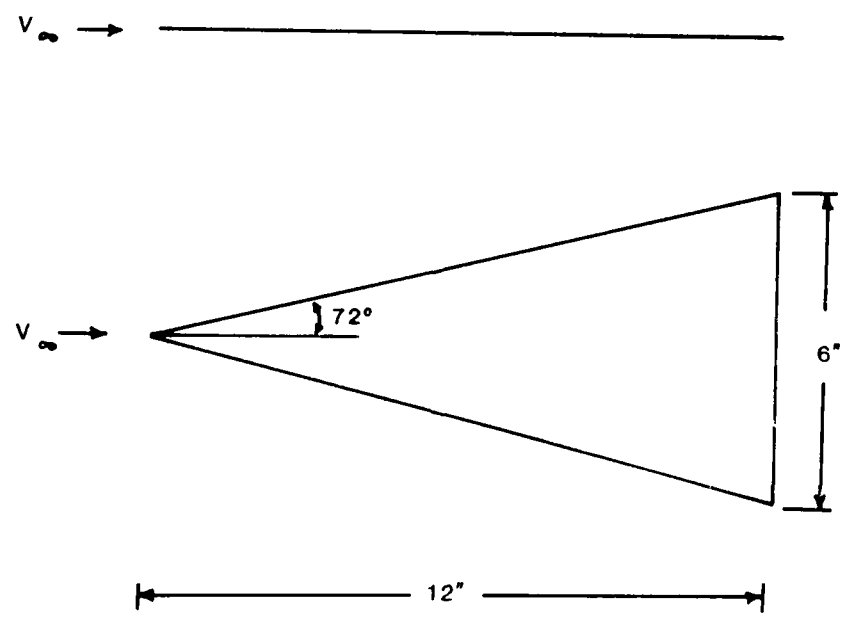

Figure 2. Model Geometry for Delta Plane

II. Background

Test engineers working at the Aeronautics Laboratory of the USAF Academy have developed an experimental technique that can measure pressure and velocity information from steady fields even with highly irregular flows. The test technique uses a multi-port pressure probe linked to a computer system that produces real-time flow field data for any geometric location in which the pressure-probe tip can be positioned. This particular seven-hole pressure probe was first developed to measure incompressible flow at the USAF Academy under the sponsorship of the NASA Ames Research Laboratory (Ref. 3). The probe's capabilities were later expanded to include supersonic testing. This probe is now being used in ongoing research to document the characteristics of lifting-surface wakes, particularly those created by the X-29 Forward-Swept Wing Flight Demonstrator. In the first wake survey, experimenters used the seven-hole probe to study a generic canard/swept-wing configuration (Ref. 5). This study of the delta and bent-plate planforms provides background information on lifting-surface wakes that will be used later in an in-depth investigation of the canard/wing wake interaction of a 1/10 scale model of the X-29 Forward-Swept Wing Demonstrator Aircraft.

The seven-hole probe used for these wake studies is shown in Figure 3. Because the probe is small (.109 inches in diameter), one can position it inside the near flow fields of moderately-sized wind tunnel models without significantly disturbing those flow fields. The position of the probe is maintained by an automated device called a traverse, which can precisely position the probe anywhere in the test section. Since this positioning traverse is controlled by the wind tunnel computer, the probe location can be loaded into the computer as a series of coordinate points.

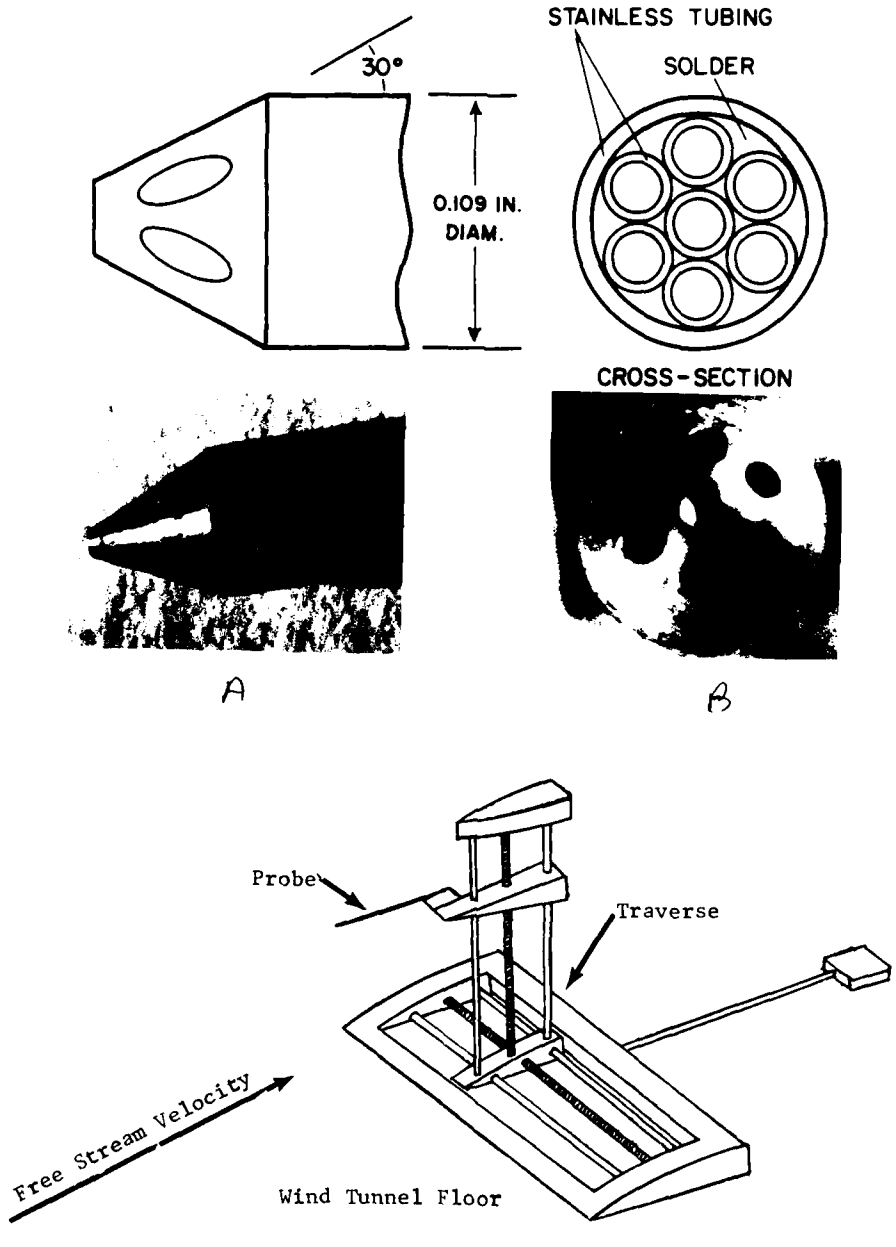

Figure 3. Seven-Hole Pressure Probe and Positioning Traverse

The probe is made up of a pressure port at its centerline surrounded by six pressure ports on its conical face. The seven pressure ports are connected to electronic pressure transducers by small-diameter tubing. With these transducers providing electrical analogs to the pressures, a computer can then directly supply the digitized values of raw pressure at these port locations.

Seven sets of fourth-order polynomial equations were used to derive flow field pressures and velocities from the raw pressure values measured at these seven pressure ports. These equations, along with the non-dimensionalized forms of their coefficients, are presented in Ref. 4. Calibration tests at known flow conditions establish the coefficients, which then remain stored in a data-acquisition computer for use with unknown flow fields. Using the raw pressure data from the seven-hole probe, these equations, with their calibrated coefficients, provide a means of calculating the more useful values of total, static, and dynamic pressures and velocity vectors at any selected point in the flow. The pressure and velocity values for each data point are recorded on high-speed disk storage for later use.

The data points for the tests are arranged in planes having common streamwise coordinates. This procedure makes it easier both to acquire and present data. The planes are chosen at various streamwise locations as measured from the trailing edge of each model. By locating the wake characteristics at each streamwise position in the flow, one can observe and interpret their development as the flow proceeds.

With a complete set of pressure and velocity data stored for each data point, one can quickly generate velocity-vector and pressure-contour plots in the data planes as testing proceeds. This insures that all of the important locations in the flow field are surveyed in each data plane. Later, these plots can be used to locate important flow

characteristics such as vorticity, wakes, and downwash for final interpretation of the lifting-surface wakes.

Figure 4 is a sample cross-velocity, flow-field data plot generated with data taken for the bent plate at 20 degrees angle of attack. This figure shows the cross-velocity vectors at the data points surveyed on the data plane immediately downstream from the trailing edge of the bent plate. These vectors represent the projection on the data planes of the total velocity vector measured at each probe location. The origin of each vector gives the geometric location of the data point; its length gives the relative magnitude of the in-plane velocity component; and the arrow head indicates the flow direction.

In Figure 4 the view is looking upstream at the port-side wing. The cross-velocity vectors indicate a strong clockwise swirling motion (typical of a streamwise vortex) centered about 1.6 inches in the negative x direction. The direction of the rotation in the cross flow is that expected about the tip vortex generated by positive lift on the port wing. The center of this motion will then be the core filament of the vortex. From these velocity fields, we can determine the locations and relative strengths of vortex systems, as well as the direction of the downwash flow field.

Pressure contour plots complement those containing the cross-velocity vectors and can be most useful in wake-location calculations. Figure 5 shows the total-pressure coefficient contours for the same data points viewed in the same direction as in Figure 4. This total-pressure coefficient is defined by total pressure comparisons between local and freestream conditions.

$$\Delta C_{P_o} = \frac{P_{o_{Local}} - P_{o_{Tunnel}}}{P_{o_{Tunnel}} - P_{o_{Tunnel}}}$$

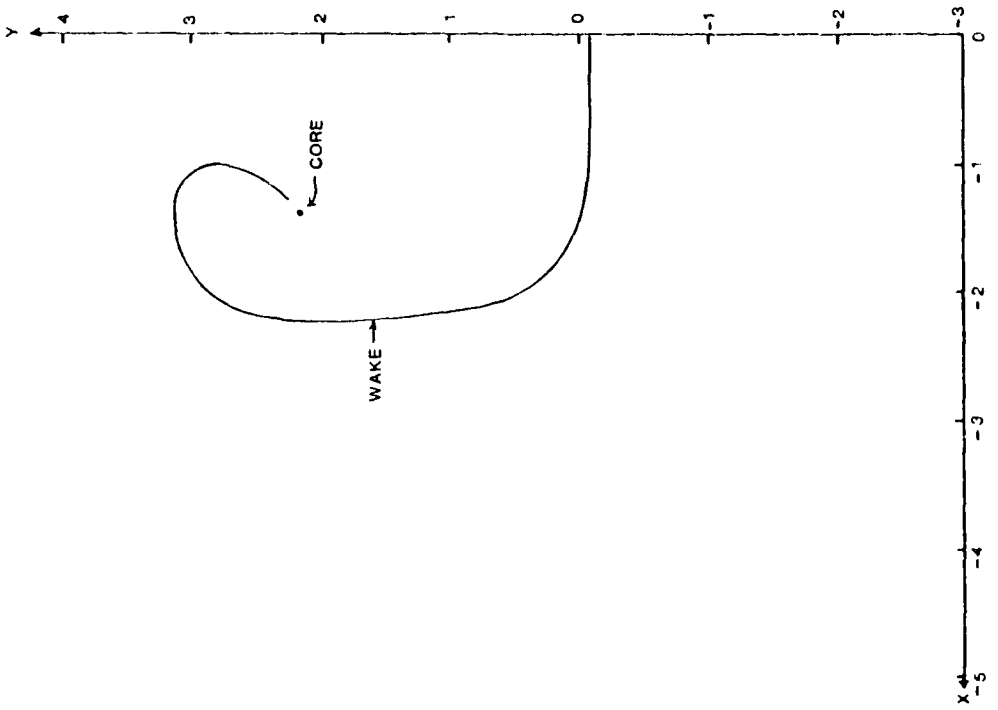

Figure 5. Example of U_{p_θ} Plot

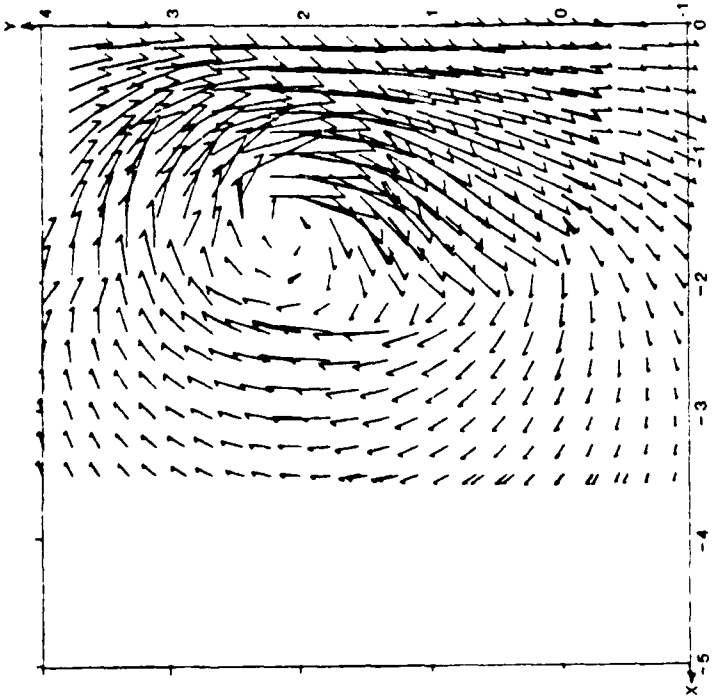

Figure 4. Example of Cross Velocity Vector Plot

The difference between local ($P_{o_{Local}}$) and freestream ($P_{o_{Tunnel}}$) total pressure is nondimensionalized by the freestream dynamic pressure. C_{p_o} becomes negative as irreversible losses in total pressure occur locally, because of viscosity in regions having large velocity gradients. These regions occur near the core of vortex filaments and in the boundary layers of lifting surfaces. In downstream flow, this loss in total pressure provides a signature, which identifies the freestream wake locations.

In Figure 5 contours of various values of C_{p_o} indicate regions where losses in total pressure have occurred. Note that the wake of the plate is apparent in the pressure values. Downstream from the tip chord of the plate, this wake wraps around the tip-vortex core. Using contour plots like those in Figure 5, we can determine the wake locations and the vortex systems (at their edges) for both the bent plate and delta planforms in each plane. The plots of their wake locations appear at the end of this report.

III. Test Apparatus

We tested two planforms in the subsonic, continuous-flow wind tunnel (described in Ref. 5) in the Aeronautics Laboratory at the USAF Academy. The freestream velocity was maintained at 100 ft/sec. The bent-plate model of Figure 1 was mounted on a thin vertical strut from the tunnel ceiling. To develop the following data, each model was set at two angles of attack; 10 and 20 degrees with respect to the freestream direction (as measured from the forward half of the model). The unit normals of the planes defining the data point streamwise locations were always parallel to the freesteam direction.

The delta planform model was also run at 10 and 20 degree angles of attack. Again, the unit normals of the planes used to organize the data points were parallel to the freestream direction.

IV. Results

The data obtained for the two planforms is presented graphically. A cross-velocity plot appears for each set of data points, followed by a second plot showing the lifting surface wake. The wake is plotted from the centerline outward, showing the way it becomes wrapped in the tip vorticity until its pressure signature cannot be distinguished from the inner field of the tip vorticity. The core location of the tip vortex is also noted. If the data plane intersects the wing planform, this too is noted. The steamwise development of the wake for different wing angles of attack can be compared for both planforms.

A. Bent-Plate Results

The bent plate data is taken from the centerline towards the port side of the plate. Since all flow configurations are symmetric about a vertical plane passing through the planform centerline, the flow field of only one side of the planform is presented to allow greater detail in the plots. The coordinate system used for all the data points has its origin at the intersection of the vertical plane of symmetry and the trailing edge of the plate. The vertical direction (perpendicular to the freesteam velocity vector) up (the positive lift side) from the plate is the positive y coordinate. The lateral direction (perpendicular to both the freestream direction and the y direction) is positive towards the starboard wingtip and is designated the positive x direction. All the plots are presented in such a way that the freesteam velocity vector is out of the data plane. Thus the plots are to be viewed as looking upstream.

The data planes for 10 degrees angle of attack are at streamwise locations relative to the trailing edge origin of -2, .2, 2, 4, 6, 9, and 12 inches. The data planes for 20 degrees angle of attack are at

locations of -2, .2, 2, 4, 6, and 11.5 inches. The data is presented in progressive steamwise locations. The cross-velocity and wake-location plots are shown for each plane.

Figures 6 through 19 show the location of the wake, the velocity field, and the vortex core for the bent plate at 10 degrees angle of attack. Figures 20 through 31 show the same at 20 degrees angle of attack. For both angles of attack and any streamwise location, the x location for the vortex core remains approximately -1.5 inches. There are, however, changes in the y location of this vortex core.

The tip vortex core location in the y direction is influenced by the direction and strength of the downwash from the lifting surface. The downwash field — and therefore the movement of the vortex core in the downwash direction — is stronger at 20 degrees angle of attack than at 10 degrees. This is evident when one compares the locations of the tip vortex core in Figure 15 and 29 or Figures 19 and 31.

B. Delta Planform Results

The results of the low aspect-ratio delta wing planform tests are presented in Figures 32 through 55. Again, the data points lie above and in the wake of the port side of the wing. The same coordinate system is used for the delta planform as was used for the bent plate, with the origin at the centerline trailing edge location of the delta planform.

The data planes for 10 degrees angle of attack are at streamwise locations relative to the trailing edge origin of -2, .2, 2, 4, 6, 9, and 12 inches. The data planes for 20 degrees angle of attack are at streamwise locations of -2, .2, 2, 4, and 6 inches. The plots of the wake locations and cross-velocity vectors for each plane of data points are presented in progressive streamwise fashion to indicate the movement

of the wake as it travels downstream from the delta wing.

The delta wing results at 10 degrees angle of attack are contained in Figures 32 through 45. The results at 20 degrees angle of attack appear in Figure 46 through 55. The highly-swept leading edge develops a strake-like vortex system that travels in both the spanwise and downwash directions as progressively downstream data planes are surveyed. The downwash velocity vectors can be seen in the velocity vector plot for each data plane. Note the clockwise rotation of the port-side, leading-edge vortex system. This is consistent with the positive lift condition created at 10 degrees angle of attack. Similar trends, only stronger, are found at 20 degrees.

The tip vortex core appears to seek the same location at either 10 or 20 degrees angle of attack: approximately -2.3 inches on the x axis and .2 inches on the y axis. This location for the tip vortex core appears to have been achieved for both angles of attack in the data plane 6 inches downstream of the trailing edge.

The shape of the delta wing's downsteam wake differs from that of the bent plate. Downstream of the delta wing, the portion of the wake that becomes wrapped around the vortex core is wrapped in a looser spiral than that found behind the bent plate. This is especially noticeable in the x locations of the outboard wake that is wrapping around the core.

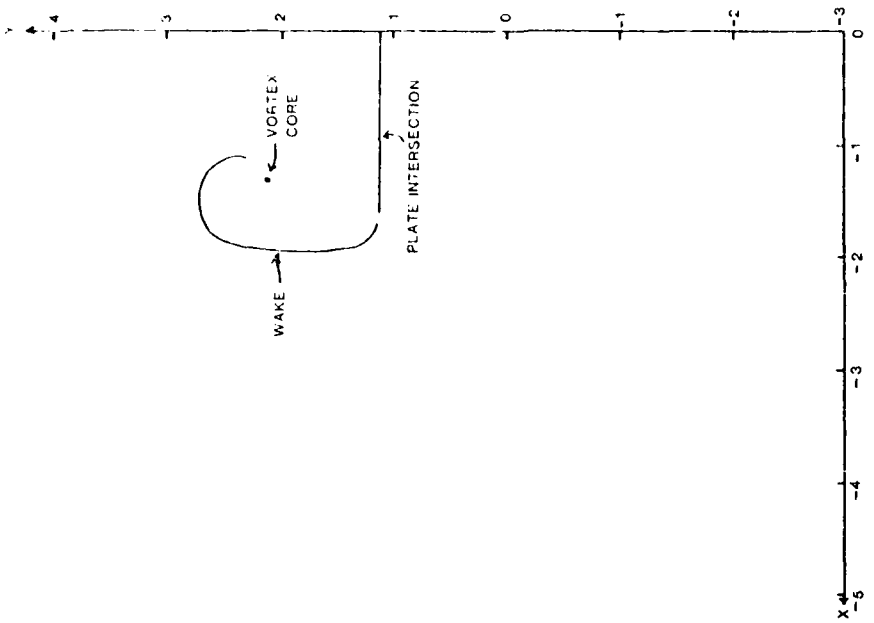

Figure 7. Bent Plate Wake Location, α = 10° and 2 Inches Upstream

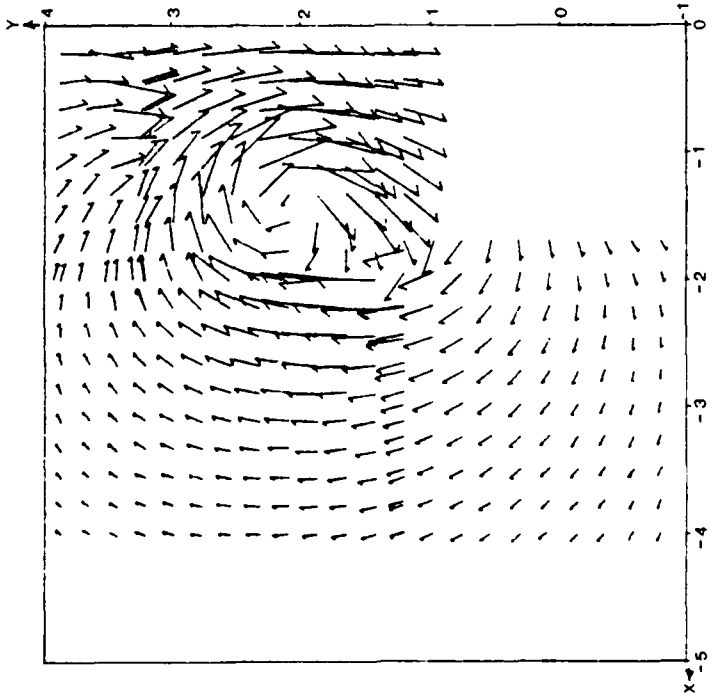

Figure 6. Bent Plate Cross Velocity Vector Plot, α = 10° and 2 Inches Upstream

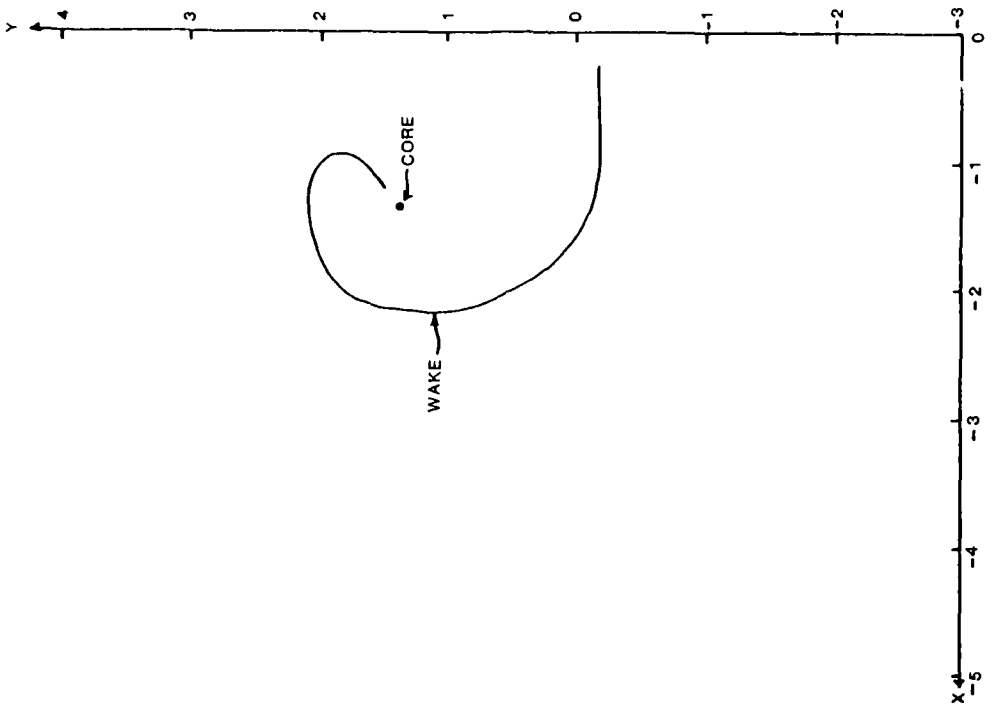

Figure 9. Bent Plate Wake Location, α = 10° and .2 Inches Downstream

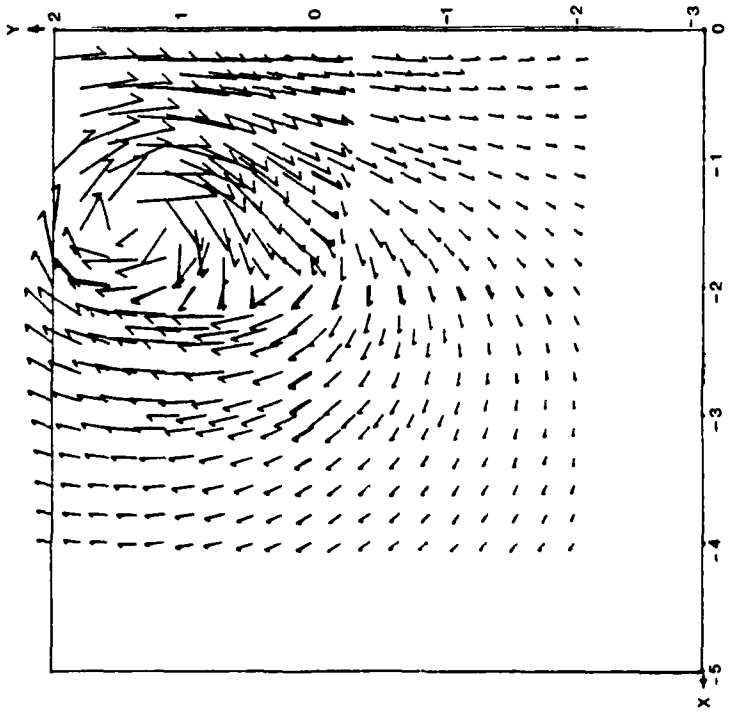

Figure 8. Bent Plate Cross Velocity Vector Plot, α = 10° and .2 Inches Downstream

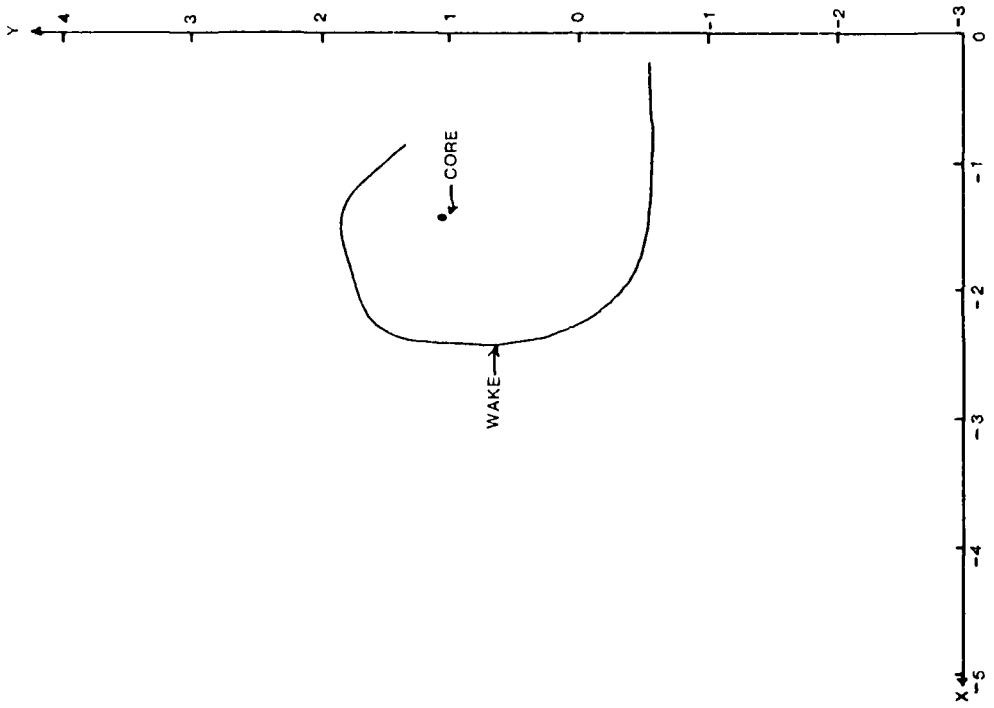

Figure 11. Bent Plate Wake Location, α = 10° and 2 Inches Downstream

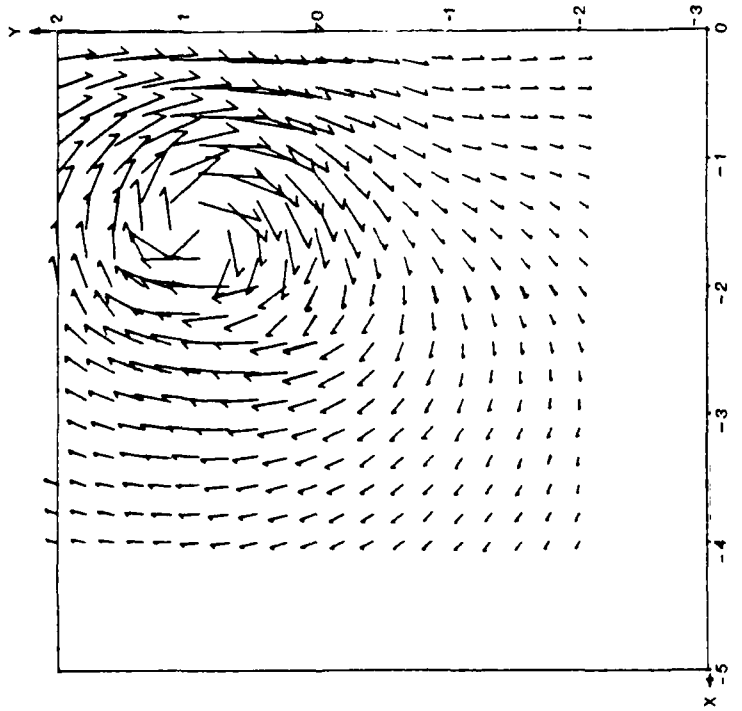

Figure 10. Bent Plate Cross Velocity Vector Plot, α = 10° and 2 Inches Downstream

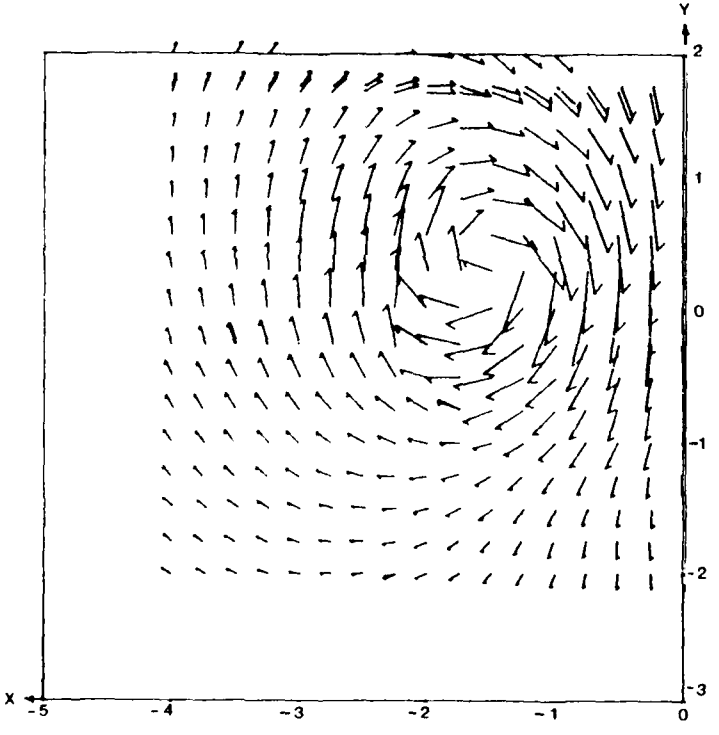

Figure 12. Bent Plate Cross Velocity Vector Plot, α = 10° and 4 Inches Downstream

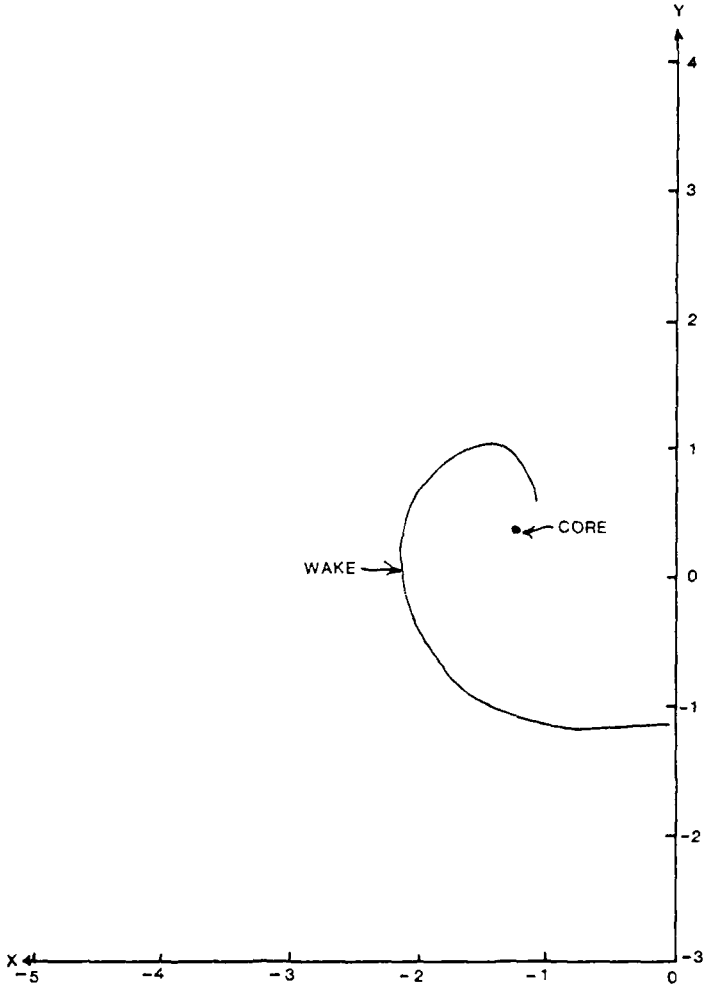

Figure 13. Bent Plate Wake Location, α = 10° and 4 Inches Downstream

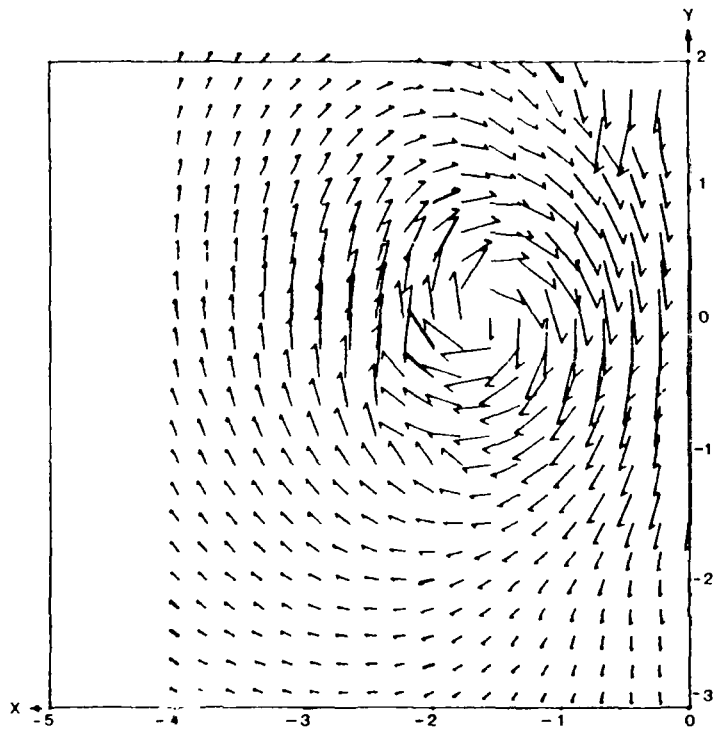

Figure 14. Bent Plate Cross Velocity Vector Plot, α = 10° and 6 Inches Downstream

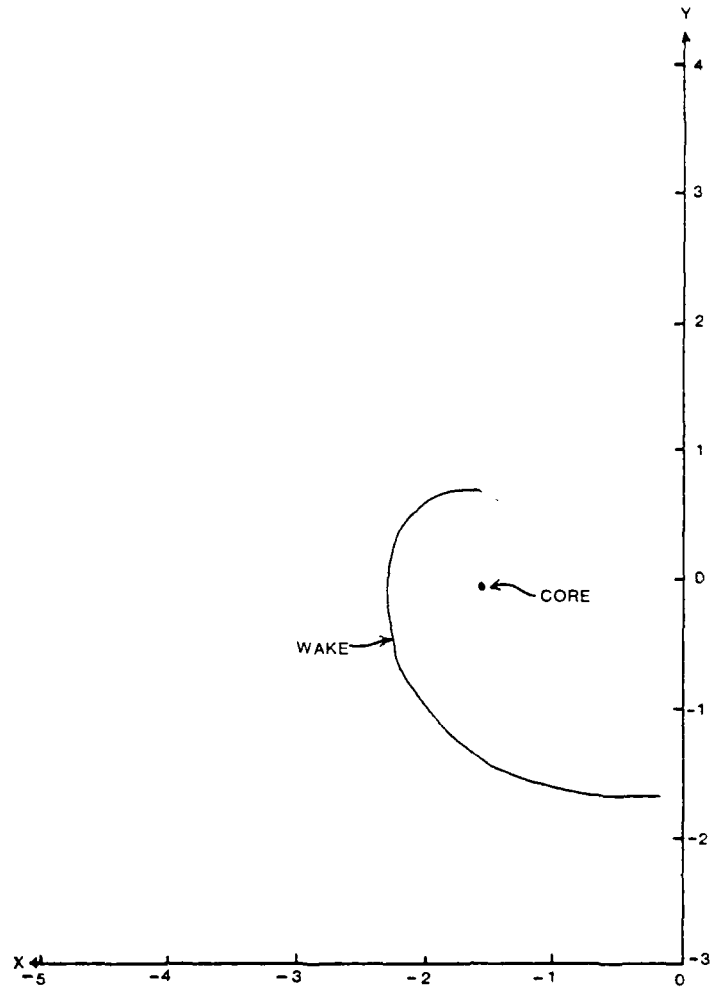

Figure 15. Bent Plate Wake Location, α = 10° and 6 Inches Downstream

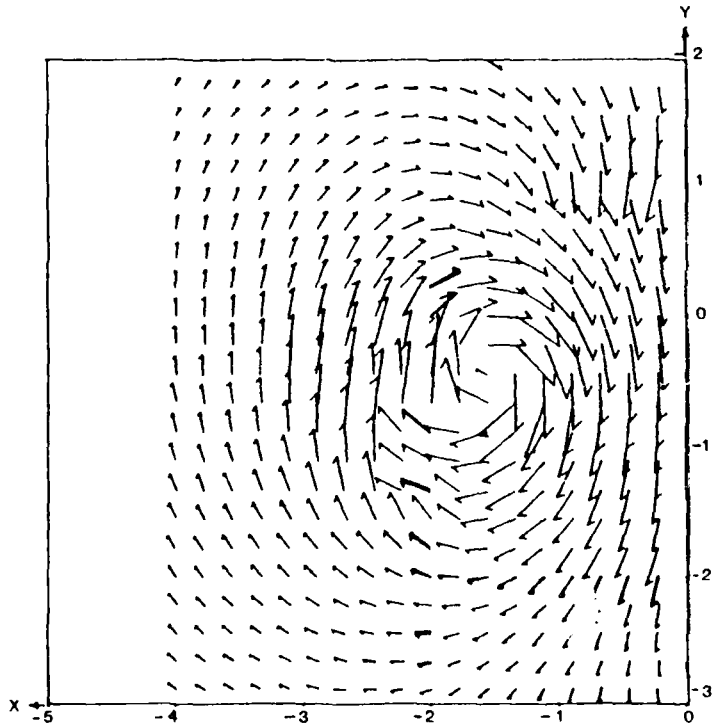

Figure 16. Bent Plate Cross Velocity Vector Plot, α = 10° and 9 Inches Downstream

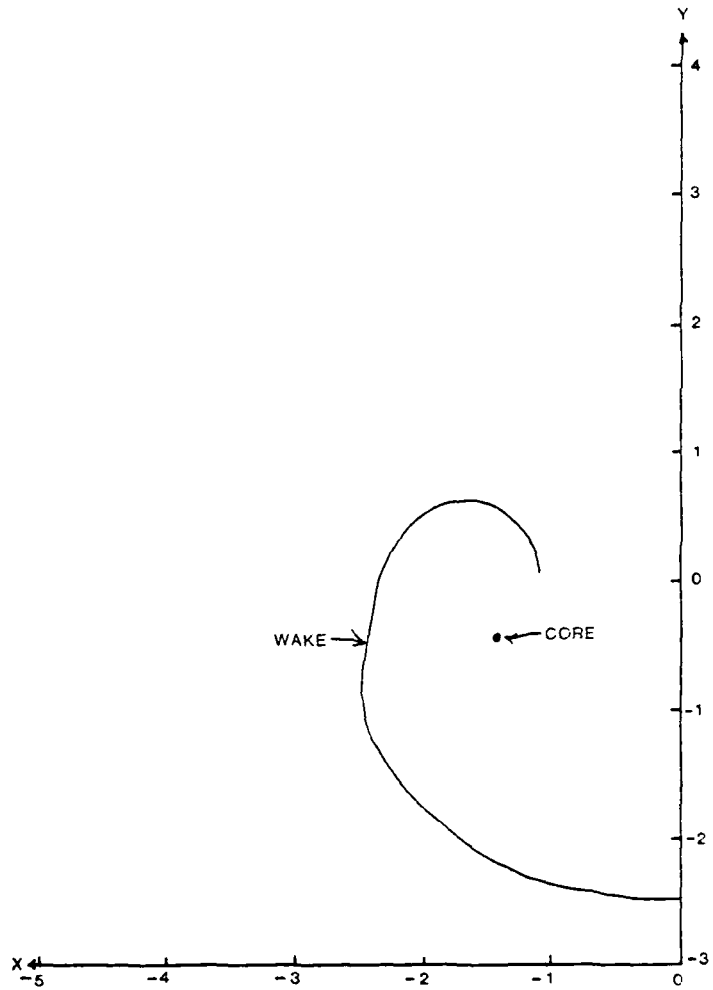

Figure 17. Bent Plate Wake Location, α = 10° and 9 Inches Downstream

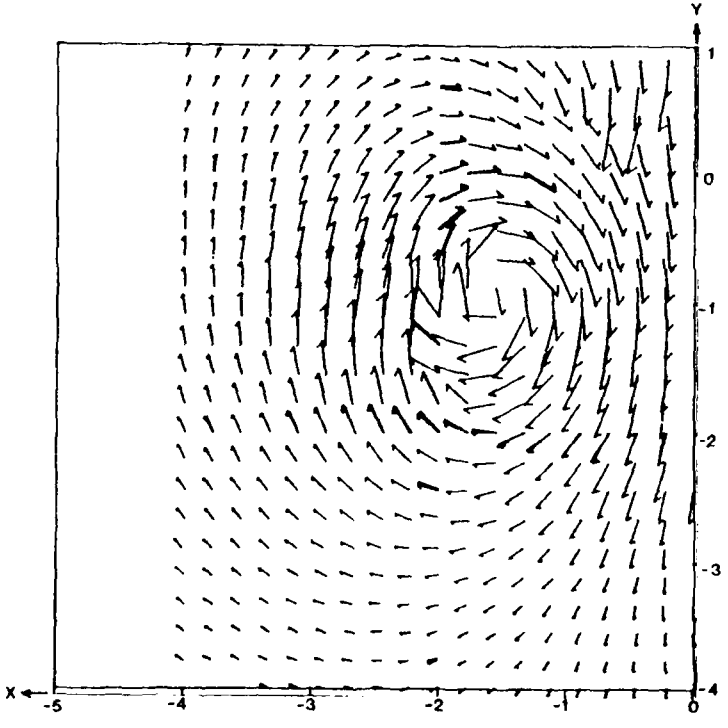

Figure 18. Bent Plate Cross Velocity Vector Plot, α = 10° and 12 Inches Downstream

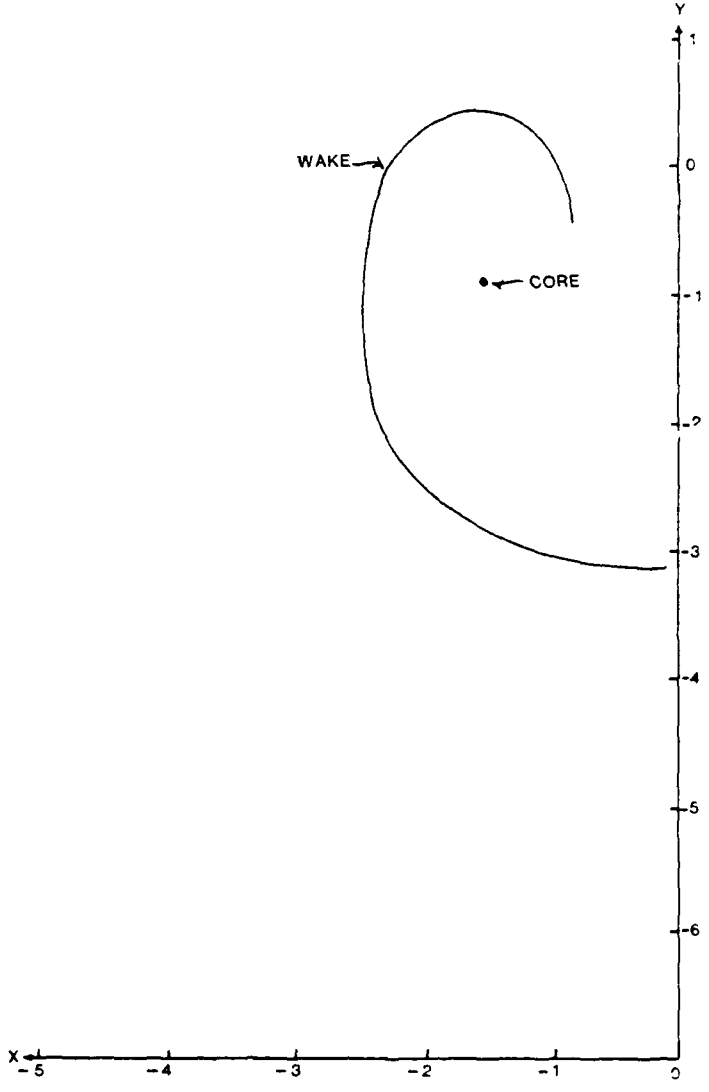

Figure 19. Bent Plate Wake Location, α = 10° and 12 Inches Downstream

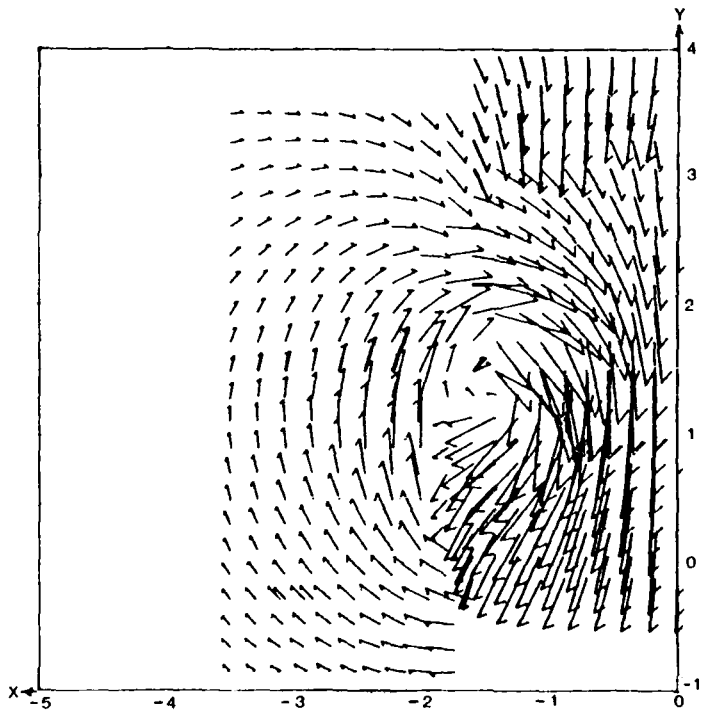

Figure 20. Bent Plate Cross Velocity Vector Plot, α = 20° and 2 Inches Upstream

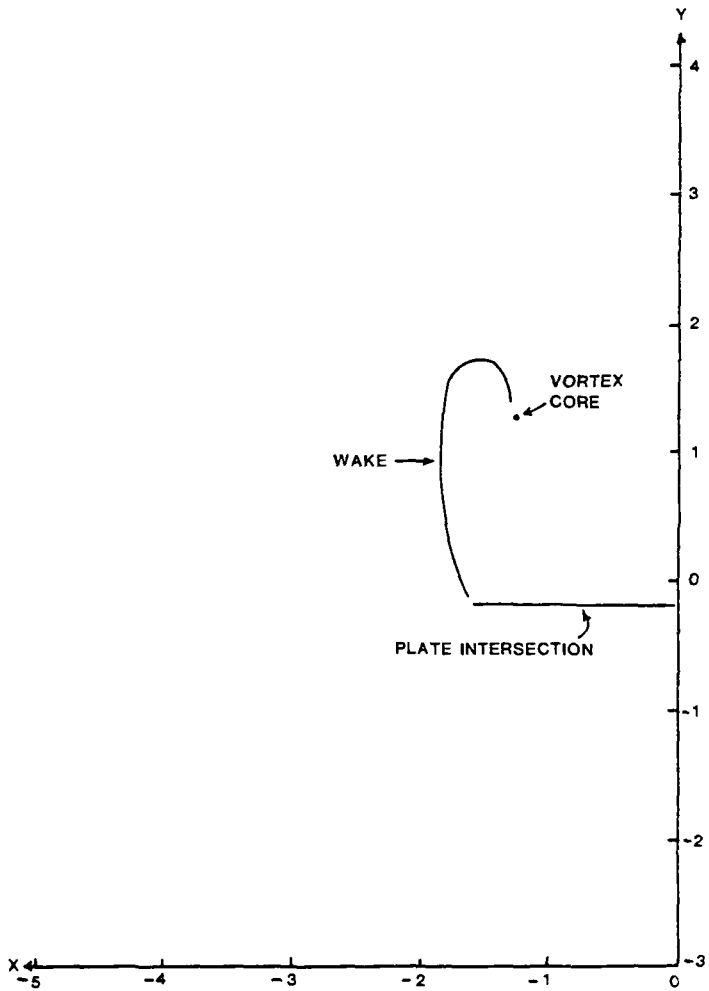

Figure 21. Bent Plate Wake Location, α = 20° and 2 Inches Upstream

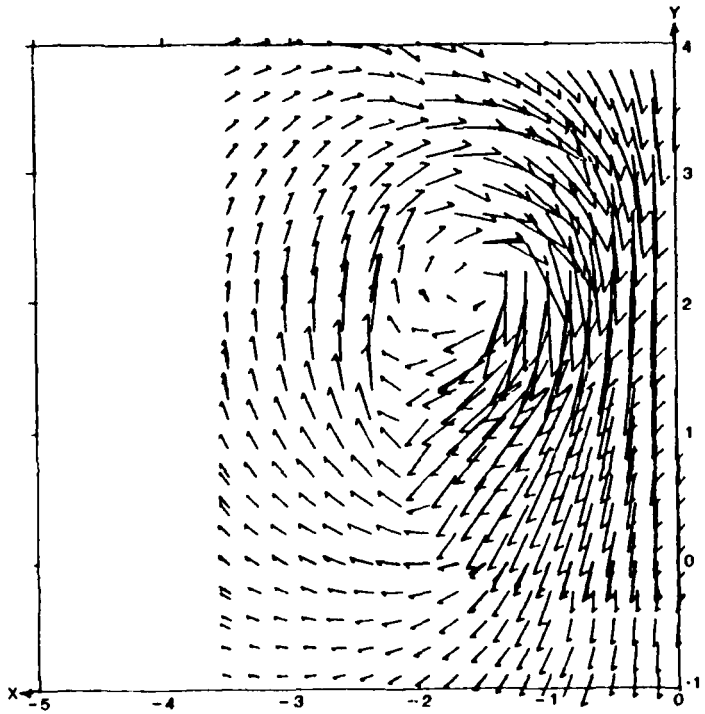

Figure 22. Bent Plate Cross Velocity Vector Plot, α = 20° and .2 Inches Downstream

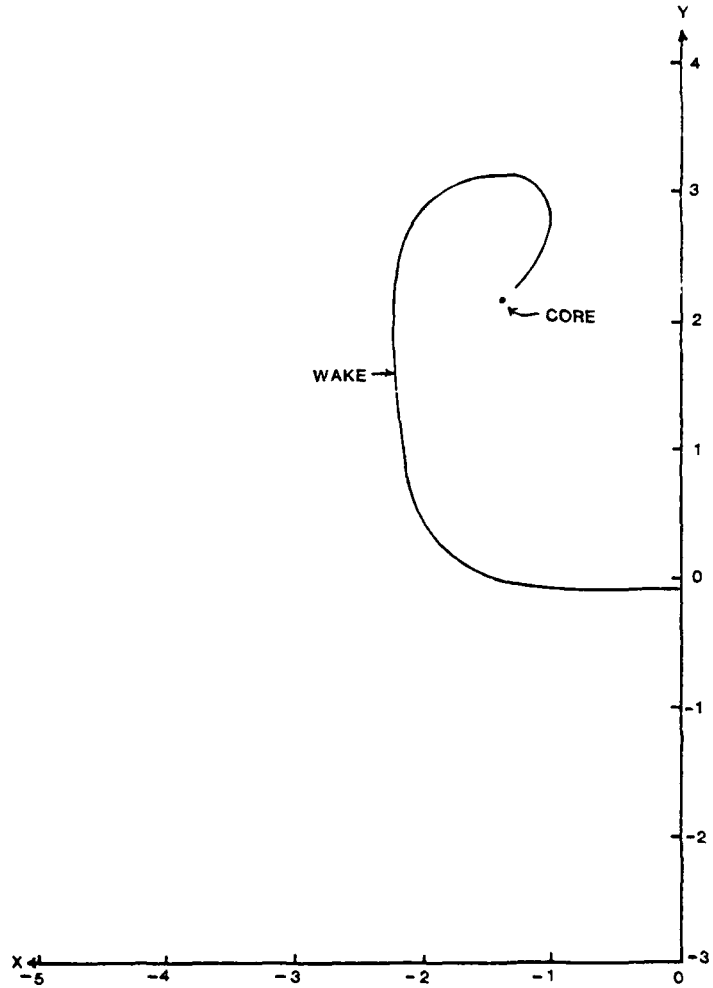

Figure 23. Bent Plate Wake Location, α = 20° and .2 Inches Downstream

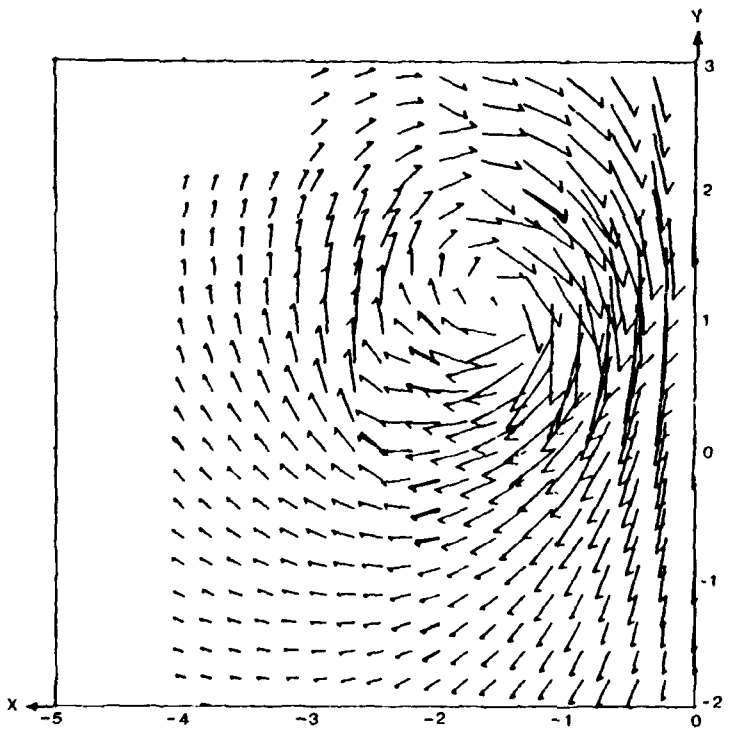

Figure 24. Bent Plate Cross Velocity Vector Plot, α = 20° and 2 Inches Downstream

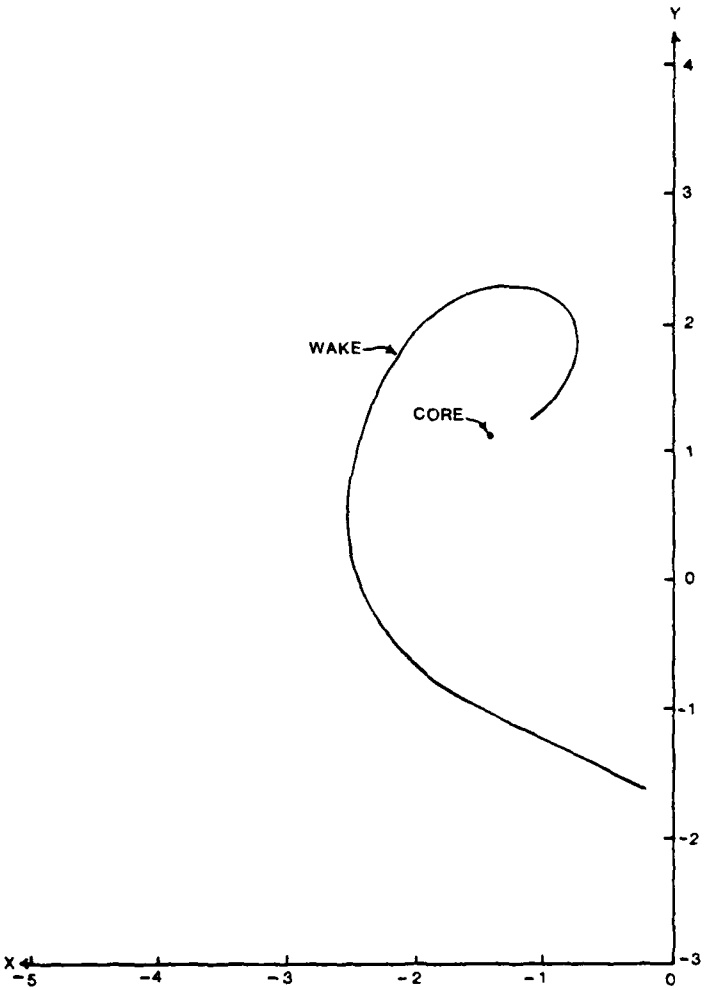

Figure 25. Bent Plate Wake Location, α = 20° and 2 Inches Downstream

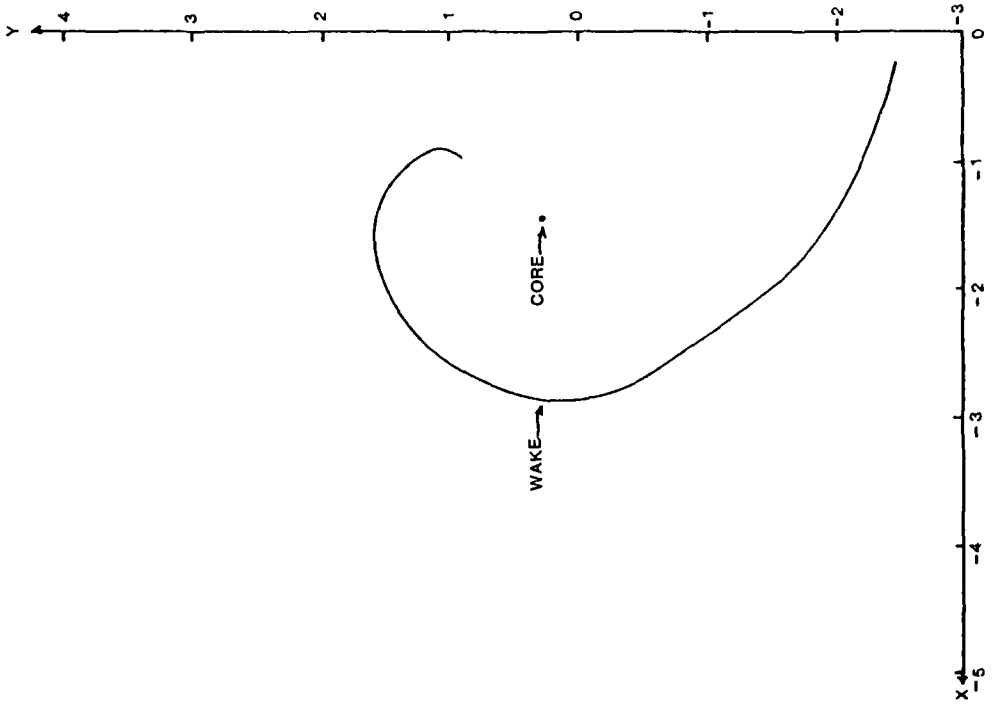

Figure 27. Bent Plate Wake Location, α = 20° and 4 Inches Downstream

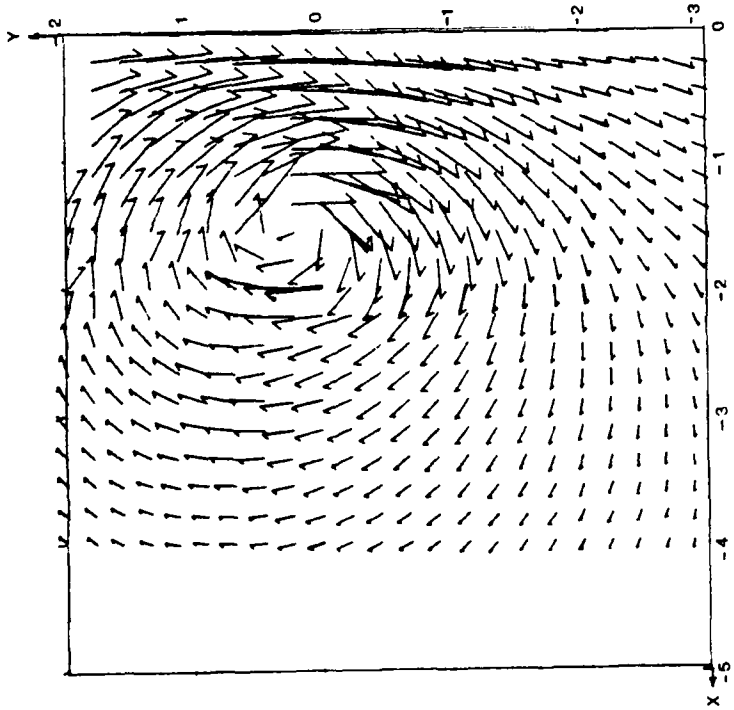

Figure 26. Bent Plate Cross Velocity Vector Plot, α = 20° and 4 Inches Downstream

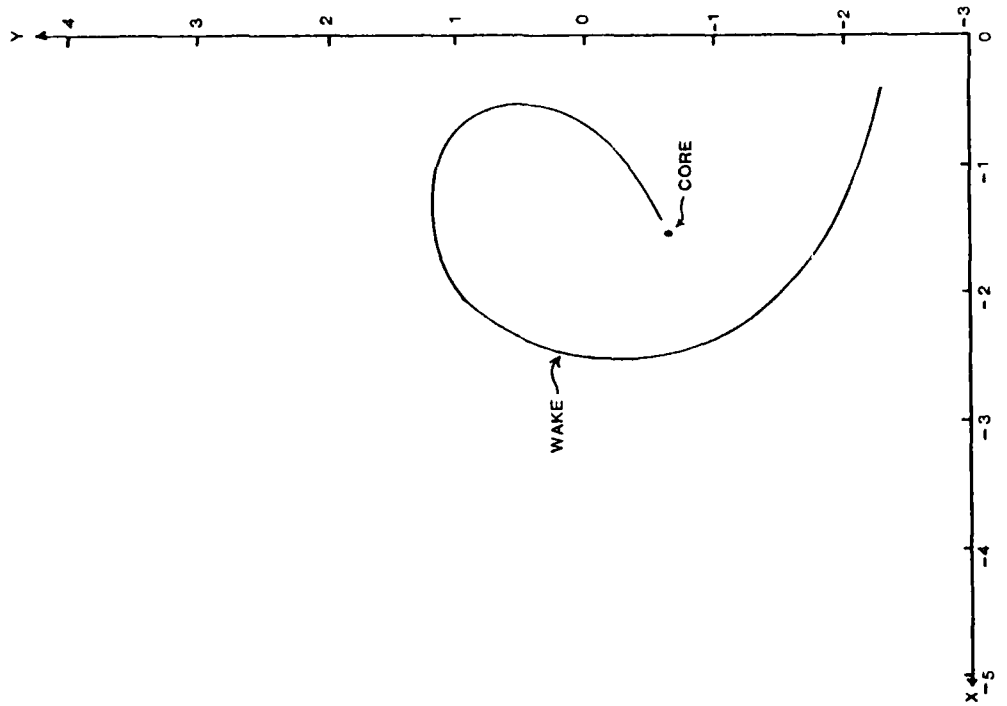

Figure 29. Bent Plate Wake Location, α = 20° and 6 Inches Downstream

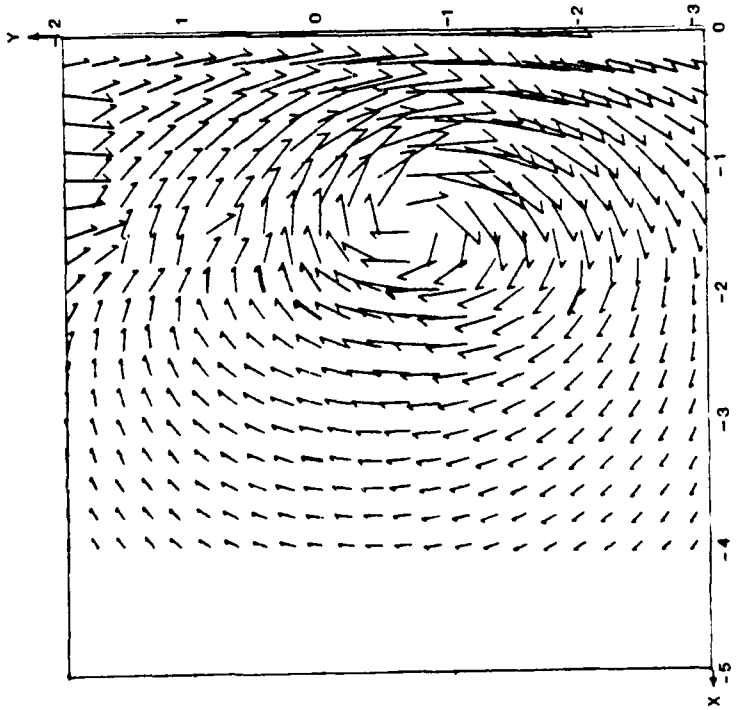

Figure 28. Bent Plate Cross Velocity Vector Plot, α = 20° and 6 Inches Downstream

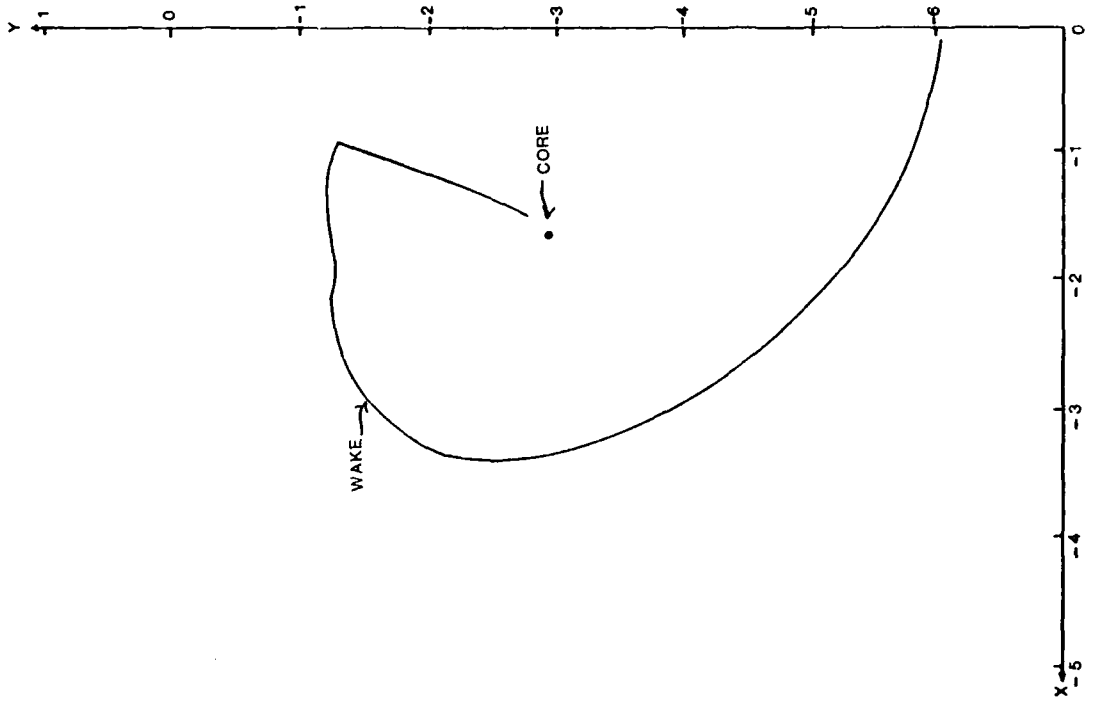

Figure 31. Bent Plate Wake Location, α = 20° and 11.5 Inches Downstream

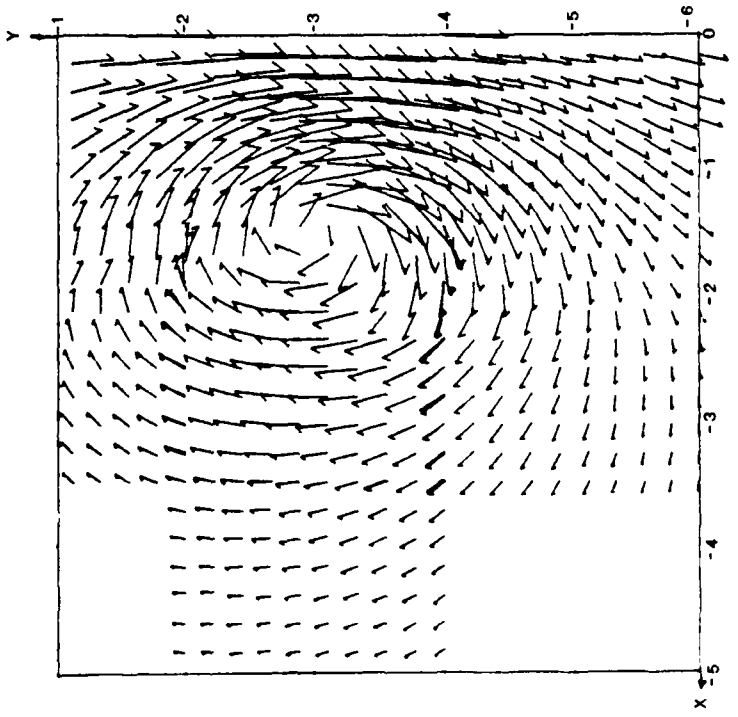

Figure 30. Bent Plate Cross Velocity Vector Plot, α = 20° and 11.5 Inches Downstream

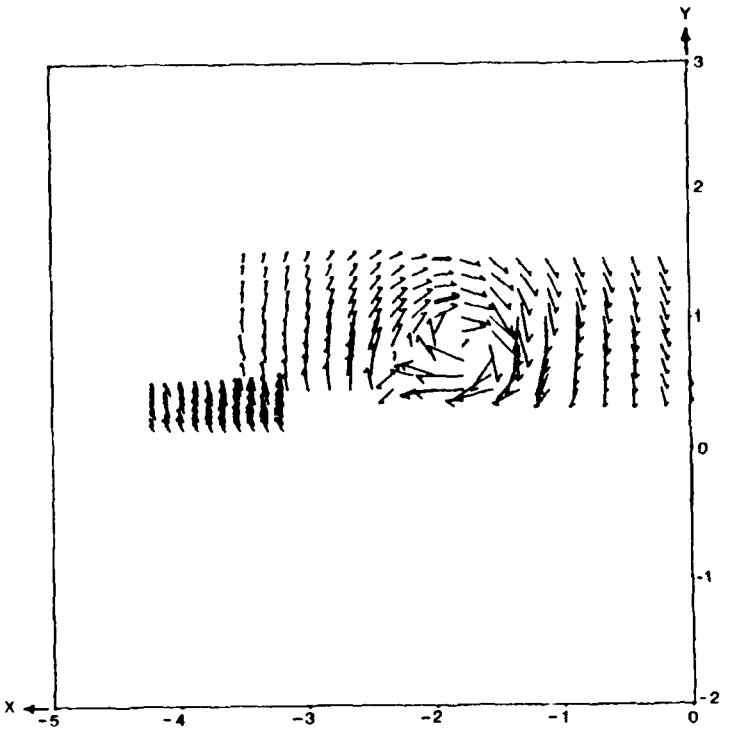

Figure 32. Delta Wing Cross Velocity Vector Plot, α = 10° and 2 Inches Upstream

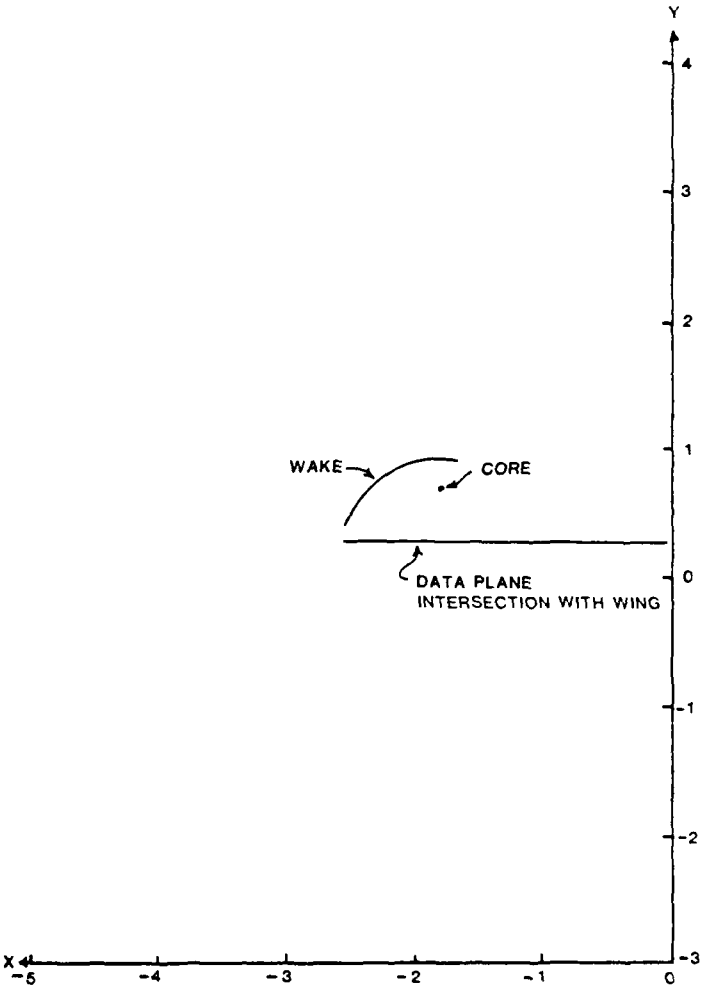

Figure 33. Delta Wing Wake Location, α = 10° and 2 Inches Upstream

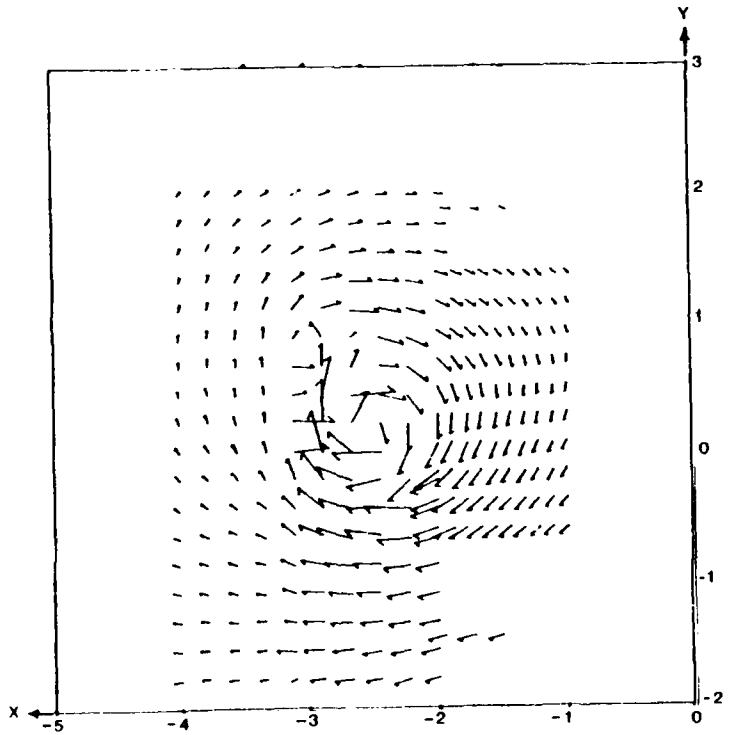

Figure 34. Delta Wing Cross Velocity Vector Plot, α = 10° and .2 Inches Downstream

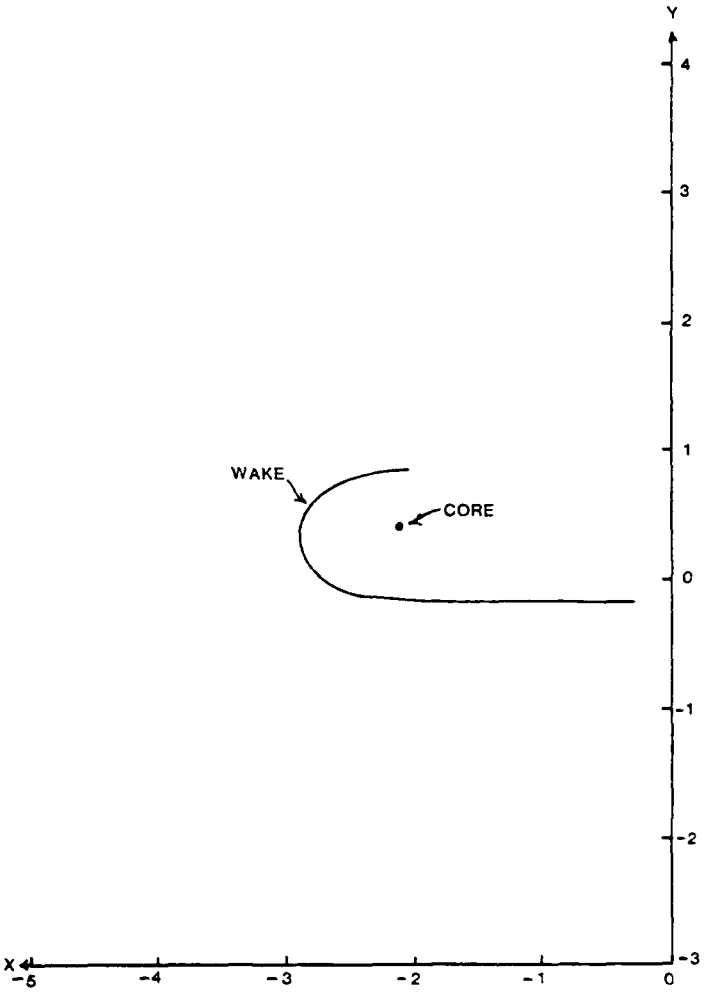

Figure 35. Delta Wing Wake Location, α = 10° and .2 Inches Downstream

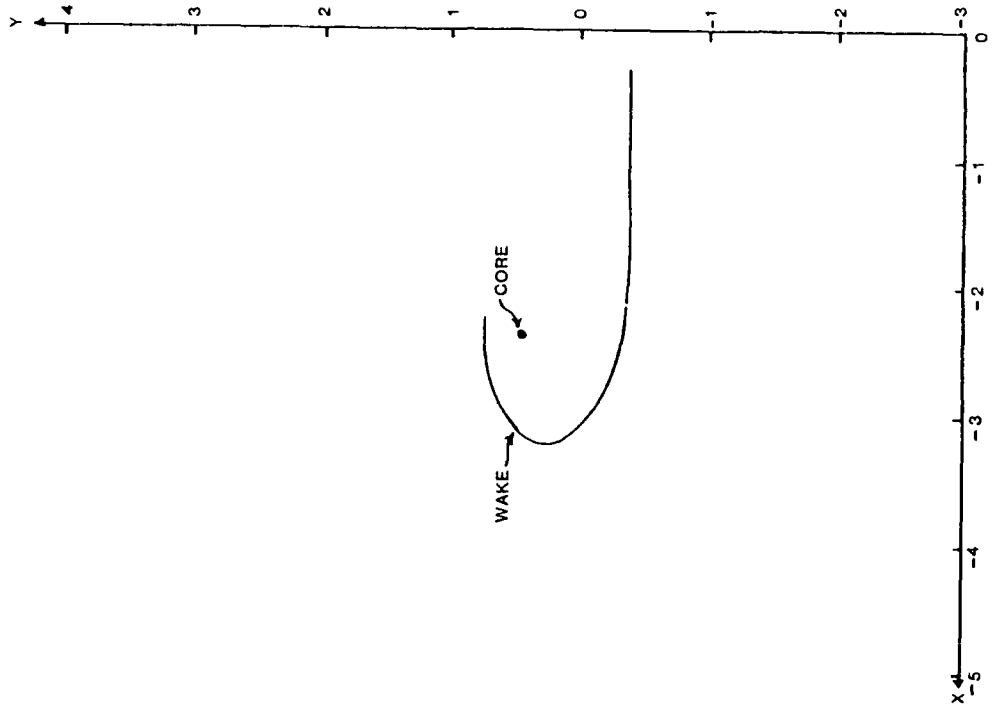

Figure 37. Delta Wing Wake Location
α = 10° and 2 Inches
Downstream

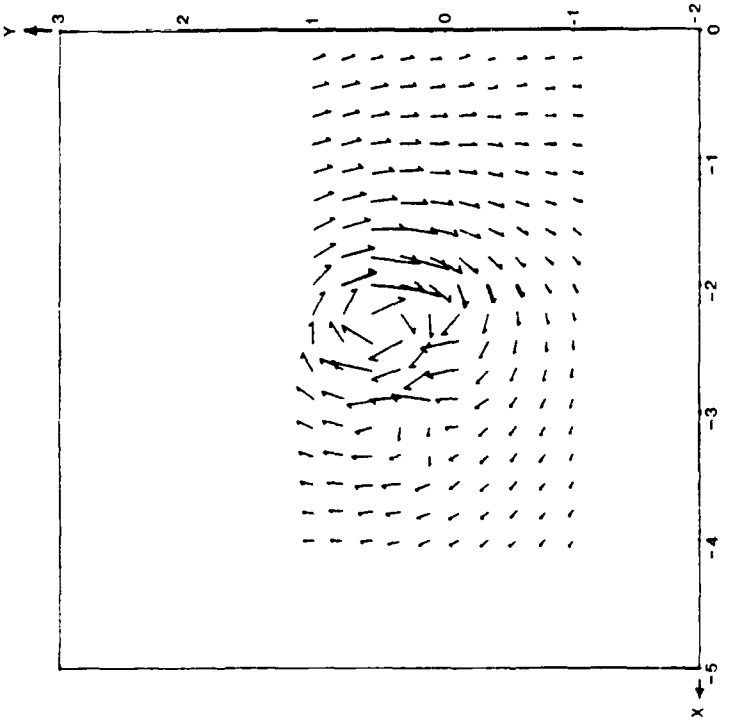

Figure 36. Delta Wing Cross Velocity
Vector Plot, α = 10° and
2 Inches Downstream

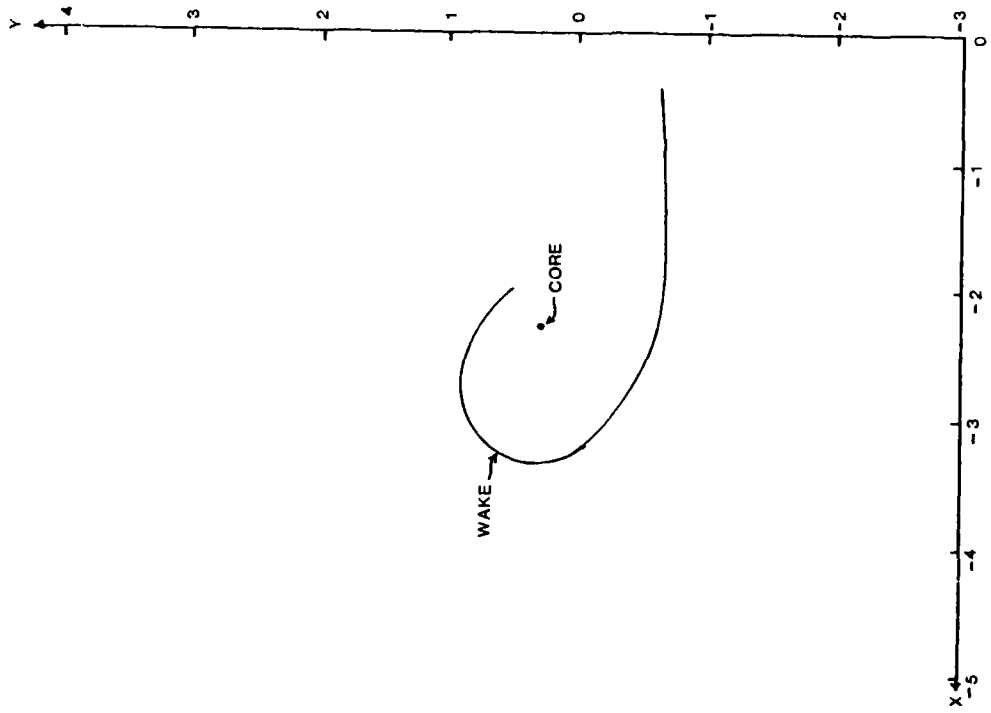

Figure 39. Delta Wing Wake Location α = 10° and 4 Inches Downstream

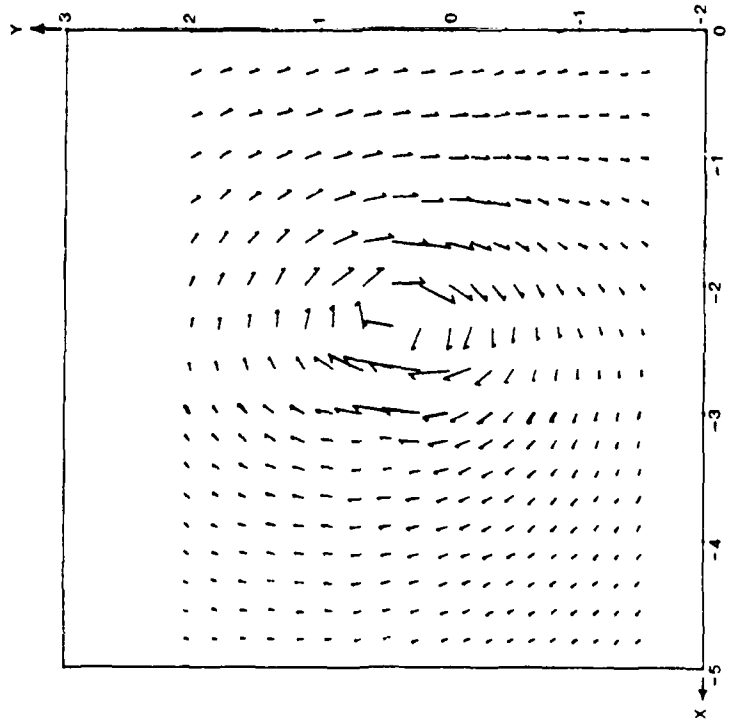

Figure 38. Delta Wing Cross Velocity Vector Plot, α = 10° and 4 Inches Downstream

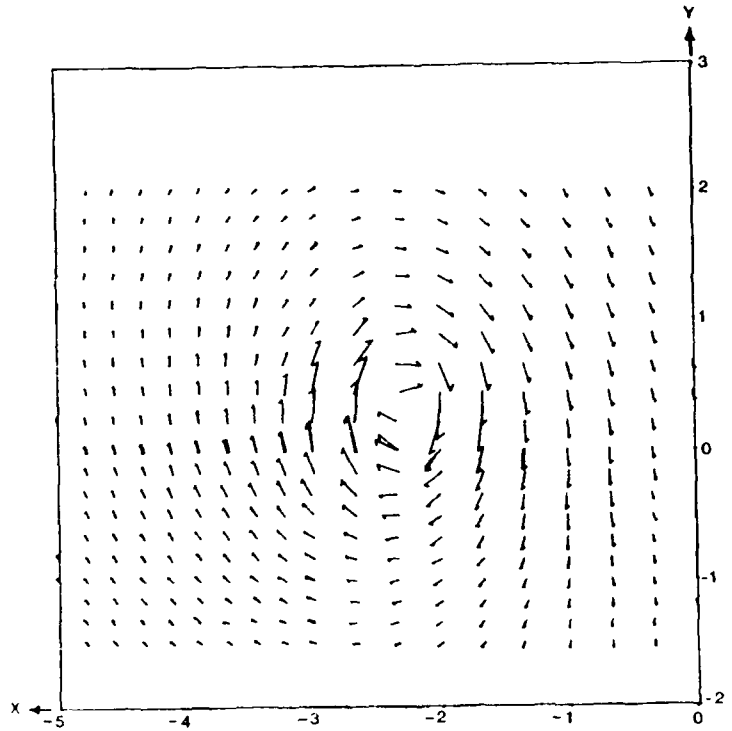

Figure 40. Delta Wing Cross Velocity Vector Plot, α = 10° and 6 Inches Downstream

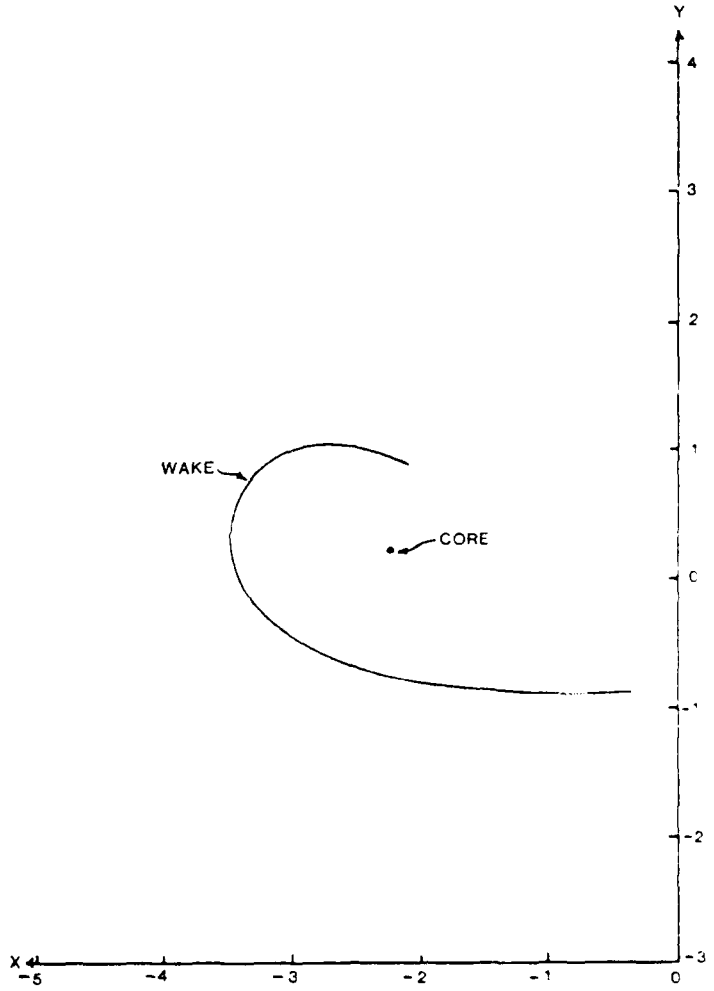

Figure 41. Delta Wing Wake Location α = 10° and 6 Inches Downstream

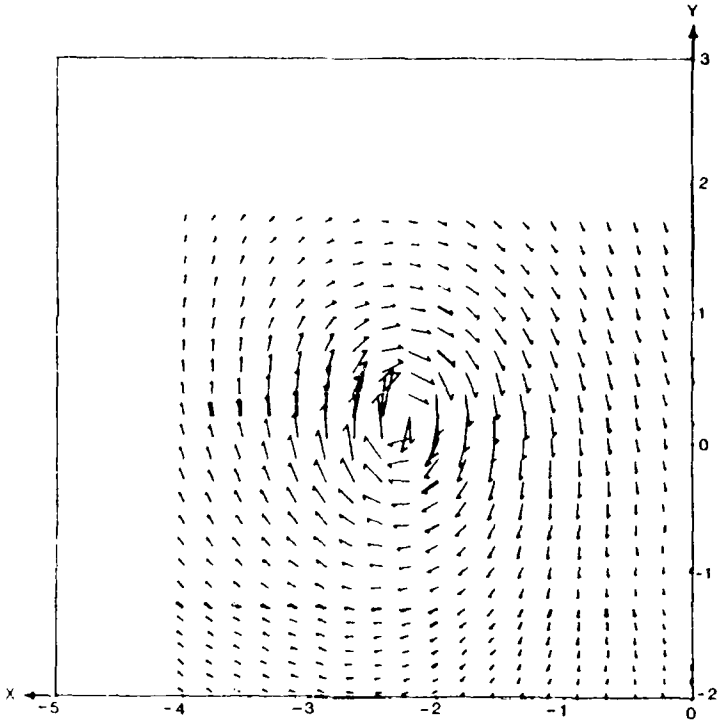

Figure 42. Delta Wing Cross Velocity Vector Plot, α = 10° and 9 Inche Downstream

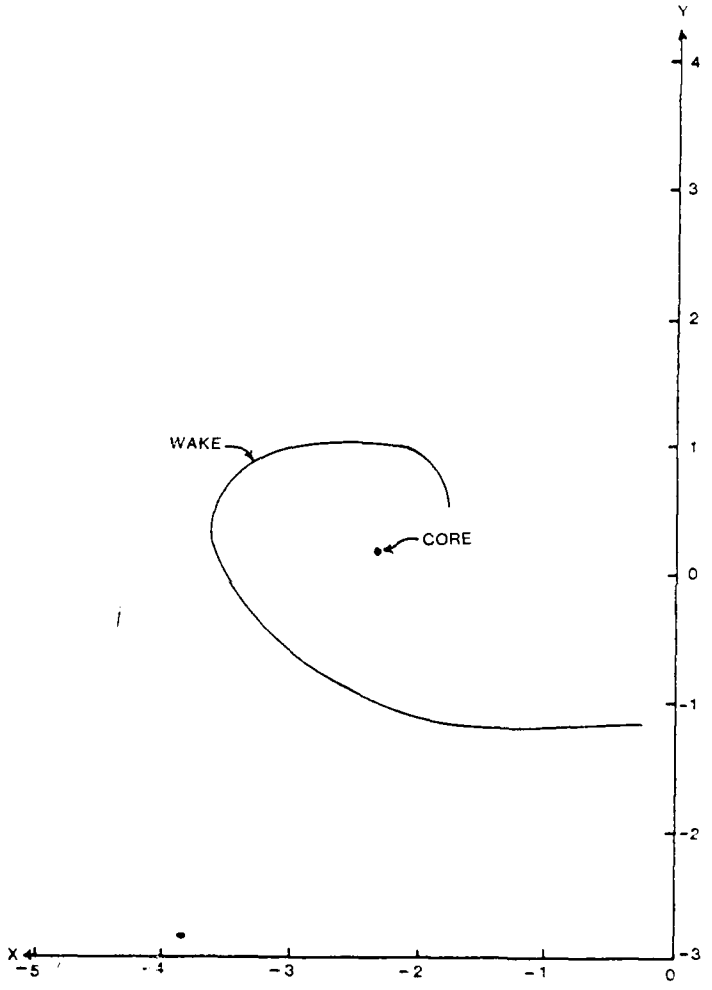

Figure 43. Delta Wing Wake Location α = 10° and 9 Inches Downstream

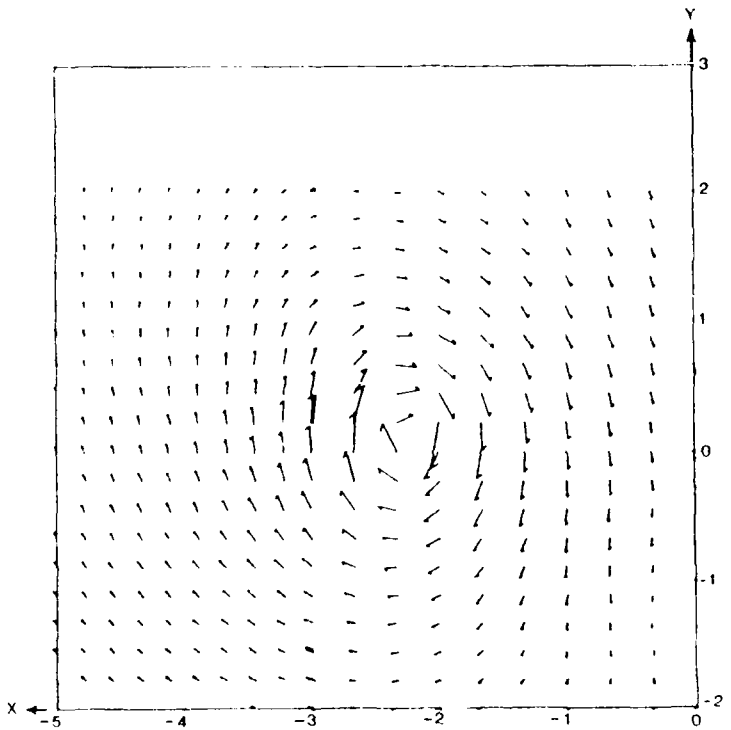

Figure 44. Delta Wing Cross Velocity Vector Plot, $\alpha = 10°$ and 12 Inches Downstream

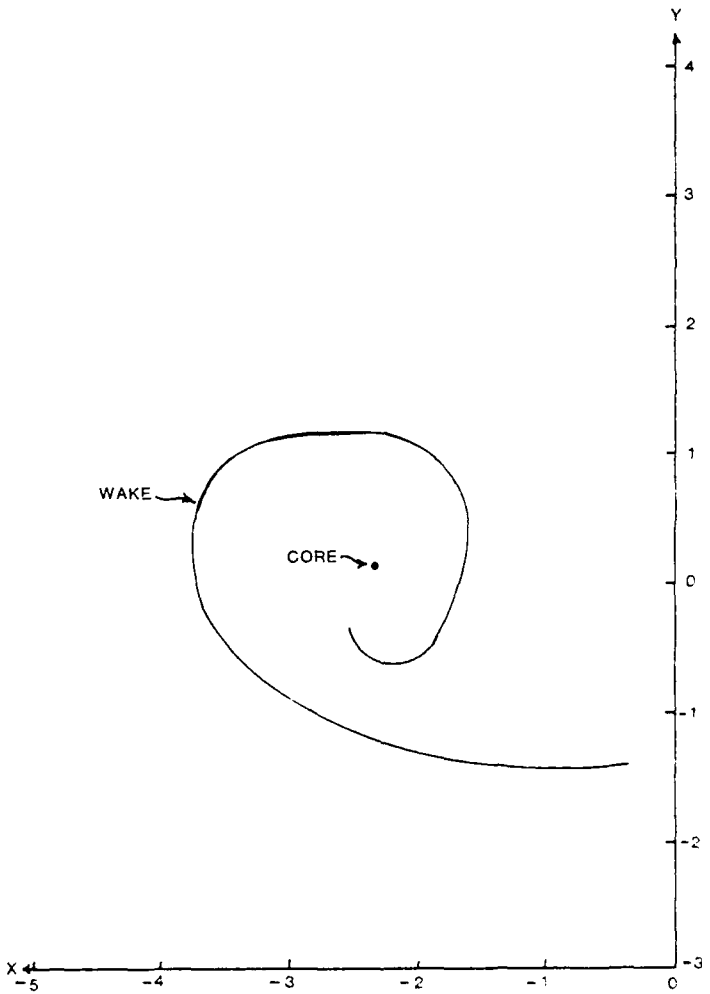

Figure 45. Delta Wing Wake Location $\alpha = 10°$ and 12 Inches Downstream

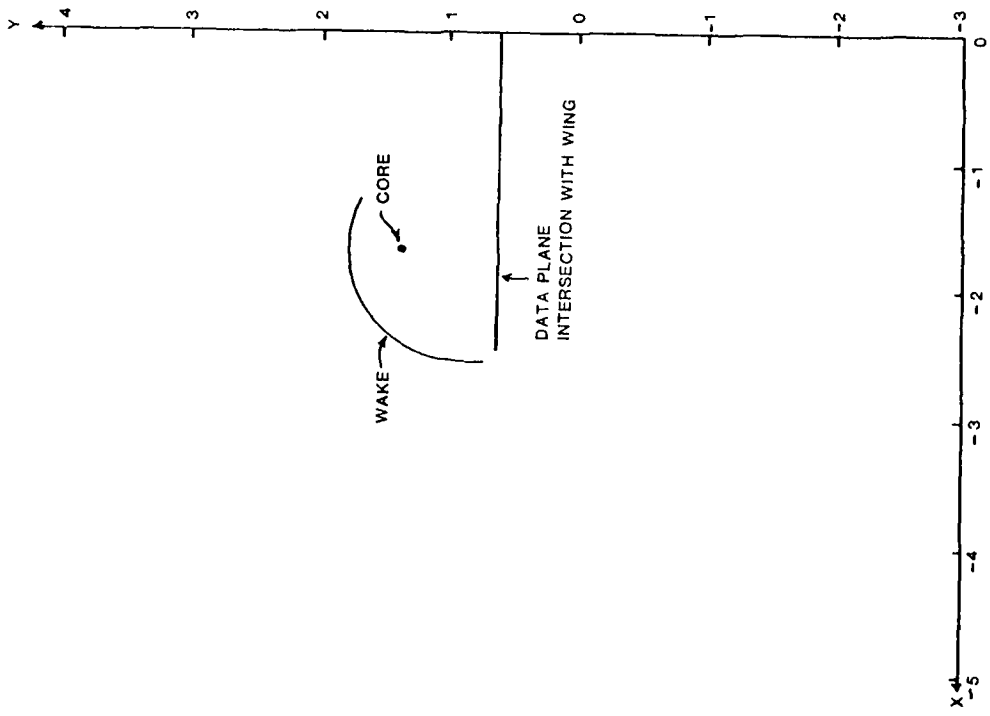

Figure 47. Delta Wing Wake Location
α = 20° and 2 Inches Upstream

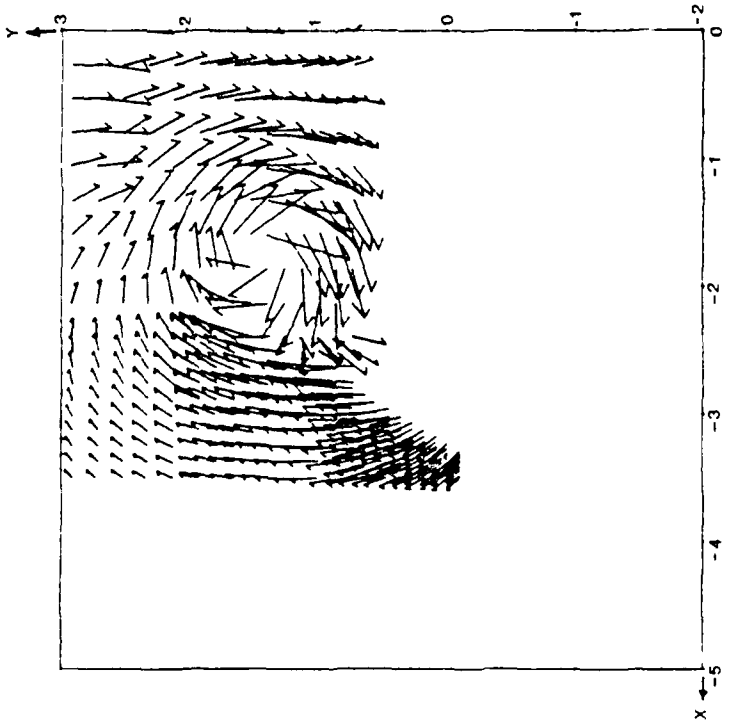

Figure 46. Delta Wing Cross Velocity
Vector Plot, α = 20° and
2 Inches Upstream

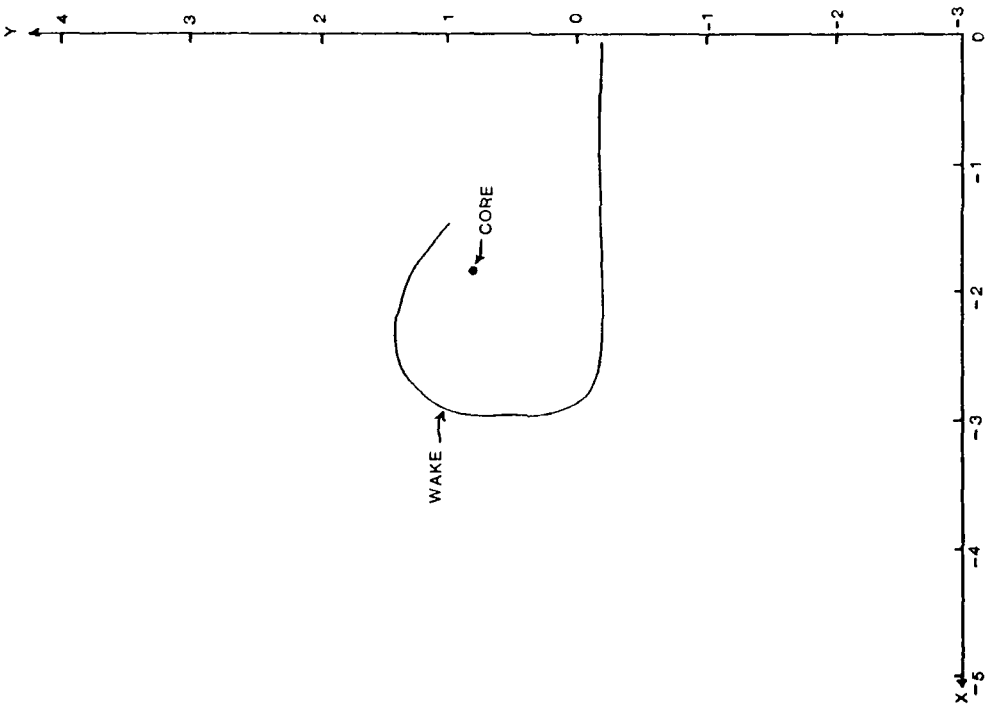

Figure 49. Delta Wing Wake Location
α = 20° and .2 Inches
Downstream

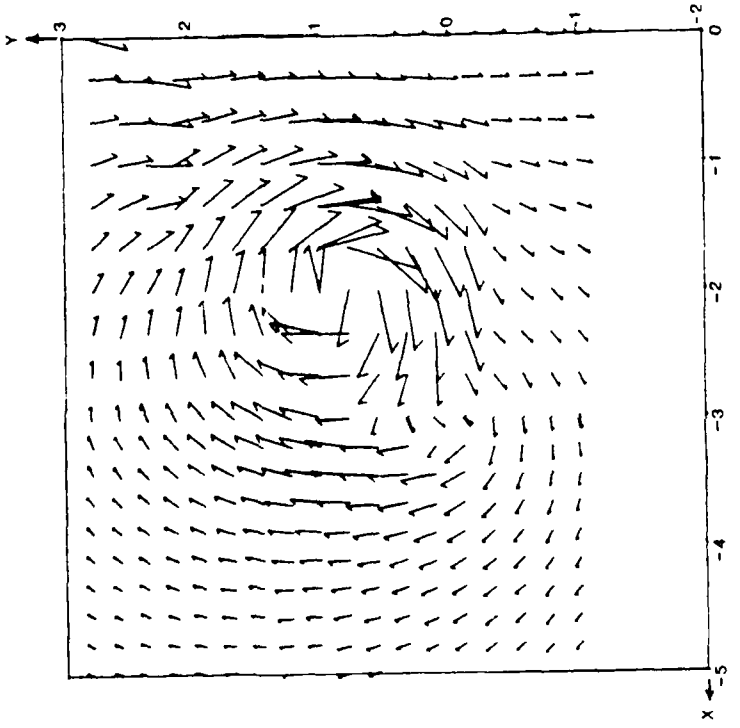

Figure 48. Delta Wing Cross Velocity
Vector Plot, α = 20° and
.2 Inches Downstream

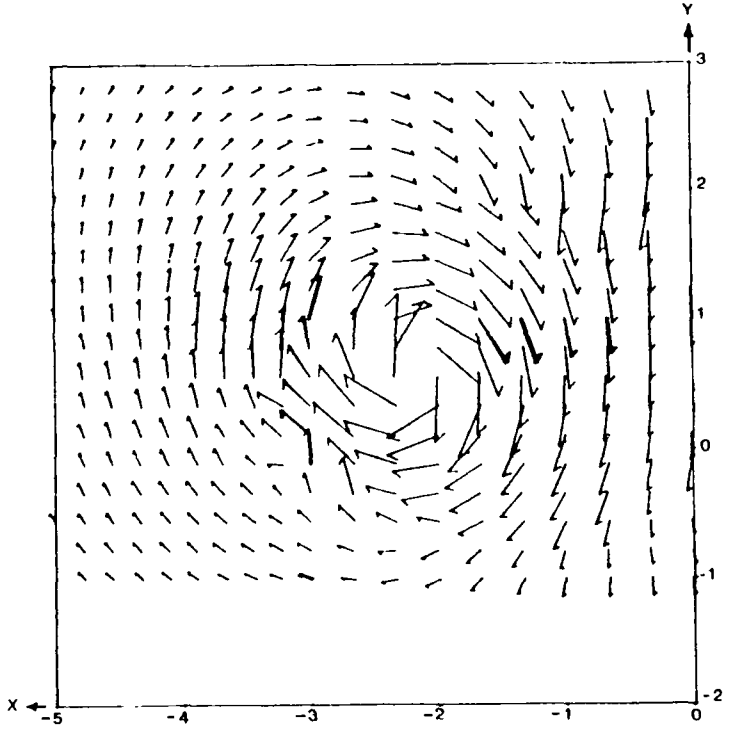

Figure 50. Delta Wing Cross Velocity Vector Plot, α = 20° and 2 Inches Downstream

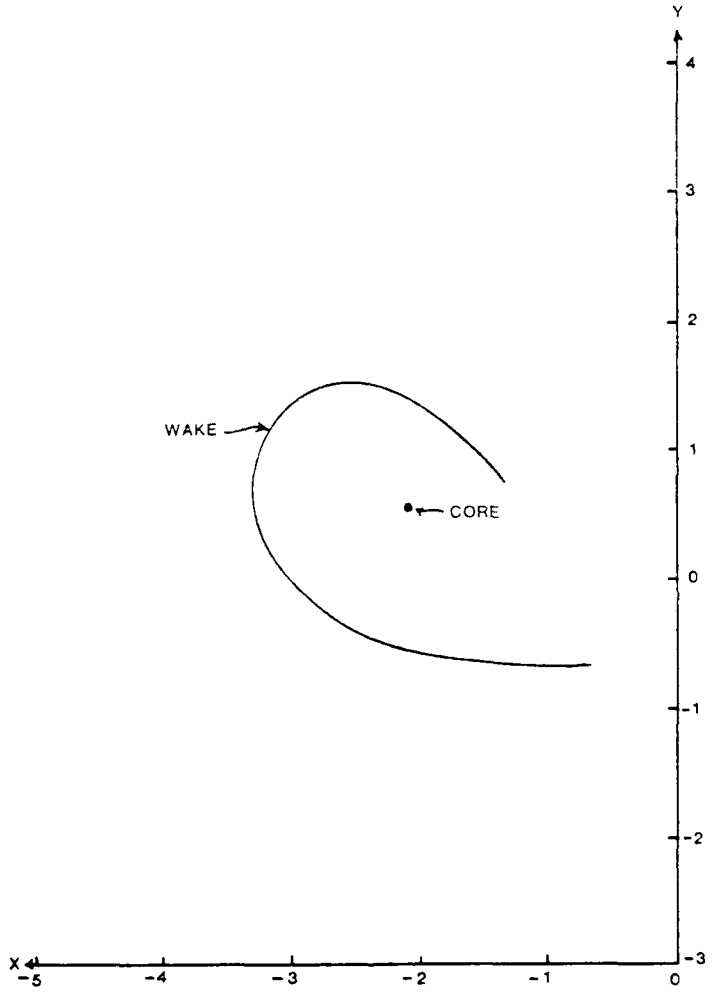

Figure 51. Delta Wing Wake Location α = 20° and 2 Inches Downstream

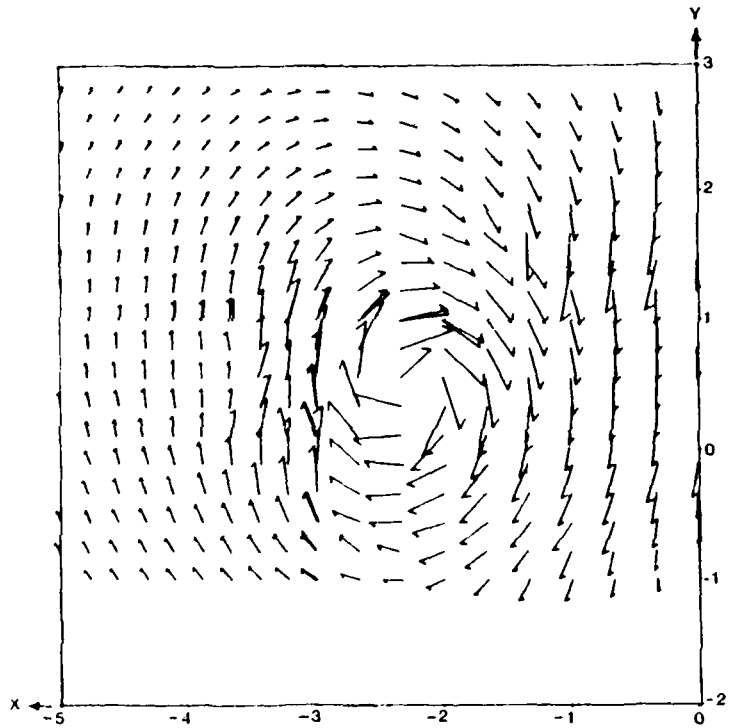

Figure 52. Delta Wing Cross Velocity Vector Plot, α = 20° and 4 Inches Downstream

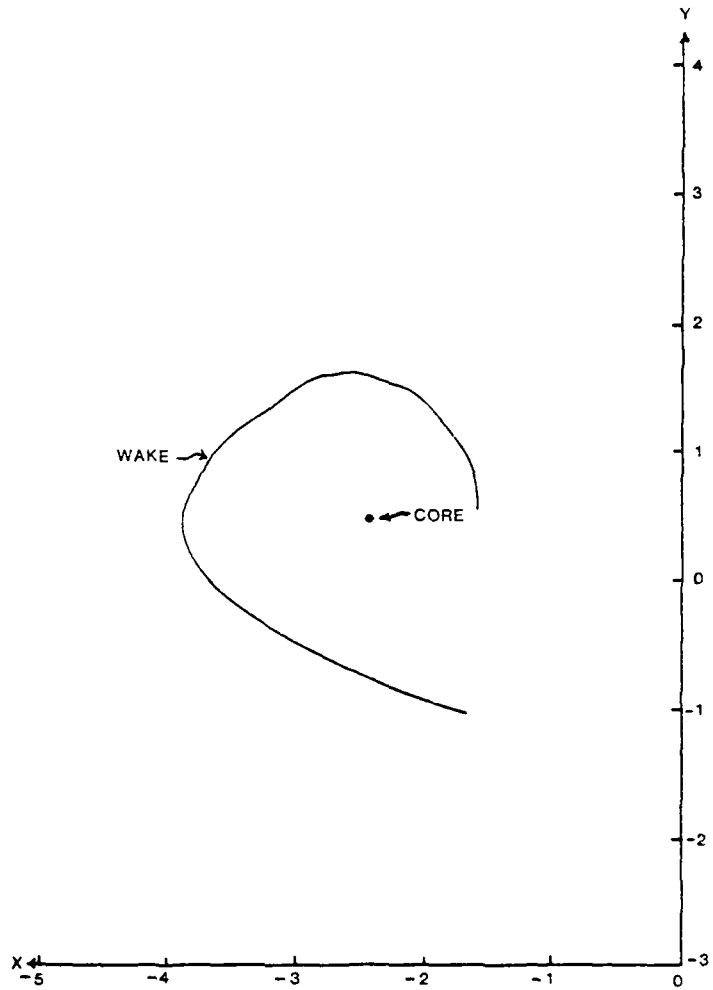

Figure 53. Delta Wing Wake Location α = 20° and 4 Inches Downstream

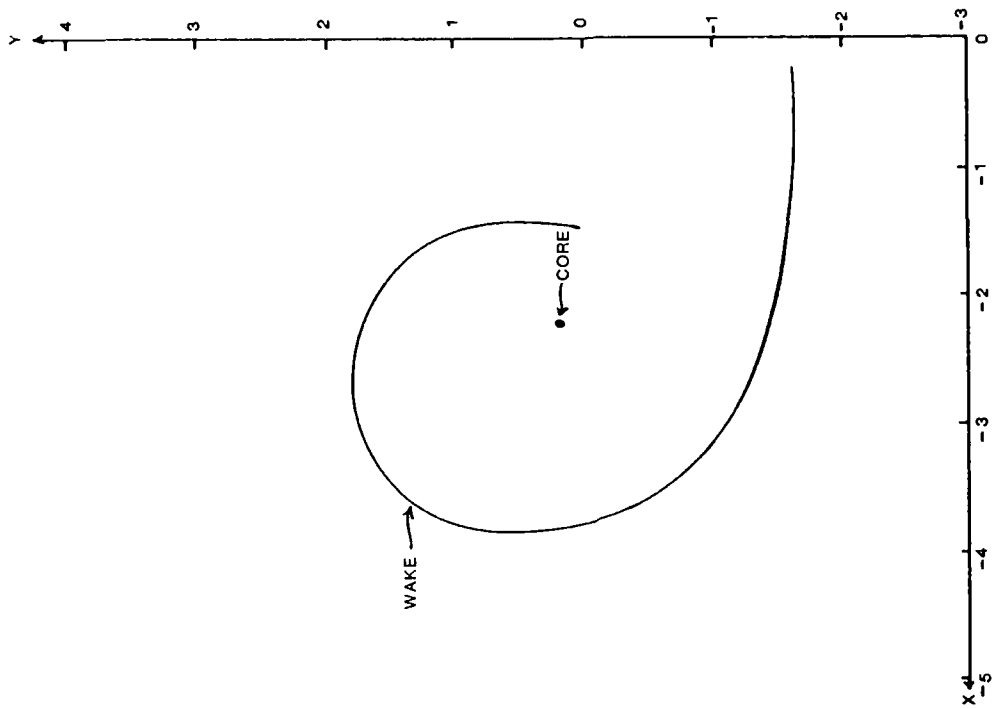

Figure 55. Delta Wing Wake Location
α = 20° and 6 Inches
Downstream

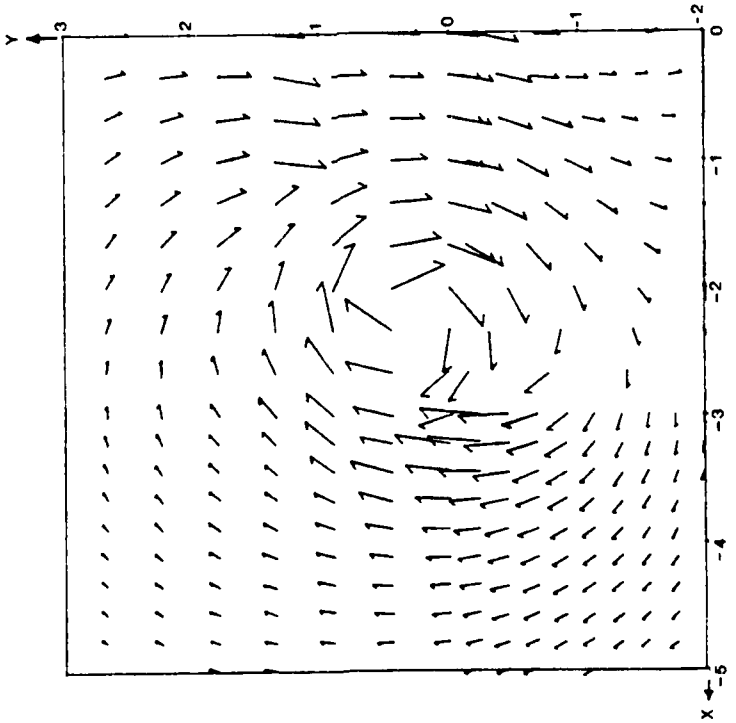

Figure 54. Delta Wing Cross Velocity
Vector Plot, α = 20° and
6 Inches Downstream

V. Conclusions

The low aspect-ratio delta wing demonstrates wing wake sensitivities to leading-edge sweep. The leading-edge sweep of the planform significantly affects both the way the wake becomes wrapped around the lifting-surface, tip-vortex system and the movement of the vortex system downstream. With large leading-edge sweep, the wake bulges in a more spanwise fashion. Also, the tip vortex moves spanwise due to sweep effects but tends to go to approximately the same downstream location relative to the delta wing trailing edge provided the angle of attack is not too large.

The bent-plate configuration addresses camber effects on wake characteristics using the 20-degree bend at midchord. The secondary vortex system caused by the discontinuity in slope at the midchord of the bent plate could not be discerned in the pressure data. This is due to the turbulence of the interior vortex flow field. The wake strength tended to determine the downstream vortex core location within the downstream range available in this test. Very little outward drift of the vortex core was noted regardless of plate angle of attack.

The actual pressure and velocity values for each data point in these test cases (recorded on magnetic tape) can be obtained by contacting the Director of the Aeronautics Laboratory, Department of Aeronautics, USAF Academy.

References

1. Wickens, R.H., "The Vortex Wake and Aerodynamic Load Distribution of Slender Rectangular Wings," Canadian Aeronautics and Space Journal, June 1967.

2. Clark, D.R., J.K. Wathman, and F.A. Dvorak, "Forward Swept Wing Configuration Evaluation and Validations of Analytic Methods,"

AFWAL-TR-82-3033, July 1982.

3. Crandall, R. and G. Sisson, "Canard Wake Measurement and Description," Aeronautics Digest, USAFA-TR-81-4, USAF Academy, May 1981.

4. Gerner, A. and G. Sisson, "Seven-Hole Probe Data Acquisition System," USAFA-TN-81-8, November 1981.

5. Griffin, K.E., "Measurement of Wake Interactions of a Canard and a Forward Swept Wing," USAFA-TN-82-4, July 1982.

SECTION II

Aeronautical History

THE EARLY DAYS OF AERONAUTICS

Sir Geoffrey I. Taylor

Editor's Note

The following article has been reprinted from the Journal of the Royal Aeronautical Society Volume 70, Number 661, January 1966, with the permission of the Royal Aeronautical Society. The author, Sir G. I. Taylor, was a prolific researcher who, in his 60 plus years as a scientist and academician, published more than 200 papers on a variety of subjects including aerodynamics, hydrodynamics, meteorology, and mechanics of solids. His career spanned the development of aeronautics from the first days of heavier-than-air aircraft to the days of manned spaceflight. His expertise and breadth of experience combine to make his recollections of the early days of aeronautics a very interesting piece of reading. Most of Taylor's published works have been collected in the four-volume set The Scientific Papers of G. I. Taylor, edited by G. K. Batchelor and published by the Cambridge University Press between 1958 and 1971. Anyone looking through these volumes can only marvel at the quality and quantity of research produced by this remarkable man.

It is always rather risky to ask old people to talk about what things were like when they were young. Having turned on the tap you may not see how to turn it off again. Fortunately there is a circumstance which keeps this trouble under control. Old people remember a lot of things when there is no call for them to do so but seldom when there is. That is the reason why I have written down most of what I can say for this lecture.

I cannot attempt to give a complete or an objective picture of aeronautical science when I started thinking about it. The best I can do is to describe a few of the things which happened to me in those days to try to convey some pictures of our primitive ideas.

My earliest aerodynamic experiences were all connected with sails. I built a boat in our home in St John's Wood while I was at school. It was before the days when woodworking firms would supply ready-made kits so I had to do all the design and construction work myself. Fig. 1 was taken while the sails my mother had made were being fitted. Those of you who know about boats will see it is old fashioned, but it was quite fast. After building the hull in my bedroom on the second floor we had

to get it through the window. It was a sash window which could be taken out. We turned the boat on its side because it was wider than the window frame. We put slings round it and attached them to a rope which we slung over a borrowed builder's pulley at the end of a joist projecting from my parents' bedroom on the top floor. After making the lower end of the rope fast to the garden roller we got the boat out of the window and left it hanging while we went down into the garden. We then detached the rope from the garden roller and my brother, my cousin, and I started to let it out. As we were doing this the boat above our heads slipped slightly in the slings. My brother let go to run upstairs to refix it and we then discovered that the boat was a little heavier than my cousin and me. Fortunately we both held on, no further slipping occurred and my brother caught us almost before we had left the ground. It was a good lesson in practical mechanics.

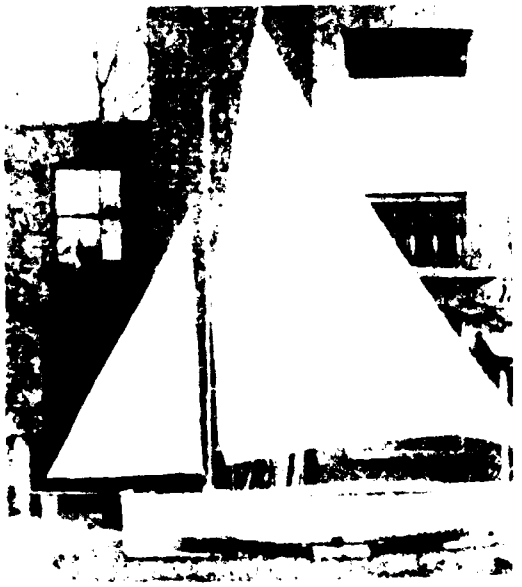

Figure 1. The boat in the garden

After launching the boat at Hammersmith I sailed down to Southend and across to Rochester, sleeping very uncomfortably with one leg down each side of the centreboard case. I did not think much in those days about the balance of aero- and hydro-dynamic forces between sails and hull. It was enough to know that sails push one along, but that voyage taught me a little about the ways of seamen. On the return journey up the Thames I met a tiresome sea and a head wind in Sea Reach. There were some 50 or 60 sailing barges beating up at the time and I managed to hook onto one of them and get a tow for the boat and a passage for me. Somewhere off Woolwich my barge was involved in a very interesting triple collision with two others, each barge hitting both of the others. One of them ultimately sank. The verbal exchanges which passed between the three skippers and their mates when we interlocked, were an eye-opener to me. I listened with admiration, never thinking that an analogous experience might one day call forth an unexpected, although of course far smaller talent in me. I was taking my 19-ton cutter before a strong wind into the sea lock at the end of the Crinan Canal when my crew failed to belay in time the rope which should stop the way. I thought we were going to ram the lockgates and in the heat of the moment said a few words about the situation. I was later told that a summer visitor who was standing on the lock side watching this manoeuvre was seen to pick up her little Peke, and stop up its ears.

The triple collision was also educative in another way. All the three skippers gave different accounts of the cause of the accident. The skipper of the barge called the "Jolly Dogs" was certainly in the wrong, but he put the blame on my skipper who, fortunately for me, was entirely correct in his actions. A pretty case was brewing for decision in the law courts and the counsel for my skipper asked me to go to his office and describe what happened. I was able to give a consistent

picture of the sequence of events and agreed to give evidence in the court. A short time afterwards the lawyer wrote that this would not be necessary because when he told the opposing lawyers that he had a truly independent witness who could describe the collision, they knew it was useless to go on, even though the witness was only a schoolboy, and they withdrew their allegations.

My first introduction to fluid mechanics as a science came through meteorology. After studying the subject in its theoretical aspect for a time, I was appointed meteorologist to the old wooden whaling ship Scotia which was chartered in 1913 by the government and the shipping companies to look for icebergs in the North Atlantic and report their positions by means of the newly invented method of wireless telegraphy. You may remember that the Titanic went down in 1912 through striking an iceberg. The Scotia was a wooden barque of 238 tons. Fig. 2 shows her quarterdeck. I took this picture one sunny morning when we were stuck in ice firm enough for me to stand on. The Scotia had been used by the explorer Bruce in the Antarctic and was equipped with an auxiliary steam engine of almost unbelievable inefficiency which would drive her up to 4 1/2 knots in a calm, although she would make about 9 knots under sail in a gale. She had two whale boats which were seldom, if ever, used on our expedition. They were the original boats used when whaling was carried out by rowing up to a whale and sticking a harpoon into it. They were very much in my way when I flew kites carrying meteorological instruments from her quarterdeck. Another obstruction was the spanker boom. I noticed that the skipper never set the spanker sail and I asked him why. He said the boom was quite rotten, but when I asked him why he kept it in position he was horrified and said, "What, cut up my spanker boom? Unthinkable!" After spending the winter in Dundee while the crew got sober enough to [illegible]

AD-A142 399 AIR FORCE ACADEMY AERONAUTICS DIGEST(U) AIR FORCE ACADEMY CO J DEJONGH ET AL. MAR 84 USAFA-TR-84-5 2/2

UNCLASSIFIED F/G 20/4 NL

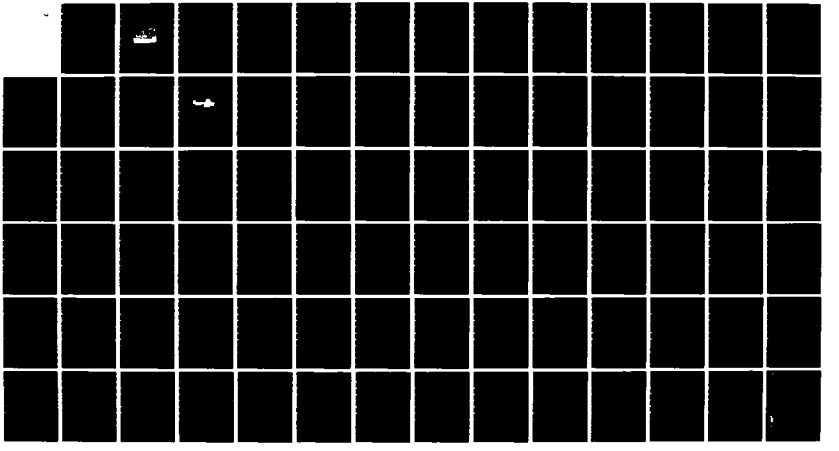

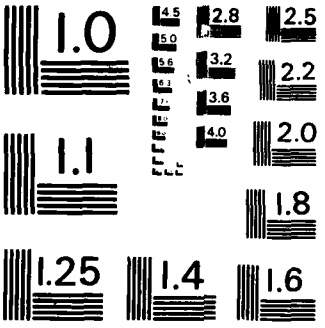

way. Most of our time was spent on the banks of Newfoundland where the iceberg-laden cold water comes south from Baffins Bay. Although the air at sea level was near freezing point the air a few hundred feet up had frequently come straight off the heated land of the American continent and was so hot that my kites felt warm to the touch when I reeled them in. It was thinking about the way heat transferred to and from the earth's surface that roused my interest in turbulence.

Figure 2. Quarter deck of the Scotia

While I was writing up the results of the Scotia expedition, war broke out on 4th August 1914. The only way I could think of in which my experience might be of value was as a meteorologist so I went to the War Office and asked whether I could give weather forecasts for military operations to the expeditionary force then being organised if telegraphic facilities could be made available. The officer whom I saw there did not seem to doubt that I could give accurate forecasts — which he might very well have done — but said that they would be of no

picture of the sequence of events and agreed to give evidence in the court. A short time afterwards the lawyer wrote that this would not be necessary because when he told the opposing lawyers that he had a truly independent witness who could describe the collision, they knew it was useless to go on, even though the witness was only a schoolboy, and they withdrew their allegations.

My first introduction to fluid mechanics as a science came through meteorology. After studying the subject in its theoretical aspect for a time, I was appointed meteorologist to the old wooden whaling ship Scotia which was chartered in 1913 by the government and the shipping companies to look for icebergs in the North Atlantic and report their positions by means of the newly invented method of wireless telegraphy. You may remember that the Titanic went down in 1912 through striking an iceberg. The Scotia was a wooden barque of 238 tons. Fig. 2 shows her quarterdeck. I took this picture one sunny morning when we were stuck in ice firm enough for me to stand on. The Scotia had been used by the explorer Bruce in the Antarctic and was equipped with an auxiliary steam engine of almost unbelievable inefficiency which would drive her up to 4 1/2 knots in a calm, although she would make about 9 knots under sail in a gale. She had two whale boats which were seldom, if ever, used on our expedition. They were the original boats used when whaling was carried out by rowing up to a whale and sticking a harpoon into it. They were very much in my way when I flew kites carrying meteorological instruments from her quarterdeck. Another obstruction was the spanker boom. I noticed that the skipper never set the spanker sail and I asked him why. He said the boom was quite rotten, but when I asked him why he kept it in position he was horrified and said, "What, go to sea without my spanker boom? Unthinkable!" After spending 24 hours at anchor off Dundee while the crew got sober enough to work the ship, we got under

value in military operations even if accurate. "Soldiers don't go into battle under umbrellas — they go whether it is raining or not." I expect he was politely telling me that the army had all the science it needed, but when six months later our people found that the French army derived great benefit from their meteorological service our meteorological office was asked to organise one; and one of its staff, Colonel Gold, did so very successfully.

Returning to the War Office, the officer asked me to leave my name and address in case anything turned up for which a scientist could be used. I went home, I must confess, rather disappointed, for I had no desire to become a dispatch rider. That evening a messenger came from the War Office saying that if I went down to the Royal Aircraft Factory at Farnborough I would be employed there as a scientist. I went there on the 5th or 6th August. What had happened in the War Office was that Major Sefton Brancker, then I think head of the flying wing of the Army had happened to go into the room of the man with whom I had just had an interview. This officer had told Brancker of my visit and asked him whether he could find any use for academic scientists in his branch. Brancker said he could use as many as he could lay his hands on. He took my name and sent his messenger at once.

On arriving at Farnborough O'Gorman, who was then the director, introduced me to a fascinating character called Teddy Busk who asked me to join his mess in Arnold House. This mess was run chiefly by members of the Naval airship section among whom was Cave-Brown-Cave who afterwards became Professor of Engineering at Southampton University. At first only Busk and I and F. M. Green were not in the Navy, but later we were joined by other civilians, F. W. Aston, the inventor of the mass spectroscope and the principal discoverer of isotopes, and Lindemann, afterwards Lord Cherwell. The mess subsequently moved to a

house called "Chudleigh"; I cannot remember who were members at the time of the move, but Farren, Glauert, R. H. Fowler, George Thomson, E. D. Adrian and Melvill Jones were certainly "Chudleighites."

When I arrived at Farnborough I was put to work in H department onto which the odd jobs that did not fit in with any other branch were decanted. It was housed in a building with a tin roof which looked out over the airfield. The aeroplanes used to come in close to the roof making a fearful noise and quite often crashed just outside our windows.

Some of the things we were set to do now seem futile in the light of hindsight, and some even then seemed rather wild, but of course we were under orders from the Army and had to do what we were told. O'Gorman, however, gave us a pretty free hand and we were able to turn down quite a number of things which could not possibly have worked. One job which was put on us, although we never thought it would be useful, was the designing of darts to be dropped on troops from aircraft. Melvill Jones and I were the principal people concerned and both he and I have described the sequence of experiments involved, so I will only give a brief account now. The French had used pointed steel "flechettes" but we found that they whirled when dropped, even though the centre of pressure when falling obliquely was well behind the centre of gravity. In any case it seemed to be a matter of prestige that we must have English darts so we designed and tested some with the necessary aerodynamic properties. Our last test was to find their distribution on the ground when dropped from an aeroplane out of a container, and we got a pilot to drop them onto an unused piece of ground. To measure their distribution we searched the ground and whenever we found the rear end of a dart projecting from it we pushed a square of paper over it to mark its position. We had just completed this work and were preparing to photograph the field when a cavalry

officer came up and asked what we were doing. When we explained that the darts which covered the field had been dropped from an aeroplane he looked at them, seeing each piercing a white square and said, in a surprised tone, "If I had not seen this I would never have believed that it was possible to make such good shooting from the air." Having finished that job, the darts were never used, not apparently for the reason we had originally raised as an objection, namely that missiles descending vertically would have a much smaller chance of hitting a standing man than the same weight of bomb going off on contact with the ground and throwing its fragments horizontally. The reason we were given was that darts were regarded as inhuman and could not be used by gentlemen.

All the things we did were not so absurd as our work on darts and by way of contrast I should like to trace one set of ideas which originated at Farnborough at that time. One of the troubles which we were asked to look at was the weakening of propeller shafts for transmitting power owing to key-ways cut in them. About this time a young man called A. A. Griffith arrived at the factory. He was obviously very able and he came and worked with me on the subject. We devised what is now called an analogue computer for obtaining mathematical solutions of the stress distribution near internal corners in keyways. Thus we formulated rough rules for deciding on the amount of rounding necessary to prevent too big a concentration of stress at the internal corners, both in torsion and in bending. This work led to our thinking about what it is that determines the strength of materials. We knew that consideration of intermolecular forces leads to an expectation that solids should be much stronger than they are and we came to the conclusion, as I think others had already done, that all materials have cracks or faults in them that entail far greater local

stresses than the mean applied stress. This qualitative idea had little value unless one could form a quantitative model for relating definable faults to the reduction in mean stress which they cause. It was a brilliant idea of Griffith's that made this possible. He pointed out that it is not necessary to know the exact distribution of stress near the sharp ends of a crack, but only the strain energy which is spread over a much larger area, and the surface energy or surface tension of the material. The condition that the crack can extend can be found by equating the loss of elastic energy during this extension to the surface energy gained. Although this idea proved very fruitful and was verified by some beautiful experiments which Griffith did at Farnborough with brittle materials, glass and quartz, it explained only the reduction in strength due to a crack. The longer the cracks the weaker the material. Griffith and I and Lockspeiser, who was also interested, knew that in fact most metals tend to get stronger when they are strained so that the Griffith crack theory could not be used to give a theoretical picture of the strength of metals. We made some unsuccessful attempts to modify the Griffith theory to include such cases. I tried to describe mathematically the situation where the stress distribution round one Griffith crack might inhibit the growth of another, and thus appear to strengthem the metal, but mathematical difficulties defeated this attempt. It was not until 19 years later, in 1934, that I formed the conception that when the Griffith crack is a shear crack which does not pull the two newly formed faces apart but allows them to slide over one another, the molecular force will still operate across it. Under these circumstances the faces may join up again, reforming the crystal structure and leaving a highly stressed region near both its ends. The stress concentrations at the two ends become what the mathematicians call singularities and the stress distributions due to each of these can

be summed as though they were independent, irrespective of how they were produced. This idea cleared up the mathematical difficulties, and the dislocation theory of the strength of metals started as an offshoot of or, in the modern phrase, a fallout from, the association of Griffith and me in our efforts to think about stress concentrations in crankshaft keyways of aircraft.

Much of our work at Farnborough consisted in designing instruments for use in aircraft and it soon became obvious to me that many of our difficulties arose because we could not form a clear picture of the experiences that pilots tried to explain to us. In many cases they did not really understand what they tried to describe and often unconsciously described as facts things that were really only their own theories about the causes of their experiences. It seemed to me that I ought to fly myself if I was going to be any use as a deviser of gadgets for use in the air. After some discussion, O'Gorman came to agree with me, but the idea that a scientist should fly appeared unorthodox and indeed unnecessary to the Service chiefs at that time, and they turned it down. Instead O'Gorman released me from his staff and in May 1915 I joined the Royal Flying Corps as a pupil in the ordinary way, leaving my scientific proclivities in abeyance. I was sent to the flying school on the old motor racing track at Brooklands and took a course on the old 1913-model Maurice Farman then called a Longhorn or a "Rumpety" for reasons which I never fathomed. It was a pusher biplane with an elevator in front and a tailplane supported on long struts behind. Its maximum speed was, I think, about 60 miles an hour and it would stall about 37 mph. One tried to land it at about 42. At that time aircraft were so scarce that pupils were not allowed to fly if there was enough wind to put a match out. We went on to the field in the calm of the early morning and again in the evening. If there was

any wind we had the day or night off. It was an easy life but to keep in it one had to learn certain rules. In my case the most important was never to touch the controls of the dual control machine on which I was being instructed. The reason for this was that the instructor to whom I had been assigned was a nervous character who had been been injured, or at any rate frightened, in a crash caused by a mistake of one of his pupils, and he decided this must not happen again, so if one of his pupils applied any appreciable force to the control or joy stick, as it was called, he reported that this man was heavy handed and would never make a good pilot. At this time many more people wanted to learn to fly than there were machines to teach them in, so the danger of being thrown out of the course was a very real one. The consequence was that the first time this instructor's pupils went solo was the first time they had taken control and consequently they were apt to do funny things on that occasion. I was fortunate because having been nearly a year at Farnborough I knew what the controls were expected to do. My first landing was too far along the field and ended in the sewage farm just outside it.

One of the things that troubled the pupils was that at the low speeds our machines would fly, a cross-wind made one seem to be side-slipping badly if one looked at the ground. People were apt to correct this by manoeuvres which gave rise to a dangerous real side-slip. Although I fear I was a bad pilot when it came to judging distances I was not bad in the air and could do the loops and steep banking that people did in those days. I was able to do fairly violent manoeuvres close to the ground because, unlike most pilots at that time, I had complete faith in my instruments and did not look at the ground till it was necessary to land on it. A rumor even went round that on one occasion this faith was misplaced because while I was turning, as I

thought about 2000 feet up, the tail of my eye caught sight of a tree quite close to. It turned out that the instrument I was relying on was the rev counter, not the altimeter.

After getting my wings, as the completion of the training course was called, in July 1915 I did a short course on what was then called reconnaissance. This consisted in flying over a farm which was supposed to be the target of artillery fire. People on the ground let off puffs of smoke in its neighborhood and we were instructed to tap out in morse code the bearing and distance of the puff from the target. At that time wireless telephony had not been invented and the transmitting apparatus had a long wire aerial with a weight at the end which the pilot had to let down when he wanted to transmit. I failed at the first attempt because I forgot to wind it up again before I landed and it was torn off near the edge of the airfield.

When I had passed the necessary tests O'Gorman asked me to return to Farnborough and rejoin his group of experimental officers. Although I had not been given a flying training as a scientist I think that the fact that nothing very dreadful occurred when I was, may have contributed to the decision of the authorities about a year later to accept other scientists like Lindemann, Farren, G. P. Thomson, Melvill Jones and others as suitable candidates for this experience.

One of the first things I did on my return to Farnborough was to design and then use apparatus for making pressure measurements over a section of a wing in flight. To understand the urge to do this work one must think of the state of the art at that time. Although Lanchester's ideas about trailing vortices were known to us, Prandtl's independent development into a usable form had not penetrated, and we had not thought of regarding wing drag as having two separable components, form drag and induced drag. To predict the aerodynamic character of the wing

we could only rely on tests of models in a wind tunnel and there was much controversy about the magnitude of scale effects. The only method for comparing model tests with full scale performance was to compare the overall performance of the whole machine with that predicted by extrapolation of the model tests and in this comparison there were so many possible sources of error that discrepancies could be attributed to a wide variety of causes according to one's fancy. It seemed to us that direct measurements of the pressure distribution of a wing in flight could be made and that a comparison could then be made between these and similar measurements over a model in a wind tunnel. I do not think that any measurements of that type had been made in 1915 when I started, so I had to design the necessary apparatus. I got the workshops to make a metal strip with 20 pressure holes and insert it in the wing of a BE2c machine. This was a really stable machine. I could not have made the measurements I did if it had not been stable. I made a multitube manometer with photographic paper which could be wound over tha bank of tubes, each of which was connected with one of the pressure holes, and arranged a light which I could switch on for an instant when I had the machine flying level and steadily on course on a calm day. Fig. 3 shows the results. In the upper section the positions of the holes are shown and in the lower the pressure coefficient for each hole over a range of speeds from 50 to 97 mph. Since I only made measurements over one section I could not achieve a comparison between the known weight of the aeroplane and the integrated upward lift produced by the observed pressure, but I did get quite good lift and drag curves for the section, and since the object of the exercise was to obtain a comparison between something which could be measured directly on a full scale wing and on a geometrically similar model wing in a wind tunnel, I had done what I set out to do. When the comparable

wind tunnel measurements were made a discrepancy was found, but this was ultimately traced to a faulty method of allowing for the effect of the tunnel walls, rather than to errors in the full-scale measurements. I think that when I wrote up my results for the R and M series in 1916 it may have been the first record of this kind, but many such measurements have been made since.

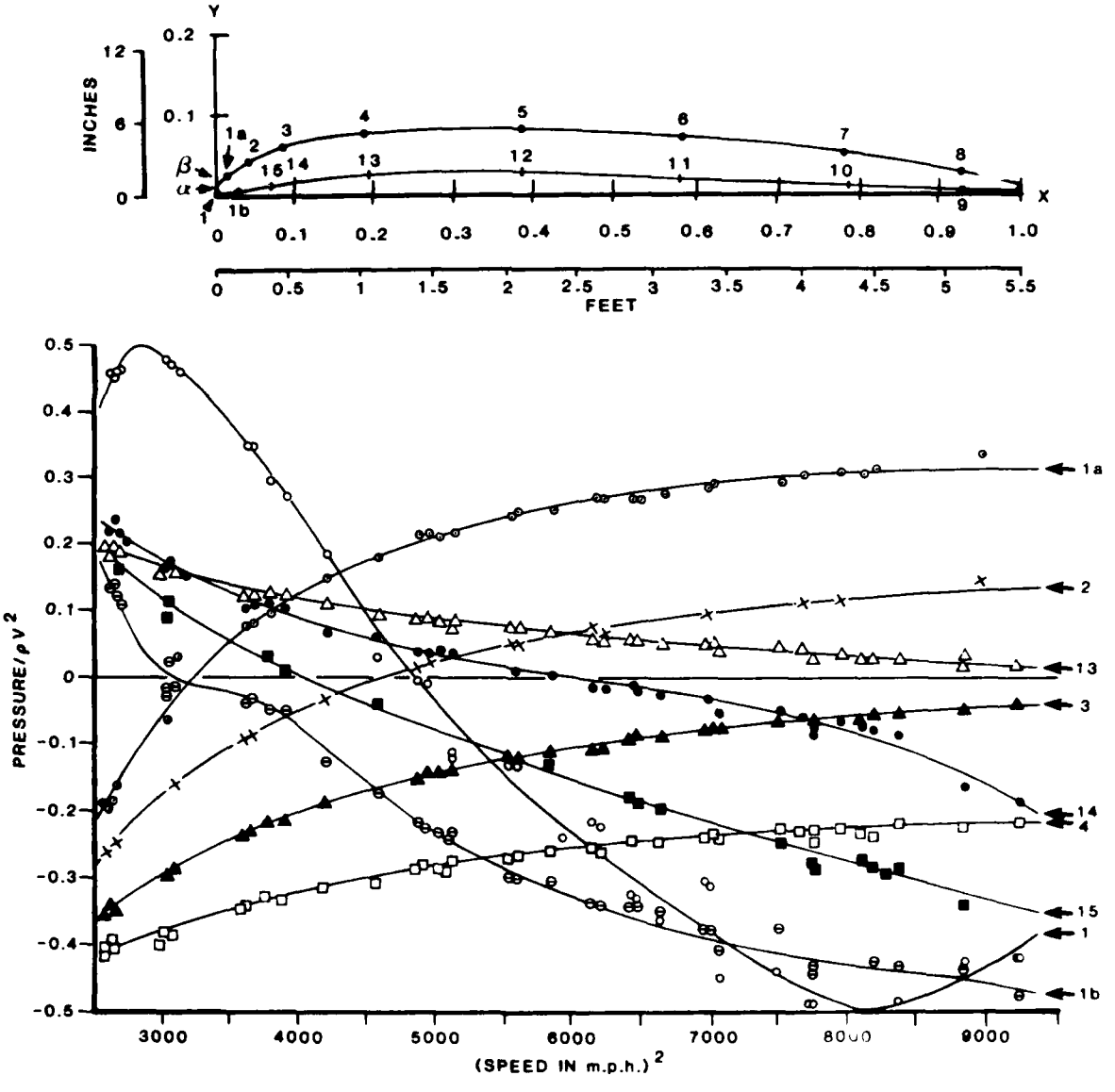

Figure 3. (Top) The position of the pressure holes
(Bottom) The pressure coefficients for each hole

Before leaving this phase of my aeronautical experience I might mention one of the less pleasant machines I used. It was the experimental machine BE2b which had warped wings instead of ailerons and was longitudinally very unstable. If it got up to 90 mph while diving, the pull on the stick was enough to require most of my strength to pull it out of its dive. I must confess that when this happened I was rather frightened. Since there must be rather few people about who have flown warped wing machines I might describe how they operated. They had no ailerons. Wings in those days were so flexible that unless they were stiffened by numerous bracing wires they could be twisted without applying much force, until the angle of incidence at the wing tip was changed by a degree or so. In warped wing machines some of the bracing wires were led to the control stick so that a movement of the stick to the right, say, would decrease the angle of incidence of the right wing tip and increase that of the left. They were very uncomfortable in gusty weather because if a gust struck one wing with greater force than the other the control wires moved the control stick with much greater force than the pilot could apply. Thus although the machine would bank on application of a steady force on the stick, the stick itself would be moving violently and uncontrollably. I found this most uncomfortable in the BE2b and also in a Caudron warped wing machine which I used.

I left Farnborough, I think, in 1917, and became a meteorological adviser to the Royal Flying Corps. One of the jobs I did then was to help organise night flying experiments and in particular to help set up in France a method devised by Bertram Hopkinson for night bombing. This was quite simple. Two searchlights were set up about a mile apart on the line to the target. Their vertical beams could be seen on most nights owing to a slight haze in the atmosphere. The pilot got them in line and set a compass course which would take him along the line

joining them. He started a stop-watch when passing over the first and stopped it at the second. By multiplying the time thus recorded by the ratio of the distance of target to distance between the searchlights the pilot estimated his time of arrival, assuming the wind remained constant. At the estimated time he dropped his bombs and went home — at least that was the theory, but it was never put into practice. We had set up the equipment in France near the south end of the line and were expecting to bomb Coblenz the next night, but happily peace was declared during the day and put a stop to the operation.

Methods like those I have described must seem very amateurish to modern aviators, but it must be remembered that the idea that one could navigate at night in an aircraft that was heavier than air was quite new and very few people could do it. I think a stimulus which made it important to fly at night was the advent of night bombing raids by rigid airships. The first time I saw one of these, it was coming down in flames. I was on leave one night at my parents' home in St Johns Wood when I was wakened by anti-aircraft fire and suddenly I saw the whole sky lit up. I realised that something spectacular must be happening and I went to the back of our house and saw an airship falling vertically in flames. I watched it till it disappeared behind a house whose garden backed onto ours. I noticed that it appeared just the same length as a chimney behind which it disappeared. I knew that most airships were then about 600 feet long so as soon as it was light enough to see anything I got out my sextant and measured the angle subtended by the chimney. I also took its compass bearing and so could pin-point the position on the map. This point lay in a NNE direction and was about 11 miles away near a place called Cuffley. There was a railway station near the spot on the Great Northern line. I took the earliest train there in the morning. I was one of the first there and saw a grisly

sight with the bodies of the crew still lying about. The whole ruined structure of the airship, which turned out to be a Schutte-Lanz, was confined to an area about equal to its cross section.

Although my only experience as an aircraft pilot was with powered aeroplanes and a parachute I have been in almost all other types except gliders, as a passenger. Perhaps the passage I enjoyed most was a trip in a free balloon. It was so beautifully quiet. During the 1914 War balloons were sometimes used at night as targets for training searchlight crews and one night I was one of three passengers and a pilot in the basket. We went up from Kennington Oval and after a short time we went into the clouds at about 4000 feet. Since we were then of no use to the searchlight crews the pilot pulled a cord and released some gas. We began to go down and very soon broke through the clouds. Putting my hand out of the basket I could feel a strong upward breeze so we were evidently descending pretty fast. After a time the pilot thought it was time to let out some sand which we carried as ballast, for otherwise we would have hit the ground. The sand rapidly dispersed and fell more slowly than the balloon so, relative to us, it went upwards. Then as our downward velocity stopped and reversed the sand caught up and filled the air all round us. It was like a sandstorm. The landing was also interesting. When he wanted to land the pilot let out a long and rather heavy rope which I should have thought would have broken any telephone wires it met. As the rope dragged along the ground it kept us at a more or less constant height of about 100 feet or less and slowed up our drift. The pilot then directed an electric torch beam downwards and as the light fell on trees or houses or gardens the illuminated patch jumped up and down. After a time it stayed down and the pilot said we must be over a field, so he pulled the gas release cord and we descended with a moderate bump and bounced I guess some 30

feet.

When the war ended I was expecting to return to Cambridge in October 1919 as lecturer in mathematics. I had half a year to spend the gratuity which the Government handed out to demobilised officers, so I was glad when Handley Page offered me the job of watching the weather and teaching celestial navigation to the navigator of his entry for the Daily Mail prize for the first direct crossing of the Atlantic. The crew consisted of H. G. Brackley, pilot, Tryggve Gran, a Norwegian, as navigator, and Admiral Mark Kerr, whose function I never really discovered. The engineer who did most of the organising was Stedman, who afterwards became head of the technical side of the Canadian Air Force. There were, if my memory is right, four competing parties who all assembled in St John's, Newfoundland, some time in May 1919. Although four firms, Vickers, Martinsyde, Sopwith and Handley Page entered, the affair was essentially a sporting event rather than an organised commercial competition. There were no aerodromes then in Newfoundland and each party set to work to make itself its own, erect a hangar if needed (in fact I do not think any were completed) and then build its machine. Fig. 4 is a photograph of the Handley Page under construction in the open. At first we all lived in the only reasonably comfortable hotel in St John's. Every morning each party rushed off to its own site and tried to get ready before the others. At the beginning of a month there were cheerful parties. This timing was a side effect of prohibition. When prohibition was introduced in Newfoundland doctors were allowed to prescribe alcohol in extreme cases for those patients who needed it medicinally. They did this at a dollar a time. One of them, I was told, prescribed about 30 000 a month. A rule was then introduced which permitted each doctor to prescribe only a limited number of "scrips" per month. At the beginning of the month, therefore,

the doctors had scrips available and parties were possible.

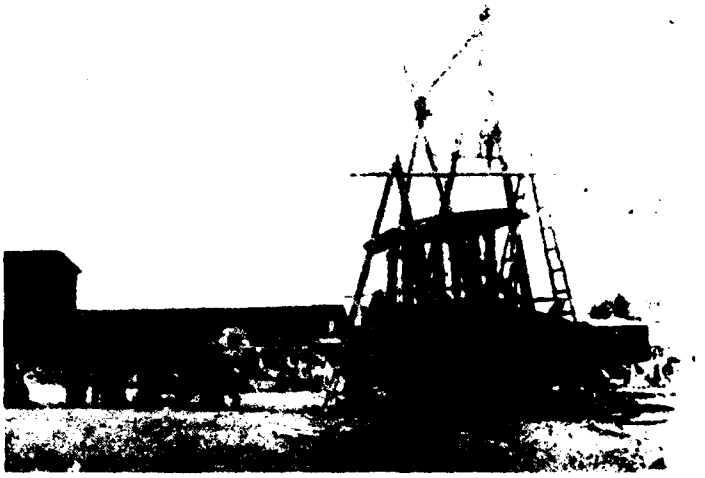

Figure 4. The Handley Page under construction in Newfoundland in 1919

The first outfit to get ready was the Martinsyde. They crashed at the take-off and were never airbourne. The navigator, a man called Morgan, was slightly injured I believe and when the papers gave out that the machine was to be repaired but that Morgan might not be able to act as navigator, people came rushing up from all over America, even from the Argentine, to offer themselves as substitutes. The hotel became so crowded one could hardly move. The next to start was the Sopwith with Hawker as pilot and McKenzie Grieve as navigator. I saw them take off, which they did apparently without difficulty. They were not heard of again for over a week, when they turned up in a Norwegian freighter. They had been picked up at sea and everyone marvelled at the ways of a beneficient providence which supplied a ship in the unfrequented area where they came down at exactly the time and place necessary to save them. The fact was that when things began to go wrong — I think an oilpipe fractured — they searched the sea for a ship and ditched

themselves alongside when they found it.

The next to take off were Brown and Alcock in the Vickers. That was a really spectacular affair. Their aerodrome was a rough stretch on some high ground behind St John's. They ran the full length without appearing to take off and disappeared from our view apparently below the level of the ground we were standing on. People near where I was standing thought they must have crashed, but in a few minutes they came back at a level which seemed to be about 100 feet and shot straight out to sea; Brown, the navigator, was not very knowledgeable about celestial navigation but he pretended to be less than he was, and I remember talking to him about how he would know where he had got to when he saw land below him on the other side. He replied "Oh well, if I see ladies in mantillas I will know it's Spain. If I see people eating frogs I will know it's France and if I see people hitting one another over the head it will be Ireland." This is not such a very exaggerated caricature of the method of navigation actually employed.

When the Vickers got across, the Handley Page, being a lot bigger than the others, had not completed her flight tests, so they wisely decided not to attempt the Atlantic crossing but to go down to New York, where they arrived after some delay caused by a forced landing in a strawberry field in Nova Scotia. One of the more absurd things that sticks in my memory was the reaction of Tryggve Gran when he heard the news that Brown and Alcock had been knighted. He was a very courageous fellow not very good at English and not very clever. He had recently married an English actress and sent her a telegram every day to tell her of his progress. When he heard that Brown and Alcock had been knighted he thought in his slow way, "If the Handley Page had got across first I would have been knighted, and then my wife would have been Lady Gran" so his telegram to her that day was, "Sorry you aren't a lady". He

couldn't think what was wrong with it.

In the years 1914-19 aeroplanes had increased greatly in numbers, power and reliability but the basic knowledge of fluid mechanics which was needed for a proper understanding of how they work had not advanced so rapidly. The advantage of reducing resistance by streamlining struts and wires was appreciated, but it was not until Melvill Jones pointed out that the part of the drag due to skin friction and turbulence could theoretically be reduced to near that of a flat plate of the same area as the wing that designers had an ideal against which they could measure their performance. The conception that drag is separable into two parts is a natural consequence of the Lanchester-Prandtl theory of lift. The combination of this theory with the Joukowsky theory of how circulation is related to aerofoil section and the boundary layer theory of surface friction, provided the main themes of aerodynamic research until speed increased so much that effects of compressibility became important.

Although these ideas provided a basis for design there was a gap between them and the classical theory of hydrodynamics, so well expounded in the great treatise of Horace Lamb. Although some of the conclusions of classical hydrodynamics had been verified experimentally, those on waves and on slow viscous flow are instances, those on flow past solid bodies had not. In particular the sphere, geometrically the simplest, is aerodynamically one of the most complex of bodies, and the inability of theory to describe flow round what seemed to be the simplest possible shape told heavily against it in the minds of practical engineers. When I returned to Cambridge in 1919 I aimed to bridge the gap between Lamb and Prandtl. In following that course I was fortunate enough to interest Rutherford who gave me a room near his own in the Cavendish Laboratory to work in. The reason for the discrepancy between classical theory of bodies moving in a fluid and what is

observed was understood at that time. The classical theory permitted perfect slipping at solid surfaces and the existence of viscosity makes this surface condition unrealistic. I therefore looked for effects in the motion of fluids which do not depend on surface conditions. One is that of rotation which affects fluid flow through the body of the fluid rather than at the solid surface. Here I found that classical theory could predict exactly in some cases how motions which themselves would not be described by that theory would be modified by rotation. Encouraged by this success I looked for and found a number of other things that could be predicted correctly by classical theory. Since then, I have witnessed an increasing willingness on the part of designers to use the work of theoretical hydrodynamicists.

At this stage I think it is time to stop before I expose my ignorance of modern aeroplanes. I am glad to have lived during the time they were simple enough for a reasonably intelligent amateur to appreciate them as mechanisms. They have developed in the kind of way, but much faster than we thought possible 40 years ago. They have also had some of the regrettable effects on our lives that I foresaw and expressed in my Wilbur Wright lecture to this Society 44 years ago. I then pointed out that every improvement in transport facilities makes it less worth while to travel on a globe of limited size because the place of arrival becomes more and more like the place of departure. Although aeroplanes have not had so detestable an effect on our country as automobiles, the activities of travel agents are forcing them along the same destructive path. You may think this an old man's view, but it is what I thought when I was young and what I still think.

By way of contrast with the primitive state of aeronautics sketched in this lecture I may mention that since writing it I travelled in comfort from Boston to London in a VC10 — neither ground nor sea were

visible at any time during our flight. Shortly after leaving the American coast our Captain told us that were were under the guidance of an automatic pilot controlled from London.

SECTION III

Propulsion

UNCERTAINTY ANALYSIS: A NEW COMPUTER SUBROUTINE

Christopher A. Boedicker*

Editor's Note

An earlier version of this paper won third place in the undergraduate division of the 1983 American Institute of Aeronautics and Astronautics Region V student paper competition.

Abstract

At the USAF Academy, I have developed and implemented a computer subroutine (UNCERT) that greatly simplifies the immense problems associated with uncertainty analyses. This paper describes the theory behind the uncertainty analysis and expl ins how this theory can be implemented in a computer program.

I. Introduction

Uncertainty analyses are vital for the test engineer. Consider this example. A firm wishes to purchase a turbine engine compressor, and the only criterion of importance is polytropic efficiency. Company A boasts an efficiency of 90 percent, and their number is guaranteed to within ± 0.1 percent. Company B has a compressor with a 91 percent efficiency, but this number can only be guaranteed to within ± 2 percent. Which compressor should the firm buy? The importance of uncertainty analysis may be somewhat clearer now.

Analyzing the uncertainty before a test gives the engineer an indication of the expected accuracy of the test results. In the absence of universally accepted standards, it is usually the engineer who determines the uncertainty values that are acceptable for a particular test. For example, in a test for which only mass flow and Mach number are calculated, an engineer may specify that he needs to know mass flow within ± 0.5 percent, but a Mach number within ± 3 percent is acceptable. If pretest uncertainties are too large, corrective action can often be taken. Specific methods for reducing uncertainty will be discussed later.

I have developed a computer subroutine called UNCERT to facilitate

*Cadet, USAF Academy

uncertainty analysis. One can attach UNCERT to a computer program that contains performance calculations in a separate subroutine. Pretest analyses show the test engineer where problems exist so corrective action can be taken, if necessary. Once the test has been completed, UNCERT provides the user with a reportable measure of the accuracy of the results. This paper discusses the theory behind the uncertainty analysis, explains how to use the subroutine, and presents the results of an actual application of the subroutine.

II. Theory

Uncertainty analysis concerns the mathematical reliability of an experiment. A detailed discussion of the theory behind uncertainty analysis appears in Ref. 3; the paragraphs below summarize the main ideas from that article.

In looking at the results of an experiment, one must distinguish between error and uncertainty. Error is a certain fixed value and refers to the difference between a measurement and the true value of a quantity. Uncertainty, on the other hand, is a measure of accuracy and represents a range of values within which the result is expected to fall.

Two types of error are associated with any measurement: random (precision) error and fixed (bias) error. Random errors occur because small, independent influences prevent the measurement system from delivering the same reading when supplied with the same input value. Deviation from the mean approximates a normal distribution (Figure 1). Standard deviation is used as a measure of the precision error, and the statistic $\bar{S}$, called the precision index, is used to estimate the standard deviation. $\bar{S}$ is given by Eqn. 1.

$$\bar{S} = \sqrt{\frac{\sum_{i=1}^{N} (X_1 - \bar{X})^2}{N - 1}} \qquad (1)$$

where N is the number of measurements, and $\bar{X}$ is the average value of individual measurements X_i. By making Z independent measurements, the standard deviation can be reduced by $\sqrt{Z}$, as shown in Eqn. (2).

$$S = \frac{\bar{S}}{\sqrt{Z}} \qquad (2)$$

Bias errors will cause repeated readings to be incorrect by roughly the same amount but for unknown reasons. Bias is determined by comparing a measurement with a known standard, an often impossible task in a laboratory situation. Judgment of the most knowledgeable instrumentation expert is often relied upon to obtain bias limits. Figure 2 illustrates how the bias error combines with the precision error to form measurement error.

The bias and precision error estimates are combined to yield an uncertainty interval. The National Bureau of Standards (NBS) and much of industry recognize a standard represented by the bias limit plus a multiple of the precision index. The uncertainty is centered about the measurement value and is evaluated using

$$U = \pm(B + t_{95}S) \qquad (3)$$

where B is the bias limit, S is the precision index, and t_{95} is the 95th percentile for the 2-tailed Student's "t" distribution. t_{95} is based on the sample size. When t = 2 (the value usually selected), Eqn. (3) becomes

$$U = \pm(B + 2S) \qquad (4)$$

This uncertainty value does not specify a statistical confidence interval, since the bias limit is based on judgment. Uncertainty, as stated earlier, is the largest error expected in the parameter of interest. The uncertainty interval is shown in Figure 3.

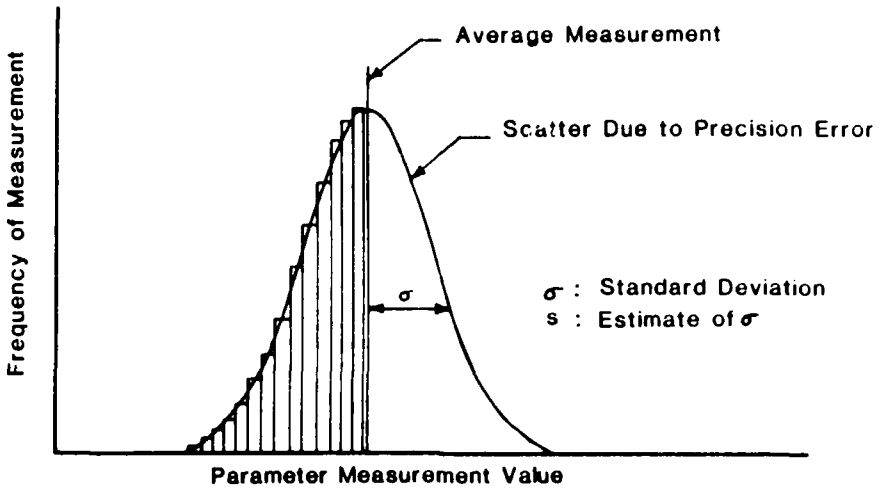

Figure 1. Precision Error

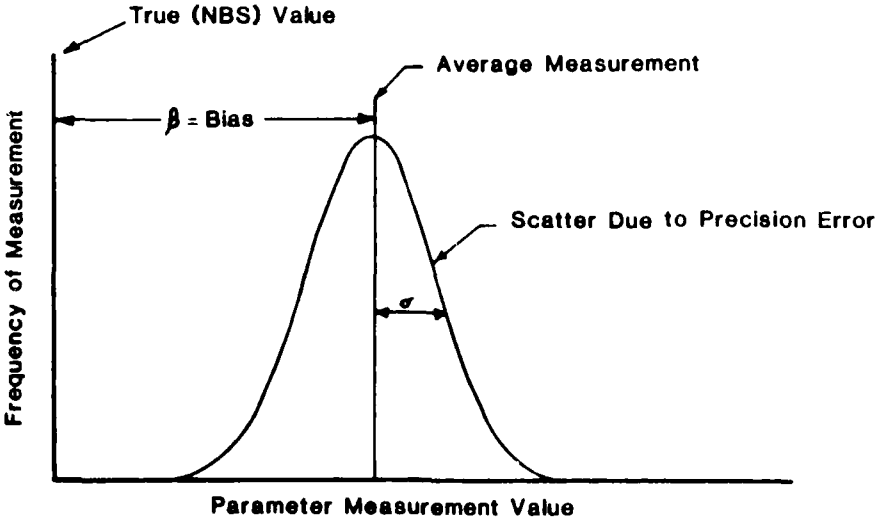

Figure 2. Bias and Precision Error

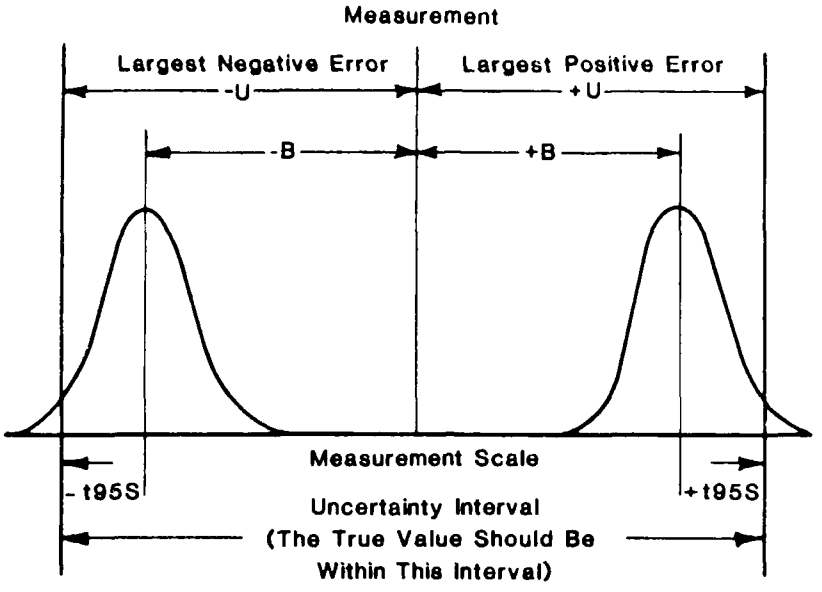

Figure 3. Measurement Uncertainty (Ref. 1)

Performance parameters are rarely measured directly in a test. Basic quantities like temperature, pressure, force, and position are determined, and performance parameters are then evaluated as a function of these more basic measurements. Errors in the measurements are propagated to the performance parameters through the particular equation for the parameter, and this propagation may be approximated by a first-order Taylor series method.

Consider a test in which there are L performance parameters or calculations based on n measurements. The bias limit for the jth calculation may be determined using

$$B_{C_j} = \sqrt{\sum_{k=1}^{n} \left(\frac{\partial C_j}{\partial M_k} B_{M_k} \right)^2} \qquad (5)$$

where C_j is the jth calculation, M_k is a measurement, and B_{M_k} is the bias limit of the kth measurement. The large M subscript specifies an

estimate of the error for a measurement; the large C subscript specifies an estimate of the error for a calculation. A similar method is used to determine the precision index for each of the calculations.

$$S_{C_j} = \sqrt{\sum_{k=1}^{n} \left(\frac{\partial C_j}{\partial M_k} \; S_{M_k} \right)^2} \qquad (6)$$

where S_{M_k} represents the precision index associated with the kth measurement. Once these numbers have been obtained, they may be added using

$$U_j = \pm \left(B_{C_j} + t_{95} S_{C_j} \right) \qquad (7)$$

to obtain the uncertainty in the jth calculation.ined parameter is the

III. Reasons for Computer Application

Although methods to determine uncertainties are available, some tests are so complex that analytic solutions to the problem cannot be obtained easily, if at all. The propagation of errors (through numerous measurements) may also prevent an analytic solution. Numerical solutions must therefore be used. The partial derivatives in Eqns. (5) and (6) must be evaluated using

$$\frac{\partial C_j}{\partial M_k} \cong \frac{\Delta C_j}{\Delta M_k} \qquad (8)$$

where C is a calculated value, and M is a measurement. To facilitate calculations, a non-dimensional number should be used:

$$\left(\frac{\partial \hat{C}_j}{\partial \hat{M}_k} \right) \cong \frac{\Delta C_j}{\Delta M_k} \left(\frac{M_k}{C_j} \right)_{nominal} \qquad (9)$$

This is the sensitivity coefficient, expressed in percent per percent.

At this point, we can use a time-saving computer subroutine to

calculate these sensitivity coefficients and then combine them with all the other proper computations to determine uncertainties.

IV. General Working of the Subroutine

The performance of a test article is usually determined by a computer program. The main part of the program is used for inputs, and the performance parameters are calculated in a separate subroutine. If such a program already exists, the UNCERT subroutine can be attached in order to yield the uncertainties in the calculations.

Bias limits (B_{M_k}'s) and precision indices (S_{M_k}'s) for each of the measurements must be input into DATA statements within the UNCERT subroutine. The values must be determined from manufacturer's data and expert opinions.

To determine the uncertainties, we must numerically evaluate partial derivatives. First, a 1 percent change in the measured parameters is made. Then the subroutine that calculates the performance parameters (TAPERF) is called (once for each measured value) to obtain a new value for the performance parameter to correspond to the new value of the measured parameter. The partial derivatives are then computed as

$$\left(\frac{\partial \hat{C}_j}{\partial \hat{M}_k}\right) \cong \frac{(C'_j - C_j) / C_j}{(M'_k - M_k) / M_k} \tag{10}$$

where

$$M'_k = 1.01\ M_k \tag{11}$$

and C'_j is the calculated value (performance parameter) evaluated using M'_j. Once the measurement bias limits, precision indices, and non-dimensional partial derivatives are available, the bias limits and precision indices for the performance parameters are found using

$$B_{C_j} = \sqrt{\sum_{k=1}^{n} \left(\frac{\partial \hat{C}_j}{\partial \hat{M}_k} B_{M_k} \right)^2} \tag{12}$$

and

$$S_{C_j} = \sqrt{\sum_{k=1}^{n} \left(\frac{\partial \hat{C}_j}{\partial \hat{M}_k} S_{M_k} \right)^2} \tag{13}$$

These can be evaluated through matrix multiplication.

$$\begin{bmatrix} \left(\frac{\partial \hat{C}_1}{\partial \hat{M}_1}\right)^2 & \cdots & \left(\frac{\partial \hat{C}_1}{\partial \hat{M}_n}\right)^2 \\ \vdots & & \vdots \\ \left(\frac{\partial \hat{C}_1}{\partial \hat{M}_1}\right)^2 & \cdots & \left(\frac{\partial \hat{C}_L}{\partial \hat{M}_n}\right)^2 \end{bmatrix} \begin{bmatrix} \left(B_{M_1}\right)^2 \\ \vdots \\ \left(B_{M_n}\right)^2 \end{bmatrix} = \begin{bmatrix} \left(B_{C_1}\right)^2 \\ \vdots \\ \left(B_{C_L}\right)^2 \end{bmatrix}$$

$$[L \times n] \qquad [n \times 1] = [L \times 1]$$

where L and n are the maximum number of calculations and measurements, respectively. The $S_{C_j}^2$ values are calculated in the same manner. A general matrix product subroutine evaluates $B_{C_j}^2$ and $S_{C_j}^2$ values, square roots are taken, and then uncertainties in the performance are determined using

$$U_j = \pm(B_{C_j} + t_{95} S_{C_j}) \tag{7}$$

where t_{95} is generally set equal to 2.0. The subroutine outputs the final values of B_{C_j} and S_{C_j}, the equation used for the uncertainty calculations, and U_j.

V. Application of Subroutine

UNCERT has been created in order to perform uncertainty analyses. A listing of the subroutine, as used within a specific example, and an

explanation of how the subroutine can be used appear in Appendix A. Because of the length of the program, only those portions necessary to understand UNCERT will be examined.

VI. Application Example

The UNCERT subroutine has been used to calculate uncertainties for a centrifugal compressor test at the Wright-Patterson AFB Aero Propulsion Lab. The main program, used to input the proper measurements, was called RUNTA (Run Test Article), and the performance was computed in a subroutine called TAPERF (Test Article Performance). The relevant parts of this program are listed in Appendix A.

The compressor to be evaluated was designed and manufactured by the Garrett Turbine Engine Company. Figure 4 shows a cross section of this compressor, with measurement station designations. This compressor has variable geometry with a flow rate of about 25 lbm/sec of air at design speed (23,000 rpm), and it develops an 8:1 pressure ratio in the single stage. RUNTA, using TAPERF, computes 64 different performance/aerodynamic parameters based on 20 different measurements. The continuity equation, velocity diagrams, and the Euler Turbomachinery equation are used with 1-dimensional, steady-flow assumptions to evaluate the compressor's performance. We also employ iterative schemes in some cases to find certain performance parameters. The final calculations involve the use of simple definitions, such as pressure recoveries or efficiencies.

The results of the RUNTA program appear in Appendix B. The nominal performance values are listed first. Then, in accordance with Dr. Abernethy's recommendations (Refs. 1 and 2), the equation for the uncertainty, the bias limits, the precision indices, and the final uncertainty values (in $\pm$ percent) are given as output.

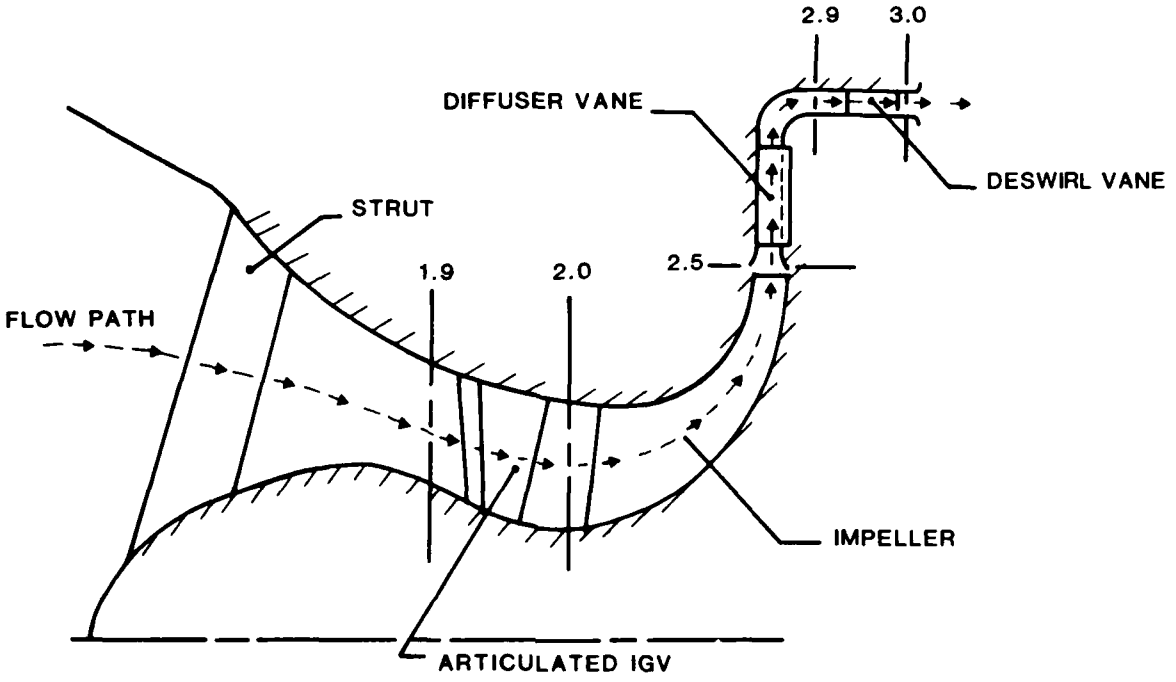

Figure 4. Compressor Flowpath and Station Designation

The results provide some interesting insights into the uncertainty analysis. Some of the uncertainties found are in excess of ±10 percent. An examination of the data shows that several different factors may have led to these high uncertainty values. First, the method we used to calculate the performance parameter may have resulted in high values for the influence coefficients. At the test article's operating point, the performance/aerodynamic parameter may have been highly sensitive to small changes in a measured value. Second, the instruments used to determine the value of the measurement may have had high bias limits and/or high precision indices. Finally, the uncertainty may have resulted from the point of operation of the test article. For example, transducers are most accurate when they are operating near 100 percent of their range. At lower values, the uncertainty associated with a transducer can increase significantly.

In looking at the results, one immediately questions the uncertainty of +0 percent listed for C(2). C(2) represents the pressure loss coefficient associated with the inlet guide vane (IGV) of the compressor (shown in Figure 4). This coefficient is evaluated using a look-up function in the performance subroutine, and it depends on the angle given to the inlet guide vane. The loss coefficient does not change its value until the IGV angle approaches 30 degrees. For this example, the IGV angle is .01 degrees. This small nominal value is used since a value of 0 degrees causes DELTAC, (C'-C)/C, to be undefined. Small changes in the IGV angle, for its small nominal value, do not change the value of the loss coefficient. The influence coefficients for this example are all 0; thus, no uncertainty is found in the loss coefficient.

An in-depth analysis of one of the uncertainty values may shed more light on the subject. The 38th calculation in the program involves the absolute Mach number at station 2.9 (Figure 4), the diffuser exit. The uncertainty in this calculated parameter [C(38)] is ±5.4 percent, as listed in Appendix B. Table I below shows the bias limits, precision indices, and uncertainties for the 5 absolute Mach numbers calculated in this example.

Table I
BIAS LIMITS (B_{C_j}), PRECISION INDICES (S_{C_j}), AND UNCERTAINTIES (U_j)
FOR 5 MACH NUMBER CALCULATIONS

Parameter	j	B_{C_j}	S_{C_j}	U_j (±%)
AM19	1	.6867 E-02	.3265 E-02	.13 E+01
AM20	5	.7249 E-02	.3447 E-02	.14 E+01
AM25	20	.5162 E-02	.5064 E-03	.62 E+00
AM29	38	.1935 E-01	.1732 E-01	.54 E+01
AM30	42	.2126 E-01	.1458 E-01	.50 E+01

The uncertainties in the absolute Mach numbers at stations 2.9 and 3.0 are both over 5 percent. Looking at Table I, one can see that the bias limits and precision indices for these calculations are significantly higher than those for the other 3 Mach numbers. Looking back at Eqns. (12) and (13), one can see that high values for the partial derivatives or the measurement bias limits or precision indices would cause high values in B_{C_j} and S_{C_j}, and thus large uncertainties. If a problem exists, there are several ways to correct it. Lower values for B_{M_k} should not be input in order to lower the overall uncertainty. The first estimate was based on expert opinion, and changing this value until a desired result is achieved defeats the purpose of the uncertainty analysis. The S_{M_k} values, however, could be lowered in order to alleviate high uncertainties. Either more or better transducers could be used to lower the S_{M_k} values. More could be used since

$$S_{M_k} \propto \frac{1}{\sqrt{Z}} \tag{14}$$

where Z is the number of transducers whose outputs are averaged together to give the measured value. However, cost and space available for transducers may be prohibitive. A final method to lower the uncertainty would be to change the equation used to calculate the parameter of interest. A different equation, if one exists, might favorably alter the value of the partial derivative.

We can use the Mach number example to illustrate some of the problems that might be encountered using a given calculation method. Since the bias limit and precision index for any given calculation are based on partial derivatives, the equation becomes very important. If static and total pressure are known at a given point, Mach number may be calculated using

$$\frac{P_T}{P_S} = \left(1 + \frac{\gamma-1}{2} M_2\right)^{\gamma/\gamma-1} \tag{15}$$

Solving for M yields

$$M = \left\{\frac{2}{\gamma-1}\left[\left(\frac{P_T}{P_S}\right)^{\gamma-1/\gamma} - 1\right]\right\}^{\frac{1}{2}} \tag{16}$$

The partial derivatives are

$$\left.\frac{\partial M}{\partial P_S}\right|_{P_T} = -\frac{1}{\gamma P_S} \frac{1}{\sqrt{\frac{2}{\gamma-1}\left[\left(\frac{P_T}{P_S}\right)^{\gamma-1/\gamma} - 1\right]}} \cdot \left(\frac{P_T}{P_S}\right)^{\gamma-1/\gamma} \tag{17}$$

$$\left.\frac{\partial M}{\partial P_T}\right|_{P_S} = \frac{1}{P_S \gamma} \frac{1}{\sqrt{\frac{2}{\gamma-1}\left[\left(\frac{P_T}{P_S}\right)^{\gamma-1/\gamma} - 1\right]}} \cdot \left(\frac{P_T}{P_S}\right)^{-1/\gamma} \tag{18}$$

The influence coefficients would be obtained by multiplying the above 2 equations by $\left.\frac{P_S}{M}\right|_{nom}$ and $\left.\frac{P_T}{M}\right|_{nom}$, respectively. Note that

$$\frac{P_T}{M} \cdot \frac{\partial M}{\partial P_T} = -\frac{P_S}{M} \frac{\partial M}{\partial P_T} \tag{19}$$

The change in the influence coefficients in the above equation with P_S/P_T (or Mach number) is shown in Figure 5.

Figure 5 shows that a Mach number calculation using Eqn. (16) is quite sensitive to errors in P_T or P_S, especially for low, subsonic Mach numbers. Table II is a list of some of the partial derivatives of the Mach numbers.

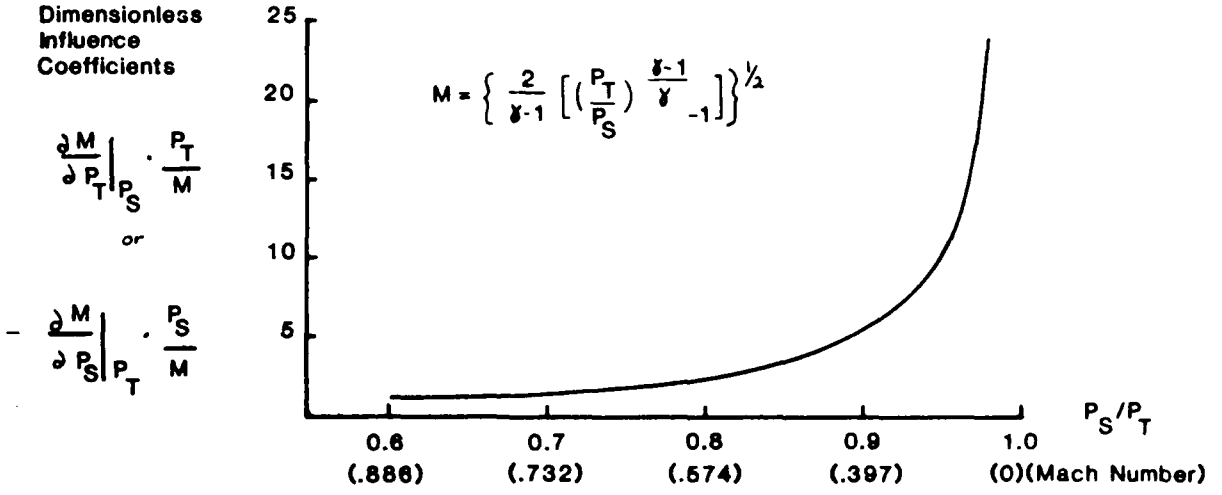

Figure 5. Mach Number Sensitivity

Table II
$\partial\hat{C}_j/\partial\hat{M}_k$: PARTIAL DERIVATIVES OF MACH NUMBERS WITH RESPECT TO STATIC AND TOTAL PRESSURES (GIVEN IN %/%)

		(M_k)				
		PS25	PS29	PS30	PT29	PT30
	AM19	0	0	0	0	0
	AM20	0	0	0	0	0
(C_j)	AM25	.1264 E+00	0	0	0	0
	AM29	.4306 E-03	.8898 E+01	0	.8191 E+01	0
	AM30	.4314 E-03	0	.9815 E-01	0	.8958 E+01

The partial derivative values shown above actually represent the percentage change in a calculated value that can be expected for a 1 percent change in a given measured value. Thus, one can expect an 8.898 percent increase in the absolute Mach number at station 2.9 for a 1 percent increase in the static pressure at that station. A negative value for a sensitivity coefficient means that one can expect a decrease in the calculated value when the measurement is increased. The partial derivatives for the Mach numbers at stations 2.9 and 3.0 (AM29 and AM30)

are very large when taken with respect to static and total pressures near the compressor exit. At stations 1.9 and 2.0, the air flow angle is known, and the continuity equation is applied in a rather simple iterative scheme to find the Mach numbers. At the impeller exit (station 2.5), the air flow angle is not known. Thus, we use the Euler Turbomachinery equation with the continuity equation in a double iteration to determine Mach number. At stations 2.9 and 3.0, we use static to total pressure ratios to find Mach number. But the possible problems with this last method have just been illustrated. The test engineer may wish to change the calculation procedure if the situation allows. An iterative scheme could be employed to find the Mach numbers at stations 2.9 and 3.0. The desired uncertainty levels and the feasibility of the change will determine whether or not the calculation procedure should be changed.

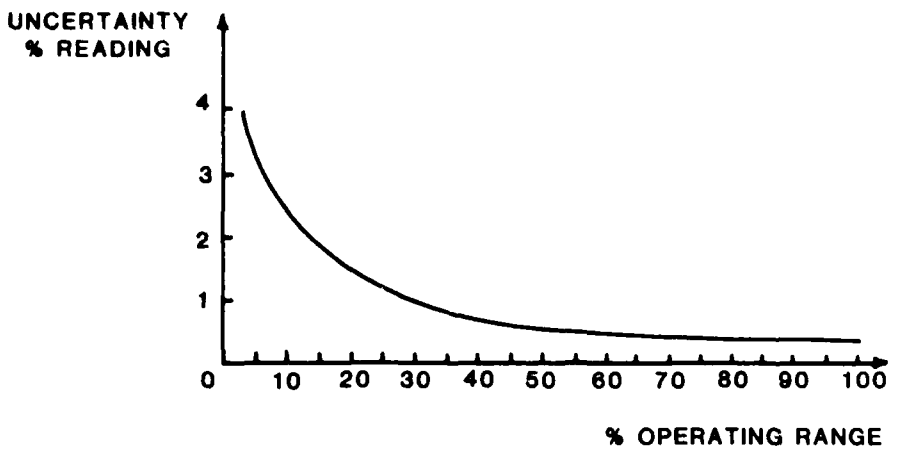

Figure 6. Uncertainty Variation with Instrument Operating Range

The operating point of the test article is very important. The uncertainty results apply to only one operating point. It has already been shown that the operating point affects the influence coefficient;

it may also affect the bias limit and precision index associated with a given transducer. Figure 6 should clarify this point. If the test article is not operating so that the transducers and instrumentation are near 100 percent of their prescribed range, then uncertainties can be higher than those obtained at a "design point." If the test must be performed far from the design point, then better or different transducers might be needed, meaning large expenditures of time and money. Unfortunately, in many cases nothing can be done. Either the uncertainties must be accepted, or the test must be cancelled. If the uncertainty analysis is performed, however, it still enables the test engineer to tell how accurate the answers from that test will be.

In summary, high uncertainties can result from many different sources. Calculation methods may lead to large sensitivity coefficients. If this is true, new calculation procedures should be sought. Also, the bias limits and precision indices may be too large. Better, more expensive transducers can be used to alleviate this problem. The measurement's precision index may be reduced by measuring the same variable with more transducers. Finally, the point of operation of the test article may cause high uncertainties. Better transducers could be used in this situation, or the engineer might choose to change transducers, depending on the specific point of operation. The feasibility of adopting many of these options depends on the time and money available to the test director.

VII. Summary

The UNCERT subroutine has been developed to perform uncertainty calculations for various experimental test articles with existing performance programs. The work required to attach the subroutine and make the required additional statements is not excessive, especially if

one considers that at present most uncertainty analyses are either very time-consuming or are never accomplished. Using the UNCERT subroutine before a test is conducted can identify potential problem areas so that the test engineer can decide whether to continue the test. If the alterations lead to excessive costs, the engineer might cancel the test before wasting large amounts of money. If the test is conducted, results of the final uncertainty analysis can be compared to the pretest analyses. The UNCERT subroutine can provide a valuable resource for any test facility.

Symbols

English Symbols

B_{C_j}	bias limit associated with a performance parameter
B_{M_k}	bias limit of an individual measurement
b_k	elemental bias limit
C_j	the jth calculation
L	total number of calculated parameters
M_k	the kth measurement
N	number of samples
n	total number of measurements
S_{C_j}	precision index associated with a performance parameter
S_{M_k}	precision index of an individual measurement
S_k	elemental precision index
$S, \bar{S}$	estimate of the standard deviation, or precision index
t_{95}	95th percentile for a 2-tailed Student's t-distribution

U_j	uncertainty; an estimate of the error
X	an observed value; an individual measurement
$\bar{X}_i$	sample average of measurements
Z	number of transducers

Greek Symbols

$(\partial \hat{C}_j / \partial \hat{M}_k)$	sensitivity (influence) coefficient
ν	degrees of freedom involved in a sample
σ	true standard deviation of repeated values of measurement

Superscripts

'	represents a new measurement or calculation value when a specified change has been made in a measured value
-	denotes a non-dimensional value

Subscripts

j	specifies a number from 1 to L
k	specifies a number from 1 to n

Computer Variable Names

ANSWER	final uncertainty value determined by U = B + 2S
BCJ	B_{C_j} values
BMK	B_{M_k} values
C	calculated value
CPRM	(C') represents the value of a calculated parameter after it has been evaluated using a value of M'
DC	dummy array containing the performance parameters calculated by the performance equations

DCODM	$(\partial\hat{C}/\partial\hat{M})$ sensitivity coefficient
DELTAC	$(C'_j - C_j)/C_j$
DELTAM	$(M'_k - M_k)/M_k$
M	measured value
MP	(M') represents the value of the measurement after a 1 percent increase in the nominal measurement has been made
SCJ	S_{C_j} values
SMK	S_{M_k} values

References

1. Abernethy, R.B., "Fluid Flow Measurement Uncertainty." Draft Revision of ISO/DIS 5168, Nov. 1981.

2. Abernethy, R.B. and J.W. Thompson, Jr., Handbook, Uncertainty in Gas Turbine Measurements, AEDC-TR-73-5, Feb. 1973.

3. Stiles, R.J. and C.A. Boedicker, An Example of Uncertainty Analysis in Compressor Testing, USAFA-TR-83-2, March 1983.

Appendix A

Computer Subroutine

To use the UNCERT subroutine, one requirement must be met: the performance of the test article must be evaluated in a separate subroutine. I will now illustrate what must be done to implement the UNCERT subroutine.

The computer program, which has been named RUNTA (Run Test Article), is listed on lines 100 through 14000. The UNCERT subroutine is shown on lines 14100 through 28400, and the general matrix product subroutine (GMPRD) is listed on lines 28600 through 30300. The performance calculations, contained in TAPERF (Test Article Performance), are given in lines 30400 through 87400.

The main part of the program, along with the performance subroutine, must be modified in order to evaluate the required partial derivatives. A 1 percent change is made in the first measurement, resulting in M'_1. The performance subroutine is then called, and C'@ values are determined based on M'_1. The partial derivative is

$$\left(\frac{\hat{C}_j}{\hat{M}_k}\right) \cong \frac{(C'_j - C_j)/C_j}{(M'_k - M_k)/M_k}$$

The nominal values of the performance parameters and the measurements (C_j and M_k) are stored and used to calculate the influence coefficients ($\partial\hat{C}_j/\partial\hat{M}_k$). M'_1 is then converted back to its nominal value, M_1. The second measurement is changed, performance parameters are evaluated, and the influence coefficients associated with M_1 are determined. This process continues until all of the influence coefficients have been

computed.

For the UNCERT subroutine to evaluate sensitivity coefficients correctly, certain assignment statements must be added to the main program and the performance subroutine. In the main program, we must place the various measurements into the M array. For example, if there are five different measurements, then the required assignment statements would resemble

```
100       M(1) = Measurement Variable Name #1
200       M(2) = Measurement Variable Name #2
300       M(3) = Measurement Variable Name #3
400       M(4) = Measurement Variable Name #4
500       M(5) = Measurement Variable Name #5
```

The variable names would correspond to the measured parameters on which the performance calculations depend. This can be seen on lines 8800 through 10700 in this Appendix.

In the performance subroutine (TAPERF), we place all of the performance calculations into a dummy array at the end of the subroutine. This is seen on lines 79800 through 86100. The values stored in the dummy array are then placed into either a C_j or C'_j array. When we use the nominal values of the measurements to evaluate the performance parameters, we can then place and store the values of these calculations in the C_j array. When a 1 percent change in a measurement (producing M'_k) is made, the resulting performance calculations are placed in the C'_j array. Once the C'_j values have been stored, we can calculate the influence coefficients using Eqn. (A1). The user must employ a "flag" so that the program can determine whether to place the performance calculations in the C_j and C'_j array. The flag, IFLAG, must be placed into COMMON blocks in both the main program and the performance subroutine (lines 2000 and 37800, respectively). Before calling the performance subroutine in the main program, the flag is set to 0 (line 10900). In the performance subroutine, the code appears on

lines 86400 through 87100. The DC array is a dummy array. For nominal performance parameters, we set the flag at 0 and transfer the D_{C_j} array values into the C_j array. Then the flag becomes 1 (line 86500) after we have made the initial D_{C_j} assignments. The C_j values are stored and can be recalled when required. When the flag is 1 (whenever one of the measured values has been altered by 1 percent), we place the dummy values into the C'_j array so we can determine the influence coefficients.

UNCERT requires certain inputs. The B_{M_k} array, containing bias limits for each of the measurements and the S_{M_k} array, containing the precision indices for each of the measurements, must be input (as fractions) within the UNCERT subroutine (lines 20100 to 20600). The B_{M_k} values come from expert opinions, manufacturers' data, or prior testing of the instrumentation against a known standard. S_{M_k} values can come from manufacturers' data or from prior testing of the instrumentation. If Z transducers are used to determine the same measurement, then

$$S_{M_k} = \frac{S_{(\text{ 1 transducer })}}{\sqrt{Z}}$$

The resulting value should be input in the S_{M_k} array.

Finally, proper array sizes must be used in the main program, the performance subroutine, and the UNCERT subroutine. When FORTRAN IV is used, as is the case in this example, array sizing must be done in COMMON statements. Although COMMON statements are not a requirement, they do facilitate the programming.

We need two array sizes in the program, L and N; L is the total number of performance parameters, and N is the total number of measurements on which the calculations depend. In the UNCERT subroutine, we must size the BCJ, SCJ, and ANSWER arrays using L. DCODM is a two-dimensional array holding the influence coefficients and must

be sized DCODM(L,N). The M'_k array, MP, must be dimensioned in a REAL declaration using N. We size the M array in the COMMON statement using N. In other COMMON statements the C and CPRM arrays are sized using L. The DIMENSION statements and proper sizing statements are seen in lines 19300 through 19900 in the subroutine.

In the main program, we must size the M, C, and CPRM arrays in the COMMON statements as was done in the UNCERT subroutine. In the performance subroutine, the C and CPRM arrays are again dimensioned in the COMMON statements. We must write the COMMON block for the M array (in the performance subroutine) as shown in lines 36200 through 36400, since the measurement values will be input into different variables. This special COMMON block could appear in either the main program or the performance subroutine, but it should not appear in the UNCERT subroutine. The COMMON block name, DSPAR here, must be consistent throughout the main program and the two subroutines. This is true for all COMMON block names.

In the call to the UNCERT subroutine (line 13700), two integer values must be passed: L and N. After all requirements have been met and modifications completed, the program can be run to yield uncertainty results. The program outputs the nominal performance of the test article, the equation for uncertainty, bias limits, precision indices, and final uncertainty values for the performance parameters. Other output statements may be added by the user.

In summary, the application of this subroutine depends on several activities. First, a computer program must be used to find the performance of the test article. Then the performance calculations must be contained in a separate subroutine. Finally, certain assignments must be made. These are listed below.

1. The various measurements must be assigned to the M array in the main program.
2. Performance calculations must be placed in dummy array DC at the end of the performance subroutine. Proper statements must be added so that these values are placed into the C or CPRM array, depending on a flag value.
3. The M, C, and CPRM arrays must be placed in COMMON statements in the main program and the two subroutines. The COMMON block for the measurements contained in the performance subroutine must be input in a special manner (see previous page).
4. All required inputs must be made. The BMK and SMK arrays must be input as fractions in the UNCERT subroutine.
5. All array sizing must be accomplished. Some of the sizing must be accomplished in the COMMON statements.
6. The UNCERT subroutine must be called with the two integer values that represent the number of performance parameters and the number of measurements, respectively.

After running the program, the user can program additional output as desired.

WORKFILE: RUNTA5 (03/06/83)

```
  100     $RESET FREE
  200     FILE  6=OUTPUT,UNIT=PRINTER,RECCND=22
  300     C***  PROGRAM RUNTA
  400     C
  500           REAL*8 UT(64)
  600           REAL J,N,NCOR
  700           REAL M,MP(20)
  800           COMMON /ROAST/ A19    ,CD19   ,A20    ,CD20   ,R20ME ,N20SHD,G,
  900          A                J     ,RG     ,TSTD   ,PSTD   ,R25   ,A25   ,BETABL,
 1000          B                CD25  ,CDTHR  ,THRCAT,ARU    ,ARL    ,CDLE  ,RLE   ,
 1100          C                ALPVLE
 1200     C
 1300     C
 1400     C
 1500           COMMON /DSPAR/ M(20)
 1600           COMMON /PARAM/ TA(64)
 1700           COMMON /NAMEE/ UT
 1800           COMMON /NUMVS/ C(64)
 1900           COMMON /PRIMS/ CPRM(64)
 2000           COMMON /FLAGG/ IFLAG
 2100     C
 2200     C
 2300     C
 2400           DATA UT /'AM19    ',',ALCS20  ',',PT20    ',',ALPH20  ',',AM20    ',
 2500          A         'V20     ',',VL20    ',',VM20    ',',U20M    ',',BETA20  ',
 2600          B         'RM20    ',',AM2SHD  ',',V20SHD  ',',BETA2S  ',',RM2SHD  ',
 2700          C         'DELH    ',',DELHC   ',',DLTCTC  ',',U25     ',',AM25    ',
 2800          D         'ALPH25  ',',BETA25  ',',RM25    ',',PRTII   ',',PRSTI   ',
 2900          E         'DEVI    ',',ETAI    ',',W2W1    ',',HRISE   ',',PAVBF   ',
 3000          F         'VU25A   ',',SF      ',',DLTOTA  ',',DLTOT   ',',PT25    ',
 3100          G         'PREC29  ',',ALCS29  ',',AM29    ',',ETAD29  ',',PREC30  ',
 3200          H         'ALCS30  ',',AM30    ',',ETAD30  ',',PRST    ',',ETAST   ',
 3300          I         'LTAPOL  ',',PSTHR   ',',PTTHR   ',',CPU     ',',CPL     ',
 3400          J         'EFFU    ',',EFFL    ',',PRECU   ',',PRECL   ',',PRECLT  ',
 3500          K         'AMLE    ',',ALFHLE  ',',AIRCD   ',',CAPRAT  ',',HPBF    ',
 3600          L         'PRTT    ',',TRTT    ',',ETATT   ',',ETAAD'/
 3700     C
 3800     C*** CONSTANTS
 3900     C
 4000           A19=110.773
 4100           CD19=.98
 4200           A20=104.391
 4300           CD20=.98
 4400           R20ME=4.93375
 4500           N20SHD=6.6175
 4600           G=32.2
 4700           J=778.16
 4800           RG=53.349
 4900           TSTD=518.688
 5000           PSTD=14.696
 5100           R25=9.998
 5200           A25=38.32605
 5300           BETABL=39.0
 5400           CD25=0.9
 5500           CDTHR=1.0
 5600           THRCAT=1.156
 5700           ARU=1.57
 5800           ARL=1.56
 5900           CDLE=0.96
 6000           RLE=10.7125
 6100           ALPVLE=75.37
 6200     C
 6300     C*** DATA SCAN PARAMETERS
 6400     C
 6500           PT19=17.401
 6600           TT20=524.190
 6700                NCOR=24.888
 6800           WAV=NCOR*(PT19/PSTD)/SQRT(TT20/TSTD)
 6900                NLOW=22999.0
```

```
 7000           N=NCOR*SQRT(TT20/TSTD)
 7100           TT30=1024.079
 7200           PS2SHD=14.205
 7300           PS25=70.590
 7400           PS29=131.886
 7500           PS30=132.500
 7600           PT29=139.889
 7700           PT30=139.800
 7800           PSTHRU=115.546
 7900           PSTHRL=107.645
 8000           PSEXU=128.972
 8100           PSEXL=129.699
 8200           PSLE=80.757
 8300           BDIFF=0.61
 8400           ALPHIG=.01
 8500           SH=0.01092
 8600           Z25=1.
 8700     C
 8800           M(1)=PT19
 8900           M(2)=TT20
 9000           M(3)=WAV
 9100           M(4)=N
 9200           M(5)=TT30
 9300           M(6)=PS2SHD
 9400           M(7)=PS25
 9500           M(8)=PS29
 9600           M(9)=PS30
 9700           M(10)=PT29
 9800           M(11)=PT30
 9900           M(12)=PSTHRU
10000           M(13)=PSTHRL
10100           M(14)=PSEXU
10200           M(15)=PSEXL
10300           M(16)=PSLE
10400           M(17)=BDIFF
10500           M(18)=ALPHIG
10600           M(19)=SH
10700           M(20)=Z25
10800     C
10900           IFLAG=0
11000     C
11100           CALL TAPERF
11200     C
11300           WRITE(6,98)
11400      98   FORMAT(1X,'NOMINAL VALUES OF CALCULATED PARAMETERS',///)
11500           WRITE(6,100)(UT(I1),I1=1,10)
11600      100  FORMAT(1X,2X,10(A6,7X)/)
11700           WRITE(6,102)(TAC(J1),J1=1,10)
11800      102  FORMAT(1X,10(E11.4,2X)//)
11900           WRITE(6,100)(UT(I2),I2=11,20)
12000           WRITE(6,102)(TAC(J2),J2=11,20)
12100           WRITE(6,100)(UT(I3),I3=21,30)
12200           WRITE(6,102)(TAC(J3),J3=21,30)
12300           WRITE(6,100)(UT(I4),I4=31,40)
12400           WRITE(6,102)(TAC(J4),J4=31,40)
12500           WRITE(6,100)(UT(I5),I5=41,50)
12600           WRITE(6,102)(TAC(J5),J5=41,50)
12700           WRITE(6,100)(UT(I6),I6=51,60)
12800           WRITE(6,102)(TAC(J6),J6=51,60)
12900           WRITE(6,104)(UT(I7),I7=61,64)
13000      104  FORMAT(1X,2X,4(A6,7X)/)
13100           WRITE(6,106)(TAC(J7),J7=61,64)
13200      106  FORMAT(1X,4(E11.4,2X)//)
13300     C
13400      60   FORMAT(1H1)
13500      63   FORMAT(1X,2X,10(A6,7X),/)
13600     C
13700           CALL UNCERT(64,20)
13800     C
13900           STOP
14000           END
```

```
14100     C*************************************************************
14200     C     NAME-
14300     C          UNCERT                          18 NOVEMBER 1982
14400     C          UNCERTAINTY CALCULATIONS
14500     C
14600     C     SYSTEM-
14700     C             BURROUGHS 6900
14800     C
14900     C     PROGRAMMER-
15000     C                  CHRISTOPHER A. BOEDICKER     CIC/USAF ACADEMY
15100     C
15200     C     PURPOSE-
15300     C              THIS MODULE CALCULATES UNCERTAINTIES IN PARAMETERS
15400     C              SPECIFIED BY THE USER.  THE METHOD IS THE ONE USED
15500     C              BY DR. ABERNETHY.
15600     C
15700     C     FUNCTIONAL AREA-
15800     C
15900     C
16000     C
16100     C     USAGE-
16200     C
16300     C
16400     C
16500     C      CALLING SEQUENCE-
16600     C
16700     C
16800     C
16900     C
17000     C      COMMON STORAGE-
17100     C                        M(ARRAY HOLDING NOMINAL MEASURED VALUES)
17200     C                        C(ARRAY HOLDING NOMINAL CALCULATED VALUES)
17300     C                        CPRM(ARRAY HOLDING VALUES OF THE CALCULATED
17400     C                             PARAMETERS AFTER A CHANGE IN THE MEASURED
17500     C                             VALUE HAS BEEN MADE)
17600     C
17700     C      EXTERNAL REFERENCES-
17800     C                             GPPRD(GENERAL MATRIX PRODUCT)
17900     C                             TAPERF(TEST ARTICLE PERFORMANCE)
18000     C
18100     C     FILES USED-
18200     C
18300     C       INPUT/OUTPUT-
18400     C                  THE BIAS LIMIT(BMK IN %) AND THE
18500     C                  PRECISION INDEX(SMK IN %) FOR EACH OF THE MEASUREMENTS
18600     C                  MUST BE INPUT.
18700     C                  BIAS AND PRECISION ERRORS, ALONG WITH THE ANSWER,
18800     C                  ARE OUTPUT FOR EACH OF THE CALCULATED PARAMETERS.
18900     C                  THESE ARE GIVEN IN PERCENT.
19000     C*************************************************************
19100           SUBROUTINE UNCERT(L,N)
19200     C
19300           DIMENSION UCOEM(64,20),RC_(64),SCJ(64)
19400           DIMENSION DELTAM(20),DELTAC(64),ANSWER(64),BMK(20),SMK(20)
19500     C
19600           REAL M,MP(20)
19700           COMMON /USPAR/ M(20)
19800           COMMON /NOMVS/ C(64)
19900           COMMON /PRIMS/ CPRM(64)
20000     C
20100           DATA BMK/.0016,.00215,.005,0.,.00215,.0016,.0016,9*.0016,2*.003,
20200          A        .002,.0025/
20300     C
20400           DATA SMK/.00047,.00017,.0025,.000016,.0001C,.00354,.00118,.00177,
20500          A        .00125,.00088,.00088,.0025,.0025,.00289,.00289,.00177,
20600          B        .0004,.0004,.00054,.001257
20700     C
20800           DO 10 K=1,N
20900           IF(M(K).EQ.0.)P(K)=.01/1.01
21000      10   MP(K)=1.01*M(K)
21100     C
21200     C
```

```
21300           DO 20 K=1,N
21400           DUM=M(K)
21500           M(K)=MP(K)
21600     C
21700           CALL TAPERF
21800     C
21900           M(K)=DUM
22000     C
22100           IF(M(K).EQ.0.)WRITE(6,15)
22200      15   FORMAT(1X,'PROGRAM STOPPED SINCE A MEASURED PARAMETER IS ZERO')
22300           IF(M(K).EQ.0.)STOP 1111
22400     C
22500           DO 17 J=1,L
22600           IF(C(J).EQ.0.)WRITE(6,16)
22700      16   FORMAT(1X,'PROGRAM STOPPED SINCE A CALCULATED PARAMETER IS ZERO')
22800           IF(C(J).EQ.0.)STOP 1112
22900      17   CONTINUE
23000     C
23100           DELTAM(K)=(MP(K)-M(K))/M(K)
23200           DO 18 J=1,L
23300           DELTAC(J)=(CPRP(J)-C(J))/C(J)
23400           DCODM(J,K)=DELTAC(J)/DELTAM(K)
23500      18   CONTINUE
23600     C
23700      20   CONTINUE
23800     C
23900           DO 70 J=1,L
24000           DO 70 K=1,N
24100           DCODM(J,K)=(DCODM(J,K))**2
24200      70   CONTINUE
24300     C
24400           DO 75 K=1,N
24500           BMK(K)=BMK(K)**2
24600           SMK(K)=SMK(K)**2
24700      75   CONTINUE
24800     C
24900           CALL GMPRD(DCODM,BMK,BCJ,L,N,1)
25000           CALL GMPRD(DCODM,SMK,SCJ,L,N,1)
25100     C
25200           DO 77 J=1,L
25300           BCJ(J)=SQRT(BCJ(J))
25400           SCJ(J)=SQRT(SCJ(J))
25500           ANSWER(J)=BCJ(J)+2.0*SCJ(J)
25600      77   CONTINUE
25700     C
25800           DO 78 J=1,L
25900           ANSWER(J)=ANSWER(J)*100.
26000      78   CONTINUE
26100     C
26200           WRITE(6,60)
26300           WRITE(6,67)
26400     C
26500           WRITE(6,60)
26600           WRITE(6,65)
26700           DO 85 J=1,L
26800           WRITE(6,66)J,BCJ(J),SCJ(J),ANSWER(J)
26900      85   CONTINUE
27000     C
27100     C
27200      60   FORMAT(1H1)
27300      61   FORMAT(1X,10(E11.4,2X))
27400      65   FORMAT(1X,5X,'PARAMETER #',7X,'BIAS LIMIT',11X,'PRECISION INDEX',
     A 6X,'UNCERTAINTY',/)
27500      66   FORMAT(1X,10X,I2,9X,E11.4,12X,E11.4,10X,E9.2)
27600      67   FORMAT(1X,10X,'THE EQUATION USED TO DETERMINE THE UNCERTAINTIES'
     A' IS',///,11X,'U = B + 2 * S',///,11X,'B IS DEFINED AS THE BIAS'
     B' LIMIT, AND S IS DEFINED AS THE PRECISION INDEX',///,11X,
     C'THE VALUE OF T95(2) COMES FROM THE TWO-TAILED STUDENTS T'
     D' DISTRIBUTION')
28100     C
28200           RETURN
28300           END
```

```
C * * * * * * * * * * * * * * * * * * * * * * * * * * * * * * * * * * * * * *
C
      SUBROUTINE GMPRD(A,B,R,N,M,L)
      DIMENSION A(1),B(1),R(1)
      IR=0
      IK=-M
      DO 10 K=1,L
      IK=IK+M
      DO 10 J=1,N
      IR=IR+1
      JI=J-N
      IB=IK
      R(IR)=0
      DO 10 I=1,M
      JI=JI+N
      IB=IB+1
   10 R(IR)=R(IR)+A(JI)*B(IB)
      RETURN
      END
C * * * * * * * * * * * * * * * * * * * * * * * * * * * * * * * * * * * * * *
C
C NAME -
C     TAPERF     5/25/82
C     GARRETT CENTRIFUGAL COMPRESSOR PERFORMANCE
C
C SYSTEM -
C     IBM 370/155 (MAIN COMPUTER)
C
C PROGRAMMERS-
C     MARK S. ORR AFWAL/POTX  PURDUE UNIVERSITY CO-OP STUDENT
C     CHRISTOPHER A. BOEDICKER  USAF ACADEMY/CS-20
C
C PURPOSE -
C     THIS MODULE DOES COMPRESSOR PERFORMANCE CALCULATIONS
C     SPECIFIED BY GARRETT
C
C FUNCTIONAL AREA -
C     MAIN COMPUTER COMPRESSOR PERFORMANCE
C
C USAGE -
C     CALLED BY IFPERF FOR EACH DATA ACQUISITION POINT THAT IS TO
C     BE PROCESSED.
C
C CALLING SEQUENCE -
C (W) EU      - MEASURED PARAMETERS ENGINEERING UNITS
C (R) PC      - PERFORMANCE CONSTANTS
C (R) MODE    - DATA ACQUISITION MODE(1=MCN,2=STATIC,3=TRAN,4=ABORT)
C (R) BAROM   - BAROMETRIC PRESSURE
C (W) KKK     - BUFFER CONTAINING COMPRESSOR CONFIGURATION CODE
C
C COMMON STORAGE -
C     NONE
C
C EXTERNAL REFERENCES -
C     ACOS , AFAN , COS , CPTBL , ITRAT2 ,ALOG , SIN , SQRT , TAN , UVAR
C
C FILES USED -
C     DATA BASE RECORD NUMBER 20 - ENGINEERING UNITS, M
C     DATA BASE RECORD NUMBER 25 - PERFORMANCE CONSTANTS, R
C
C INPUT/OUTPUT -
C     NONE
C
C * * * * * * * * * * * * * * * * * * * * * * * * * * * * * * * * * * * * * *
      SUBROUTINE TAPERF
C     DIMENSION ALPH(18),CC(64),CPRM(64)
C   LINE ABOVE REPLACED WITH LINE BELOW TO DELETE C (DIM AT 3370), AND
C   CPRM (DIM AT 3380).
      DIMENSION ALPH(18),CC(64)
      REAL J,N,MU25,MCOR,M(20)
      COMMON /KONST/ A19    ,CD19   ,A20    ,CD2C   ,R2OME ,R2OSHD,G,
     A               J      ,RG     ,TSTD   ,PSIC   ,M25   ,A25   ,BETABL,
     B               CD25   ,CDTHR  ,THRCAT,ARU    ,AHL   ,CDLE  ,RLE   ,
     C               ALPVLE
```

```
35900     C
36000     C
36100     C
36200           COMMON /USPAR/ PT19  ,TT20  ,WAV   ,N     ,TT30  ,PS2SHD,PS25  ,
36300          A               PS29  ,PS30  ,PT29  ,PT30  ,PSTHRU,PSTHRL,PSEXU ,
36400          B               PSEXL ,PSLE  ,RDIFF ,ALPHIG,SH,Z25
36500     C
36600           COMMON /PARAM/ AM19  ,ALOS20,PT20  ,ALPH20,AM20  ,V20   ,
36700          A               VU20  ,VM20  ,U20M  ,BETA20,RP20  ,AM2SHD,
36800          B               V2OSHD,BETA2S,RP2SHD,DELP  ,DELHC ,DLTCTC,
36900          C               U25   ,AM25  ,ALPH25,BETA25,RM25  ,PRTTI ,
37000          D               PRSTI ,DEVI  ,ETAI  ,W2W1  ,HRISE ,PAVBF ,
37100          E               VU25A ,SF    ,DLTCTA,DLTCT ,PT25  ,PREC29,
37200          F               ALOS29,AM29  ,ETAD29,PREC30,ALOS30,AM30  ,
37300          G               ETAD30,PRST  ,ETAST ,ETAFCL,PSTHR ,PTTHR ,
37400          H               CPU   ,CPL   ,EFFU  ,EFFL  ,PRECU ,PRECL ,
37500          I               PRECLT,AMLE  ,ALPHLE,AINCD ,CAPRAT,HPBF,
37600          J               PRTT  ,TRTT  ,ETATT ,ETAAD
37700     C
37800           COMMON /FLAGG/ IFLAG
37900           COMMON /NORVS/ C(64)
38000           COMMON /PRIMS/ CPRM(64)
38100     C
38200           DATA ALPH/0.0,60.0,0.0,14.1,0.0,.02,5.0,.02,10.0,.02,20.0,.02,
38300          A30.0,.0205,40.0,.026,60.0,.039/
38400     500   FORMAT(5X,E12.5)
38500           GC=32.2
38600           PI=3.14159
38700           FA=0.0
38800           HC=0.0
38900     C*** CALCULATE HSTD BASED ON TSTD
39000           CALL CPTBL(TSTD,HSTD,RPSTD,FA,HC,SH,1,RG,GAMMA,CP,RA,CX)
39100     C*** CALCULATE GAM2,HT20,AND RP20 AT TT20
39200           CALL CPTBL(TT20,HT20,RP20,FA,HC,SH,1,RG,GAM2,CP,RA,CX)
39300     C
39400     C
39500     C*** ITERATE FOR AM19
39600           G1=.5*(GAM2+1.0)/(GAM2-1.0)
39700           G2=.5*(GAM2-1.0)
39800           WDTM1=0.0
39900           WDTM2=0.0
40000           AM19=.5
40100           AMN4=1.0
40200           WDTM=WAV*SQRT(TT20)/(PT19*CD19*A19)
40300     5     CONTINUE
40400     C
40500                 DUM1=GAM2*GC/RG
40600                 IF(DUM1.LT.0.0) WRITE(6,500) DUM1
40700                 IF(DUM1.LT.0.0) STOP 1001
40800     C
40900           WDTM3=SQRT(GAM2*GC/RG)*AM19*((1.0+G2*(AM19**2))**(-G1))
41000           IF(ABS(WDTM3-WDTM).LT..0001) GOTO 7
41100           CALL ITRAT2(WDTM1,AMN1,WDTM2,AMN2,WDTM3,AM19,WDTM,AMN4)
41200           GOTO 5
41300     7     CONTINUE
41400     C*** TABLE LOOKUP FOR ALOS20
41500           ALOS20=UVAM(ALPH,ALPHIG)
41600     C
41700     C
41800     C*** CALCULATE PSPT19
41900           PSPT19=(1.0+G2*(AM19**2))**(-(GAM2/(GAM2-1.0)))
42000           DPTIGV=PT19*ALLS20*(1.0-PSPT19)
42100           PT20=PT19-DPTIGV
42200           DIGV=0.0
42300           ALPH20=ALPHIG*PI/180.
42400     C*** ITERATE FOR AM20
42500           WDTM1=0.0
42600           WDTM2=0.0
42700           AM20=.5
42800           AMN4=1.0
42900           WDTM=WAV*SQRT(TT20)/(PT20*CD20*A20*COS(ALPH20))
```

```
43000    15    CONTINUE
43100    C
43200    C
43300          WDTM3=SQRT(GAM2*GC/RG)*AM2O*((1.0+G2*(AM2O**2))**(-G1))
43400          IF(ABS(WDTM3-WDTP).LT..0001) GOTO 17
43500          CALL ITRAT2(WDTM1,AMN1,WDTM2,AMN2,WDTM3,AM2O,WDTM,AMN4)
43600          GOTO 15
43700    17    CONTINUE
43800    C
43900    C
44000               DUM2=1.0+G2*(AM2O**2)
44100               IF(DUM2.LT.0.0) WRITE(6,500) DUM2
44200               IF(DUM2.LT.0.0) STOP 1002
44300    C
44400          V2AT2O=AM2O/SQRT(1.0+G2*(AM2O**2))
44500    C
44600               DUM3=GAM2*GC*RG*TT2O
44700               IF(DUM3.LT.0.0) WRITE(6,500) DUM3
44800               IF(DUM3.LT.0.0) STOP 1003
44900    C
45000          AT2O=SQRT(GAM2*GC*RG*TT2O)
45100          V2O=V2AT2O*AT2O
45200          VU2O=V2O*(SIN(ALPH2O))
45300          VM2O=V2O*(COS(ALPH2O))
45400          U2OM=2.0*PI*N*R2OME/(60.*12.)
45500          BETA2O=ATAN((U2OM-VU2O)/VM2O)
45600          RM2O=AM2O*(COS(ALPH2O)/COS(BETA2O))
45700    C
45800               DUM4=(((PT2O/PS2SHD)**(G2*2./GAM2))-1.0)/G2
45900               IF(DUM4.LT.0.0) WRITE(6,500) DUM4
46000               IF(DUM4.LT.0.0) STOP 1004
46100    C
46200    C
46300    C
46400          AM2SHD=SQRT((((PT2O/PS2SHD)**(G2*2./GAM2))-1.0)/G2)
46500    C
46600               DUM5=1.0+G2*(AM2SHD**2)
46700               IF(DUM5.LT.0.0) WRITE(6,500) DUM5
46800               IF(DUM5.LT.0.0) STOP 1005
46900    C
47000          VAT2SD=AM2SHD/SQRT(1.0+G2*(AM2SHD**2))
47100          V2OSHD=VAT2SD*AT2O
47200          VU2SHD=V2OSHD*SIN(ALPH2O)
47300          VM2SHD=V2OSHD*COS(ALPH2O)
47400          U2SHD=U2OM*R2OSHD/R2OME
47500          BETA2S=ATAN((U2SHD-VU2SHD)/VM2SHD)
47600          RM2SHD=AM2SHD*COS(ALPH2O)/COS(BETA2S)
47700          W2OSHD=RM2SHD*SQRT(GAM2*GC*RG*TT2O/(1.0+G2*(AM2SHD**2)))
47800    C*** CALCULATE HT2O AT TT2O
47900          CALL CPTBL(TT2O,HT2O,RP2O,FA,HC,SH,1,RG,GM2,CP2,NN,CX)
48000    C*** CALCULATE HT3O AT TT3O
48100          CALL CPTBL(TT3O,HT3O,RP3O,FA,HC,SH,1,RG,GAP3,CP3,NN,CX)
48200    C
48300    C
48400          DELH=HT3O-HT2O
48500          DELHC=DELH*TSTO/TT2O
48600          HT3OC=HSTD+DELHC
48700    C*** CALCULATE TT3OC AT HT3OC
48800          CALL CPTBL(TT3OC,HT3OC,RP3OC,FA,HC,SH,2,RG,GM3C,CP3C,NN,CX)
48900          DTTC=TT3OC-TSTD
49000          DLTGTC=DTTC/TSTD
49100    C*** CALCULATE CP AT ((TT3OC+TT2O)/2.0
49200          T3CSD2=(TT3OC+TT2O)/2.0
49300          CALL CPTBL(T3CSD2,E,HP,FA,HC,SH,1,RG,GAM3CS,CPIAV,NN,CX)
49400          U25=U2OM*R25/R2OME
49500    C*** ITERATE FOR TS25
49600          TT3CM1=0.0
49700          TT3CM2=0.0
49800          TS25=TT3C
49900          TSN4=TT3O-10.
50000    C
```

```
50100           VU25=(CPIAV*DTTC*GC*J*L2CP*VU20)/U25
50200           PCA=PS25*CD25*A25
50300     C
50400           Q=0.
50500     C
50600     25    CONTINUE
50700           CALL CPTBL(TS25,E,RP,FA,HC,SH,1,RG,GAM25,CP,AN,CX)
50800     C
50900                IF(GAM25.EQ.0.0) STOP 5525
51000     C
51100           BB1=(VU25**2.)/(GAM25*GC*RG*TT30C)
51200           G3=.5*(GAM25-1.0)
51300           AA=G3*(G3**2)*BB1
51400           BB2=1.0-(GAM25-1.0)*BB1
51500     C
51600                DUM6=RG/(GAM25*GC)
51700                IF(DUM6.LT.0.0) WRITE(6,500) DUM6
51800                IF(DUM6.LT.0.0) STOP 1006
51900     C
52000           CC=-BB1*(((Z25*WAV*SQRT(TT30)/PCA)*SQRT(RG/(GAM25*GC)))**2
52100     C
52200                DUM7=(BB2**2)-4.*AA*CC
52300                IF(DUM7.LT.0.0) WRITE(6,500) DUM7
52400                IF(DUM7.LT.0.0) STOP 1007
52500                DUM8=(-BB2+SQRT(DUM7))/(2.*AA)
52600                IF(DUM8.LT.0.0) WRITE(6,500) DUM8
52700                IF(DUM8.LT.0.0) STOP 1008
52800     C
52900           AM25=SQRT((-BB2+SQRT((BB2**2)-4.*AA*CC))/(2.*AA))
53000           TT3CM3=TS25*(1.0+G3*(AM25**2))
53100     C
53200           Q=Q+1.
53300           IF(Q.GT.40.)WRITE(6,993)TT3CM3,TT30C
53400           IF(Q.GT.40)GOTO 27
53500      993  FORMAT(1X,'TT3CM3=',F15.9,3X,'TT30C=',F15.9,5X,'LOOP EXITED')
53600     C
53700           IF(ABS(TT3CM3-TT30C).LT..001) GOTO 27
53800     C
53900           IF(Q.GE.20.)TT3CM3=TT3CM3+.25
54000     C
54100           CALL ITRAT2(TT3CM1,TSN1,TT3CM2,TSN2,TT3CM3,TS25,TT30C,TSN4)
54200     C
54300           GOTO 25
54400     27    CONTINUE
54500     C
54600     C
54700                G3A252=1.0+G3*(AM25**2)
54800     C
54900                DUM9=GAM25*GC/(RG*TT30)
55000                IF(DUM9.LT.0.0) WRITE(6,500) DUM9
55100                IF(DUM9.LT.0.0) STOP 1009
55200     C
55300                SQGRT=SQRT(GAM25*GC/(RG*TT30))
55400     C
55500                DUM10=BB1
55600                IF(DUM10.LT.0.0) WRITE(6,500) DUM10
55700                IF(DUM10.LT.0.0) STOP 1010
55800     C
55900           ALPH25=ATAN(SQRT(BB1)*(G3A252)*(PS25*CD25*A25/(Z25*WAV)))*SQGRT)
56000     C
56100                DUM11=GAM25*GC*RG*TT30C
56200                IF(DUM11.LT.0.0) WRITE(6,500) DUM11
56300                IF(DUM11.LT.0.0) STOP 1011
56400     C
56500                DUM12=1.0+G3*(AM25**2)
56600                IF(DUM12.LT.0.0) WRITE(6,500) DUM12
56700                IF(DUM12.LT.0.0) STOP 1012
56800     C
56900           V25=AM25*SQRT(GAM25*GC*RG*TT30C)/SQRT(1.0+G3*(AM25**2))
57000           VM25=V25*COS(ALPH25)
57100           BETA25=ATAN(U25/VM25-TAN(ALPH25))
57200           RP25=AM25*COS(ALPH25)/COS(BETA25)
57300           PT25=PS25*((1.0+G3*(AM25**2))**(GAM25/(GAM25-1.0)))
```

```
57400           PRTTI=PT25/PT19
57500           PRSTI=PS25/PT19
57600           DEVI=BETA25-(BETABL*PI/180.)
57700           PSI=VU25/U25
57800           PHI=VM25/U25
57900           HIN=HT20
58000           HEX=HT30
58100     C*** CALCULATE HISEN(HPISEN) WHERE HPISEN=HP20*PRTTI
58200           HPISEN=HP20*PRTTI
58300     C
58400                DUM23R=HPISEN
58500                IF(DUM23R.LE.0.0) WRITE(6,500) DUM23R
58600                IF(DUM23R.LE.0.0) STOP 1023
58700     C
58800           CALL CPTBLC(TISEN,HISEN,PPISEN,FA,HC,SH,3,RG,CAMISE,CPISE,NN,CX)
58900           ETAI=(HISEN-HIN)/(HEX-HIN)
59000           W2W1=VM25/(W20SHD*COS(BETA25))
59100           HRISE=HEX-HIN
59200           PAVBF=PS25*(1.0-(U25**2)/(16.*GC*RG*TT30))
59300           MU25=(2.257E-8)*(TT30**(1.5))/(TT30C+198.6)
59400           RHO=PAVBF*144./(Z25*RG*TT30)
59500     C
59600     C
59700           REN=RHO*U25*R25/(12.*MU25*GC)
59800           CMBF=0.03194/(REN**0.2)
59900     C
60000     C
60100           CM=RHO*(U25**2)*CMBF*(R25**3)/(1728.*2.*GC)
60200           HPBF=CM*N*2.*PI/33000.
60300           DFDEL=550.*HPBF/(J*WAV)
60400           HAERO1=HRISE-DFDEL
60500           HAERO2=HEX-DFDEL
60600           VU25A=(GC*J*HAERO1*U20M*VU20)/U25
60700     C
60800     C
60900           SF=VU25A/(U25-VM25*TAN(BLTABL*PI/180.))
61000     C*** CALCULATE TAERO(HAERO2)
61100           CALL CPTBLC(TAERO,HAERO2,RPAERO,FA,HC,SH,2,RG,GAMAER,CPAER,NN,CX)
61200           DLTOTA=(TAERO-TT20)/TT20
61300           DLTOT=(TT30-TT20)/TT20
61400     C*** CALCULATE GAMC((TT30+TT20)/2.)
61500           T312AV=(TT30+TT20)/2.0
61600           CALL CPTBLC(T3T2AV,H32AV,RP32AV,FA,HC,SH,1,RG,GAMC,CP32AV,NN,CX)
61700           PT25=PT19*((DLTOT*ETAI+1.0)**(GAMC/(GAMC-1.0)))
61800           PREC29=(PS29-PS25)/(PT25-PS25)
61900           ALOS29=(PT25-PT29)/(PT25-PS25)
62000     C*** CALCULATE GAMD((TT30+TS25)/2.0)
62100           TST25A=(TT30+TS25)/2.0
62200           CALL CPTBLC(T3T25A,H325AV,RP325A,FA,HC,SH,1,RG,GAMD,CP325A,NN,CX)
62300     C
62400                DUM13=(2./(GAMD-1.))*(((PS29/PT29)**(-(GAMD-1.)/GAMD))-1.)
62500                IF(DUM13.LT.0.0) WRITE(6,500) DUM13
62600                IF(DUM13.LT.0.0) STOP 1013
62700     C
62800     C
62900     C
63000           AM29=SQRT((2./(GAMD-1.0))*(((PS29/PT29)**(-(GAMD-1.)/GAMD))-1.))
63100           TS29=TT30/(1.0+((GAMD-1.0)/2.)*(AM29**2))
63200           ETAD29=(((PS29/PS25)**((GAMD-1.)/GAMD))-1.)/((TS29/TS25)-1.)
63300           PREC30=(PS30-PS25)/(PT25-PS25)
63400           ALOS30=(PT25-PT30)/(PT25-PS25)
63500     C
63600                DUM14=(2./(GAMD-1.))*(((PS30/PT30)**(-(GAMD-1.)/GAMD))-1.)
63700                IF(DUM14.LT.0.0) WRITE(6,500) DUM14
63800                IF(DUM14.LT.0.0) STOP 1014
63900     C
64000           AM30=SQRT((2./(GAMD-1.))*(((PS30/PT30)**(-(GAMD-1.)/GAMD))-1.))
64100           TS30=TT30/(1.+.5*(GAMD-1.)*(AM30**2))
64200           ETAD30=(((PS30/PS25)**((GAMD-1.)/GAMD))-1.)/((TS30/TS25)-1.)
64300           PRTT=PT30/PT19
64400           PRST=PS30/PT19
64500     C*** CALCULATE HISEN(HPISET) WHERE HPISET=HP20*PRTT
```

```
      RPISET=RP20*PRTT
C
           DUM24R=RPISET
           IF(DUM24R.LE.0.0) WRITE(6,500)
           IF(DUM24R.LE.0.0) STOP 1024
C
      CALL CPTBL(TISENT,HISENT,RPISET,FA,HC,SH,3,RG,GAMIST,CPISET,NN,CX)
C*** CALCULATE HISENS(RPISES) WHERE RPISES=RP20*PRST
      RPISES=RP20*PRST
C
           DUM25R=RPISES
           IF(DUM25R.LE.0.0) WRITE(6,500) DUM25R
           IF(DUM25R.LE.0.0) STOP 1025
C
C
C
      CALL CPTBL(TISENS,HISENS,RPISES,FA,HC,SH,3,RG,GAMISS,CPISES,NN,CX)
      ETATT=(HISENT-HT20)/(HT30-HT20)
      ETAST=(HISENS-HT20)/(HT30-HT20)
      PHIREF=0.57839
C
           DUM15L=RP20
           IF(DUM15L.LE.0.0) WRITE(6,500) DUM15L
           IF(DUM15L.LE.0.0) STOP 1015
C
      PHIT20=(RG*ALOG(RP20)/J)+PHIREF
C
           DUM16L=RP30
           IF(DUM16L.LE.0.0) WRITE(6,500) DUM16L
           IF(DUM16L.LE.0.0) STOP 1016
C
      PHIT30=(RG*ALOG(RP30)/J)+PHIREF
C*** CALCULATE PHIISE(RPISET)
C
           DUM17L=RPISET
           IF(DUM17L.LE.0.0) WRITE(6,500) DUM17L
           IF(DUM17L.LE.0.0) STOP 1017
C
C
C
      PHIISE=(RG*ALOG(RPISET)/J)+PHIREF
      ETAPOL=(PHIISE-PHIT20)/(PHIT30-PHIT20)
C
C
      PSTHR=(PSTHRG+PSTHRL)/2.0
      ATHR=THRCAT*BDIFF*21.
      G4=2./(GAM3+1.0)
      G5=.5*(GAM3+1.0)/(GAM3-1.0)
      G6=.5*(GAM3-1.0)
      WDTM1=0.0
      WDTM2=0.0
      AMTHR=.5
      AMN4=1.0
      WDTM=WAV*SQRT(TT30)/(CDTHR*ATHR*PSTHR)
35    CONTINUE
C
C
           DUM18=GAM3*GC/RG
           IF(DUM18.LT.0.0) WRITE(6,500) DUM18
           IF(DUM18.LT.0.0) STOP 1018
C
           DUM19=1.0+G6*(AMTHR**2)
           IF(DUM19.LT.0.0) WRITE(6,500) DUM19
           IF(DUM19.LT.0.0) STOP 1019
C
      WDTM3=SQRT(GAM3*GC/RG)*AMTHR*SQRT(1.0+G6*(AMTHR**2))
      IF(ABS(WDTM3-WDTM).LT..0001) GOTO 37
      CALL ITRAT2(WDTM1,AMN1,WDTM2,AMN2,WDTM3,AMTHR,WDTM,AMN4)
      GOTO 35
37    CONTINUE
      PTTHR=PSTHR*((1.0+G6*(AMTHR**2))**(GAM3/(GAM3-1.0)))
      CPU=(PSEXU-PSTHRL)/(PTTHR-PSTHRU)
```

```
71800           CPL=(PSLXL-PSTHRL)/(PTTHR-PSTHRL)
71900           AASTHR=(G4*((1.0+G6*(AMTHR**2))**G5))/AMTHR
72000           AASEXU=AASTHR*ARL
72100           AASEXL=AASTHR*ARL
72200           AAS1=0.0
72300           AAS2=0.0
72400           AMEXU=.5
72500           AMN4=1.0
72600     45    CONTINUE
72700     C
72800     C
72900           AAS3=(G4*((1.+G6*(AMEXL**2))**G5))/AMEXU
73000           IF(ABS(AAS3-AASEXU).LT..0001)GO TO 47
73100           CALL ITRAT2(AAS1,AMN1,AAS2,AMN2,AAS3,AMEXU,AASEXU,AMN4)
73200           GO TO 45
73300     47    CONTINUE
73400     C
73500     C
73600           AAS1=0.0
73700           AAS2=0.0
73800           AMEXL=.5
73900           AMN4=1.0
74000     55    CONTINUE
74100     C
74200     C
74300           AAS3=(G4*((1.0+G6*(AMEXL**2))**G5))/AMEXL
74400           IF(ABS(AAS3-AASEXL).LT..0001) GOTO 57
74500           CALL ITRAT2(AAS1,AMN1,AAS2,AMN2,AAS3,AMEXL,AASEXL,AMN4)
74600           GOTO 55
74700     57    CONTINUE
74800     C
74900     C
75000           PREXU=(1.0+G6*(AMEXU**2))**(-(GAM3/(GAM3-1.0)))
75100           PSEXUI=PREXU*PITHR
75200           PREXL=(1.0+G6*(AMEXL**2))**(-(GAM3/(GAM3-1.0)))
75300           PSEXLI=PREXL*PITHR
75400           EFFU=(PSEXU-PSTHRU)/(PSEXUI-PSTHRU)
75500           EFFL=(PSEXL-PSTHRL)/(PSEXLI-PSTHRL)
75600           PRECU=(PSEXU-PSTHRU)/(PTTHR-PSTHRU)
75700           PRECL=(PSEXL-PSTHRL)/(PTTHR-PSTHRL)
75800           PRECLT=(PSTHR-PS25)/(PT25-PS25)
75900           PRLE=PSLE/PT25
76000     C
76100     C
76200     C
76300                DUM20=((PRLE**(-(GAM3-1.0)/GAM3))-1.0)/G6
76400                IF(DUM20.LT.0.0) WRITE(6,500) DUM20
76500                IF(DUM20.LT.0.0) STOP 1020
76600     C
76700           AMLE=SQRT(((PRLE**(-(GAM3-1.0)/GAM3))-1.0)/G6)
76800     C
76900                DUM21=GAM3/(RG*GC)
77000                IF(DUM21.LT.0.0) WRITE(6,500) DUM21
77100                IF(DUM21.LT.0.0) STOP 1021
77200     C
77300                DUM22=1.0+G6*(AMLE**2)
77400                IF(DUM22.LT.0.0) WRITE(6,500) DUM22
77500                IF(DUM22.LT.0.0) STOP 1022
77600     C
77700     C
77800     C
77900           CHI=SQRT(GAM3/(RG*GC))*AMLE*SQRT(1.0+G6*(AMLE**2))
78000           AEFF=WAV*SQRT(TT30)/(CHI*PSLE*GC)
78100           CD=AEFF/(2.0*PI*RLE*BDIFF)
78200           ALPHLE=ARCOS(CD/CDLE)
78300           ATNCD=ALPHLE-ALPVLE*PI/180.
78400           CAPRAT=ATHR/AEFF
78500           PRTT=PT30/PT19
78600           THTT=TT30/TT20
78700           ETAAD=(PHTT**((GAMC-1.)/GAMC)-1.)/(THTT-1.)
78800     C
78900           ALPH20=ALPH20*180./PI
```

```
79000           BETA20=BETA20*180./PI
79100           BETA2S=BETA2S*180./PI
79200           ALPH2S=ALPH2S*180./PI
79300           BETA2S=BETA2S*180./PI
79400           DEVI=DEVI*180./PI
79500           ALPHLE=ALPHLE*180./PI
79600           AINCD=AINCD*180./PI
79700     C
79800           DC(1)=AM19
79900           DC(2)=ALDS20
80000           DC(3)=PT20
80100           DC(4)=ALPH20
80200           DC(5)=AM20
80300           DC(6)=V20
80400           DC(7)=VU20
80500           DC(8)=VM20
80600           DC(9)=U20M
80700           DC(10)=BETA20
80800           DC(11)=RM20
80900           DC(12)=AM2SHD
81000           DC(13)=V20SHD
81100           DC(14)=BETA2S
81200           DC(15)=RM2SHD
81300           DC(16)=DELH
81400           DC(17)=DELHC
81500           DC(18)=DLTUTC
81600           DC(19)=U25
81700           DC(20)=AM25
81800           DC(21)=ALPH25
81900           DC(22)=BETA25
82000           DC(23)=RM25
82100           DC(24)=PRTTI
82200           DC(25)=PRSTI
82300           DC(26)=DEVI
82400           DC(27)=ETAI
82500           DC(28)=M2WI
82600           DC(29)=HRISE
82700           DC(30)=PAVBF
82800           DC(31)=VU25A
82900           DC(32)=SF
83000           DC(33)=DLTETA
83100           DC(34)=DLTOT
83200           DC(35)=PT25
83300           DC(36)=PREC29
83400           DC(37)=ALDS29
83500           DC(38)=AM29
83600           DC(39)=ETAD29
83700           DC(40)=PREC30
83800           DC(41)=ALDS30
83900           DC(42)=AM30
84000           DC(43)=ETAD30
84100           DC(44)=PRST
84200           DC(45)=ETAST
84300           DC(46)=ETAPOL
84400           DC(47)=PSTHR
84500           DC(48)=PTTHR
84600           DC(49)=CPU
84700           DC(50)=CPL
84800           DC(51)=EFFU
84900           DC(52)=EFFL
85000           DC(53)=PRECU
85100           DC(54)=PRECL
85200           DC(55)=PRECLT
85300           DC(56)=AMLE
85400           DC(57)=ALPHLE
85500           DC(58)=AINCD
85600           DC(59)=CAPRAT
85700           DC(60)=HPBF
85800           DC(61)=PRTT
85900           DC(62)=TRTT
```

```
86000           DC(63)=ETATT
86100           DC(64)=ETAAD
86200     C
86300     C
86400           IF(IFLAG.NE.0)GO TO 800
86500           IFLAG=IFLAG+1
86600           DO 700 I=1,64
86700      700  C(I)=DC(I)
86800           RETURN
86900     C
87000      800  DO 900 I=1,64
87100      900  CPRM(I)=DC(I)
87200     C
87300           RETURN
87400           END
```

Appendix B

Sample Equations

NOMINAL VALUES OF CALCULATED PARAMETERS

AM19	ALOS20	PT20	ALPH20	AM20	V20	VU20	VM20	U20M	BETA20
.4332E+00	.2000E-01	.1736E+02	.1000E-01	.4696E+00	.5175E+03	.9032E-01	.5175E+03	.9955E+03	.6253E+02
RP20	AP2SHD	V20SHD	BLTA2S	RM2SHD	DELH	DELHC	OLTOTC	U25	AM25
.1018E+01	.5432E+00	.5943E+03	.6600E+02	.1336E+01	.1229E+03	.1216E+03	.9543E+00	.2017E+04	.1146E+01
ALPH25	BETA25	RM25	PRTTI	PRSTI	DEVI	ETAI	M2M1	MRISE	PAVDF
.7082E+02	.4421E+02	.5253E+00	.9142E+01	.4657E+01	.5206E+01	.9062E+00	.5005E+00	.1229E+03	.6065E+02
VU25A	SF	OLTOTA	OLTOT	PT25	PREC29	ALOS29	AM29	ETAD29	PREC30
.1317E+04	.9525E+00	.9481E+00	.9536E+00	.1593E+03	.6912E+00	.2185E+00	.2930E+00	.7628E+00	.6982E+00
ALOS30	AM30	ETAD30	PRST	ETAST	ETAPOL	PSTHR	PTTHR	CPU	CPL
.2195E+00	.2794E+00	.7633E+00	.7615E+01	.8083E+00	.8756E+00	.1116E+03	.1423E+03	.9518E+00	.6364E+00
EFFU	EFFL	PRECU	PRECL	PRECLT	AMLE	ALPHLE	AINCD	CAPRAT	NPBF
.7626E+00	.9132E+00	.5618E+00	.6364E+00	.4624E+00	.1041E+01	.7351E+02	-.1856E+01	.1324E+01	.3048E+02
PRTI	EFTI	ETATI	ETAAD						
.8036E+01	.1954E+01	.8365E+00	.8358E+00						

THE EQUATION USED TO DETERMINE THE UNCERTAINTIES IS

U = B + 2 + S

B IS DEFINED AS THE BIAS LIMIT, AND S IS DEFINED AS THE PRECISION INDEX THE VALUE OF T95(2) COMES FROM THE TWO-TAILED STUDENTS T DISTRIBUTION

PARAMETER #	BIAS LIMIT	PRECISION INDEX	UNCERTAINTY
1	.6867E-02	.3265E-02	.13E+01
2	0.	0.	0.
3	.1609E-02	.4729E-03	.26E+00
4	.3000E-02	.4000E-03	.38E+00
5	.7249E-02	.3447E-02	.14E+01
6	.7232E-02	.3303E-02	.14E+01
7	.7829E-02	.3328E-02	.14E+01
8	.7232E-02	.3303E-02	.14E+01
9	0.	.1600E-04	.32E-02
10	.2706E-02	.1236E-02	.52E+00
11	.1817E-02	.8522E-03	.35E+00
12	.5795E-02	.9226E-02	.24E+01
13	.5574E-02	.8726E-02	.23E+01
14	.1798E-02	.2826E-02	.74E+00
15	.1514E-02	.1934E-02	.54E+00
16	.5030E-02	.2737E-03	.56E+00
17	.6252E-02	.4014E-03	.71E+00
18	.6108E-02	.3922E-03	.69E+00
19	0.	.1600E-04	.32E-02
20	.5162E-02	.5064E-03	.62E+00
21	.2052E-02	.7265E-03	.35E+00
22	.1257E-01	.1997E-02	.17E+01
23	.9710E-02	.1670E-02	.13E+01
24	.7779E-02	.1278E-02	.10E+01
25	.2252E-02	.1268E-02	.48E+00
26	.1067E+00	.1696E-01	.14E+02
27	.2237E-02	.7297E-03	.37E+00
28	.9160E-02	.2137E-02	.13E+01
29	.5030E-02	.2737E-03	.56E+00
30	.1639E-02	.1180E-02	.40E+00
31	.5067E-02	.2766E-03	.56E+00
32	.5391E-02	.8309E-03	.71E+00
33	.6233E-02	.4033E-03	.70E+00
34	.6198E-02	.4011E-03	.70E+00
35	.7634E-02	.1189E-02	.10E+01
36	.1416E-01	.4544E-02	.23E+01
37	.5032E-01	.1052E-01	.71E+01
38	.1935E-01	.1732E-01	.54E+01
39	.9119E-02	.2382E-02	.14E+01
40	.1415E-01	.3639E-02	.21E+01
41	.5003E-01	.1047E-01	.71E+01
42	.2126E-01	.1458E-01	.50E+01
43	.9066E-02	.2326E-02	.14E+01
44	.2252E-02	.1334E-02	.49E+00
45	.6353E-02	.9488E-03	.83E+00
46	.4672E-02	.5599E-03	.56E+00
47	.1132E-02	.1769E-02	.47E+00
48	.2696E-02	.1498E-02	.57E+00
49	.2288E-01	.3228E-01	.87E+01
50	.1510E-01	.1929E-01	.54E+01
51	.2393E-01	.3145E-01	.87E+01
52	.1522E-01	.1903E-01	.53E+01
53	.2288E-01	.3228E-01	.87E+01
54	.1510E-01	.1929E-01	.54E+01
55	.1429E-01	.5710E-02	.26E+01
56	.6360E-02	.1716E-02	.97E+00
57	.1800E-02	.5367E-03	.30E+00
58	.7446E-01	.2126E-01	.12E+02
59	.8121E-02	.2314E-02	.13E+01
60	.2643E-02	.1370E-02	.54E+00
61	.2252E-02	.9959E-03	.42E+00
62	.3026E-02	.1958E-03	.34E+00
63	.6387E-02	.7472E-03	.79E+00
64	.6400E-02	.7483E-03	.79E+00

SECTION IV

Engineering Education

ONE-DIMENSIONAL UNSTEADY ISENTROPIC GAS FLOW (Part II)

Daniel H. Daley*

Editor's Note

This article is the second in a two-part tutorial series presenting new insights into familiar topics. Part I (in the last issue of the Digest) examined the wave equation and its solutions. Part II applies the wave equation to unsteady isentropic flow of a perfect gas.

I. Nonlinear, One-Dimensional, Unsteady Flow

The following equations govern nonlinear, one-dimensional, unsteady flow:

Continuity,

$$\frac{\partial \rho}{\partial t} + u \frac{\partial \rho}{\partial x} + \rho \frac{\partial u}{\partial x} = 0 \tag{1}$$

Euler's equation,

$$\frac{\partial u}{\partial t} + u \frac{\partial u}{\partial x} + \frac{1}{\rho} \frac{\partial p}{\partial x} = 0 \tag{2}$$

and the Isentropic relations,

$$p = \left(\frac{p_1}{\rho_1^{k}} \right) \rho^{k} \tag{3}$$

$$T = \left(\frac{T_1}{\rho_1^{k-1}} \right) \rho^{k-1} \tag{4}$$

$$c = \left(\frac{c_1}{\rho_1^{\frac{k-1}{2}}} \right) \rho^{\frac{k-1}{2}} \tag{5}$$

---

*Colonel, USAF, Permanent Professor and Head, DFAN

In these equations, p = pressure, u = velocity in the x direction, ρ = density, T = temperature, c = the speed of sound, and k = ratio of specific heats. The subscript 1 designates some known reference state. This set of five equations relates the five dependent variables (ρ, u, p, T, and c) to the two independent variables of position and time (x,t). Since p is a function of ρ only as given by Eqn. (3), we can write ∂p/∂x in Eqn. (2) as

$$\frac{\partial p}{\partial x} = \frac{dp}{d\rho} \frac{\partial \rho}{\partial x} = c^2 \frac{\partial \rho}{\partial x}$$

where $c^2 = dp/d\rho$. When we substitute the above expression for ∂p/∂x in Eqn. (2), the result is three equations in the three unknowns (ρ, u, and c) — Eqns. (1), (6) [modified from Eqn. (2)], and (5) — as follows:

$$\frac{\partial \rho}{\partial t} + u \frac{\partial \rho}{\partial x} + \rho \frac{\partial u}{\partial x} = 0 \qquad (1)$$

$$\frac{\partial u}{\partial t} + u \frac{\partial u}{\partial x} + \frac{c^2}{\rho} \frac{\partial \rho}{\partial x} = 0 \qquad (6)$$

$$c = \left(\frac{c_1}{\rho_1^{\frac{k-1}{2}}} \right) (\rho) \qquad (5)$$

These equations are exact as long as the motion under consideration is isentropic. Under that condition, a solution of the equations would completely describe ρ, u, and c in terms of x and t for a system of gas contained in a constant area tube (Figure 1).

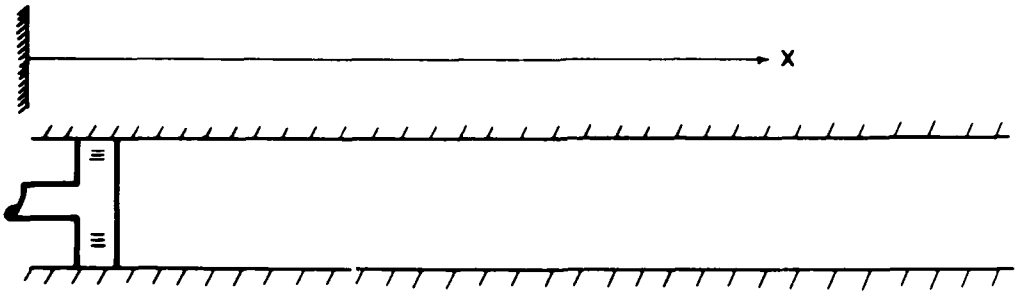

Figure 1. Unsteady One-Dimensional Gas Flow Model Piston Is the Source of Disturbances in Gas Properties

We can then find the pressure and temperature through Eqns. (3) and (4). Since terms such as u ($\partial u/\partial x$) make the equations nonlinear, however, they are not easily solved. There are two methods for arriving at a solution. One is based on small perturbations in ρ and u and leads to the classical wave equation. The other, the method of characteristics, originated by Riemann and Earnshaw in the nineteenth century, leads to a stepwise solution of the nonlinear equations, a procedure that is more exact than the linear solution. In the next section, we will linearize the equations to obtain the so-called acoustic equations.

II. Linearized One-Dimensional Unsteady Flow

Consider small perturbations in density and velocity from an initial uniform condition with property values of ρ_1, p_1, T_1, and c_1 and zero stream velocity. The small perturbation in density is $\delta\rho = \rho - \rho_1$, and the small perturbation in speed is $\delta u = u - 0 = u$. Here we introduce a non-dimensional perturbation density, $\bar{\rho}$, defined by

$$\bar{\rho} = \frac{\rho-\rho_1}{\rho_1} = \frac{\delta\rho}{\rho_1}$$

so that

$$\rho = \rho_1 (1 + \bar{\rho})$$

Substituting ρ as given by this expression into Eqns. (1), (6), and (5), and placing Eqn. (5) into Eqn. (6), the equations become

$$\frac{\partial \bar{\rho}}{\partial t} + \frac{\partial u}{\partial x} + u \frac{\partial \bar{\rho}}{\partial x} + \bar{\rho} \frac{\partial u}{\partial x} = 0$$

$$\frac{\partial u}{\partial t} + u \frac{\partial u}{\partial x} + c_1^2 \left(1 + \bar{\rho} \right)^{k-2} \frac{\partial \bar{\rho}}{\partial x} = 0$$

We can now linearize. This means neglecting terms that are small compared to other terms in the equation. Thus, we drop terms that contain products of small perturbation quantities. In addition, since $\bar{\rho}$ is small compared to 1, we drop $\bar{\rho}$ relative to unity in the last term of the second equation. These operations give the following linear equations:

$$\frac{\partial \bar{\rho}}{\partial t} + \frac{\partial u}{\partial x} = 0 \tag{7}$$

$$\frac{\partial u}{\partial t} + c_1^2 \frac{\partial \bar{\rho}}{\partial x} = 0 \tag{8}$$

Since $\partial^2 u/\partial x \partial t = \partial^2 u/\partial t \partial x$, we can differentiate the first equation with respect to t and the second with respect to x and equate them to get

$$c_1^2 \frac{\partial^2 \bar{\rho}}{\partial x^2} = \frac{\partial^2 \bar{\rho}}{\partial t^2} \tag{9}$$

Similarly, because $\partial^2\bar{\rho}/\partial x\,\partial t = \partial^2\bar{\rho}/\partial t\,\partial x$, we obtain

$$c_1^2 \frac{\partial^2 u}{\partial x^2} = \frac{\partial^2 u}{\partial t^2} \tag{10}$$

which was discussed in Part I of this series. Eqns. (9) and (10), which are in the form of the wave equation, show that any disturbances in density and speed propagate through the gas without change at the speed of sound in the undisturbed gas, c_1.

If we write the general solution to Eqn. (10) as

$$u = \delta u = f(x - c_1 t) + g(x + c_1 t) \tag{11}$$

then, since $\bar{\rho}$ is related to u through Eqns. (7) and (8), the solution to Eqn. (9) must be

$$\bar{\rho} = \frac{\delta\rho}{\rho_1} = \frac{1}{c_1} f(x - c_1 t) = \frac{1}{c_1} g(x + c_1 t) \tag{12}$$

One can verify that Eqns. (7) through (10) are all satisfied by Eqns. (11) and (12). If we consider only simple rightward- and leftward-propagating waves (for which g = 0 and f = 0, respectively) we can write Eqns. (11) and (12)

$$\frac{\delta\rho}{\rho_1} = \pm \frac{\delta u}{c_1} \tag{13}$$

where the + and - signs refer to rightward- and leftward-propagating simple waves.

Here is the interpretation of Eqn. (13). If the piston (Figure 1) imparts a positive incremental change in velocity, δu, to the gas particles adjacent to the piston face, this disturbance will propagate to the right through the gas at the speed c_1. This disturbance in particle velocity is accompanied by a positive increment in gas density given by Eqn. (13). If we move the piston to the left, imparting a negative increment in δu, then this rightward-propagating disturbance

in particle speed is accompanied by a decrease in gas density. Similar remarks apply to the density effect produced by leftward- [negative sign in Eqn. (13)] propagating disturbances in particle speed generated by a piston placed at the right-hand end of the tube (Figure 1).

For example, suppose the piston of Figure 1 imparts a sinusoidal velocity disturbance to the air particles adjacent to the piston face, so that at t = 0 the gas velocity distribution in the tube is

$$\delta u = 10 \frac{\text{ft}}{\text{sec}} \sin 2\pi \frac{x}{4 \text{ ft}}$$

$$0 \leq x \leq 2 \text{ ft.}$$

The perturbation density distribution in the gas is then given by Eqn. (13) with the plus sign. Thus, if $c_1 = 1000$ ft/sec and $\rho_1 = 0.076$ lbm/ft^3, corresponding to standard air conditions, then

$$\delta\rho = \rho_1 \frac{\delta u}{c_1}$$

$$= 0.076 \frac{\text{lbm}}{\text{ft}^3} \frac{10 \frac{\text{ft}}{\text{sec}} \sin \frac{2\pi x}{4 \text{ ft.}}}{1000 \text{ ft/sec}}$$

$$= 0.00076 \frac{\text{lbm}}{\text{ft}^3} \sin \frac{2\pi x}{4 \text{ ft.}} \quad @ \; t = 0$$

These disturbances in δu and $\delta\rho$ propagate through the gas along the rightward characteristics (Figure 2).

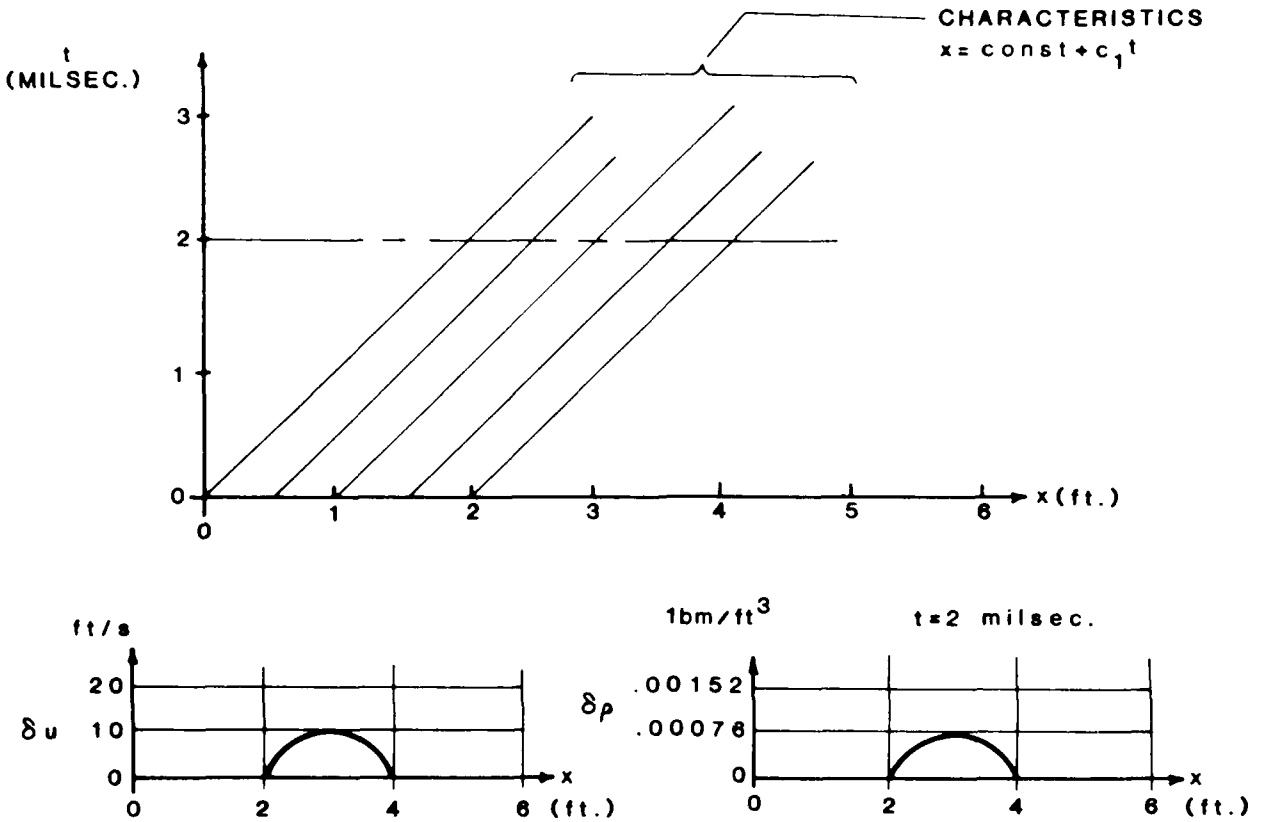

Figure 2. Particle Velocity and Accompanying Density Disturbances Advancing Through a Gas

III. Pressure and Temperature Disturbances Accompanying a Particle Velocity Perturbation

The final result of the preceding section shows that a disturbance (δu, in gas-particle velocity imparted by, for example, a piston) propagates through the gas at the speed of sound, c_1. Accompanying this disturbance in gas particle speed is a density disturbance given by

$$\frac{\delta\rho}{\rho_1} = \pm \frac{\delta u}{c_1}$$

But we must also find the perturbations in pressure and temperature accompanying the density and particle-speed disturbances. These are given by the isentropic relations, Eqns. (3) and (4), which take the following form when written in terms of the perturbation density, $\bar{\rho}$,

$$p = \left(\frac{p_1}{\rho_1^k}\right)\rho^k = \frac{p_1}{\rho_1^k}\left[\rho_1\,(1+\bar{\rho})\right]^k = p_1\left[1+k\bar{\rho}+\ldots\right]$$

Or, dropping terms of higher order than $\bar{\rho}$ in the above binomial expansion,

$$p = p_1\,(\,1 + k\,\bar{\rho}\,)$$

we can write the equation, using $\delta p = p - p_1$, as

$$\frac{\delta p}{p_1} = k\,\frac{\delta\bar{\rho}}{\rho_1} \tag{14}$$

Similarly, Eqn. (4) gives

$$\frac{\delta T}{T_1} = (\,k - 1\,)\,\frac{\delta\rho}{\rho_1} \tag{15}$$

Using these results, we can determine the pressure and temperature disturbances associated with the velocity and density disturbances illustrated by Figure 2. According to Eqn. (14), when $p_1 = 1680$ ltf/ft^2 at time $t = 0$,

$$\delta p = kp_1\left(\frac{\delta\rho}{\rho_1}\right) = kp_1\left(\frac{\delta u}{c_1}\right)$$

$$\delta p = \left[1.4(1680\ \text{psfa})\right]\ 10^{-2}\sin 2\pi\,\frac{x}{4\ \text{FT.}}$$

$$\delta p = 23.5\,\frac{\text{lbf}}{\text{ft}^2}\sin 2\pi\,\frac{x}{4\ \text{ft.}}$$

And according to Eqn. (15), if $T_1 = 415$ degrees R, then at $t = 0$ the temperature disturbance is

$$\delta T = (k-1)\,T_1\left(\frac{\delta\rho}{\rho_1}\right) = (k-1)\,T_1\left(\frac{\delta u}{c_1}\right)$$

$$\delta T = (0.4)\ (415^{\circ}R)\ 10^{-2} \sin 2\pi \frac{x}{4\ ft.}$$

$$\delta T = 1.66^{\circ}R \sin 2\pi \frac{x}{4\ ft.}$$

We can locate these disturbances graphically at any time t by reference to the characteristics of Figure 2. But in this particular example, it is just as easy to write the equation for each property disturbance in the gas. Since we are dealing only with rightward-traveling waves, each disturbance must be written using the argument $(x - c_1 t)$. In terms of this variable the property disturbances are

$$\delta u = 10\ ft/sec \sin \left[\frac{2\pi}{4\ ft} (x - c_1\ t)\right]$$

$$\delta \rho = 0.00076\ lbm/ft^3 \sin \left[\frac{2\pi}{4\ ft} (x - c_1\ t)\right]$$

$$\delta p = 2.35\ lbf/ft^2 \sin \left[\frac{2\pi}{4\ ft} (x - c_1\ t)\right]$$

$$\delta T = 1.66^{\circ}R \sin \left[\frac{2\pi}{4\ ft} (x - c_1\ t)\right]$$

This example describes rightward-propagating simple waves. But we can obtain similar results for leftward-propagating simple waves by letting a minus sign represent the relation between density and particle velocity in Eqn. (13).

IV. Finite Isentropic Waves

The essence of the linearized theory presented in the preceding section lies in the concept (resulting from the linearization of the governing equations) that small perturbations in gas properties travel through the gas at a constant wave speed, c_1. In relation to wave

speed, we ignore the effects of variation in the speed of sound and gas-particle velocity. But if the gas disturbances are not sufficiently small, we must allow for the change in speed of the wave from point to point.

Consider an isentropic but finite rightward-traveling compression wave in a gas (Figure 3). We can approximate the continuous curves forming the waves of u, ρ, and c versus position in the manner of calculus by the infinitesimal step "curves" shown. In this procedure, the disturbances propagate through the gas as an infinite number of infinitesimal pulses. Because each pulse produces infinitesimal changes (du, $d\rho$, dc, etc.) in the gas properties, it travels into the gas in front of the pulse at the speed of sound c (always plus) in that gas. The gas itself has a velocity u (vector quantity). Relative to the stationary wall of the tube containing the gas, the pulse speed or local wave speed w (always positive) is

$$w = c \pm u \tag{16}$$

where the plus sign applies to rightward-traveling waves (Figure 3) and the minus sign applies to leftward-moving waves. Since c and u vary throughout the wave, the wave speed also varies from point to point on the wave.

We can find the wave speed at any point on an isentropic finite wave in terms of the gas velocity. First, the local speed of sound is

$$c = c_1 \left(\frac{\rho}{\rho_1}\right)^{\frac{k-1}{2}} \tag{17}$$

Second,

$$du = \pm c \frac{d\rho}{\rho} \tag{18}$$

where the plus sign refers to rightward- and the minus sign to leftward-moving waves. We obtain this result by application of the mass conservation principle to flow through a control surface surrounding and

riding with a pulse traveling at speed W (Figure 4).

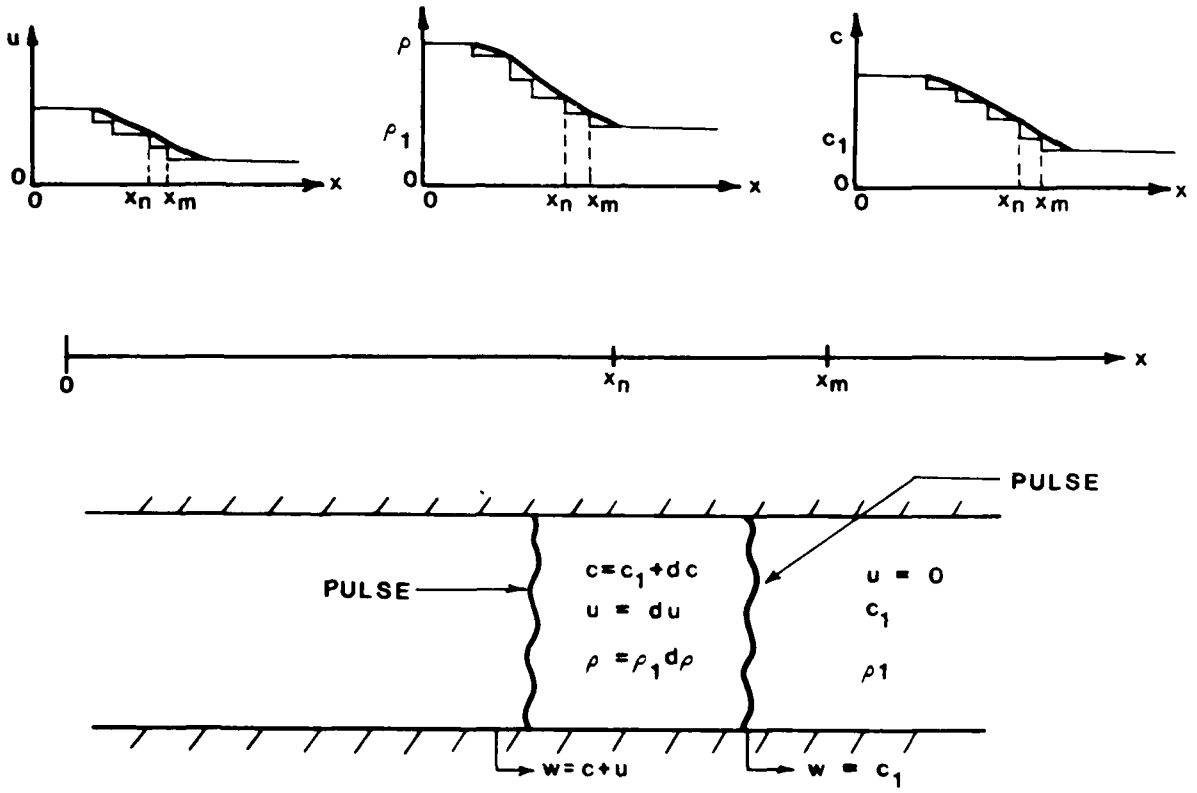

Figure 3. Compression Wave Considered as a Series of Infinitesimal Pulses Moving Through a Gas in a Tube

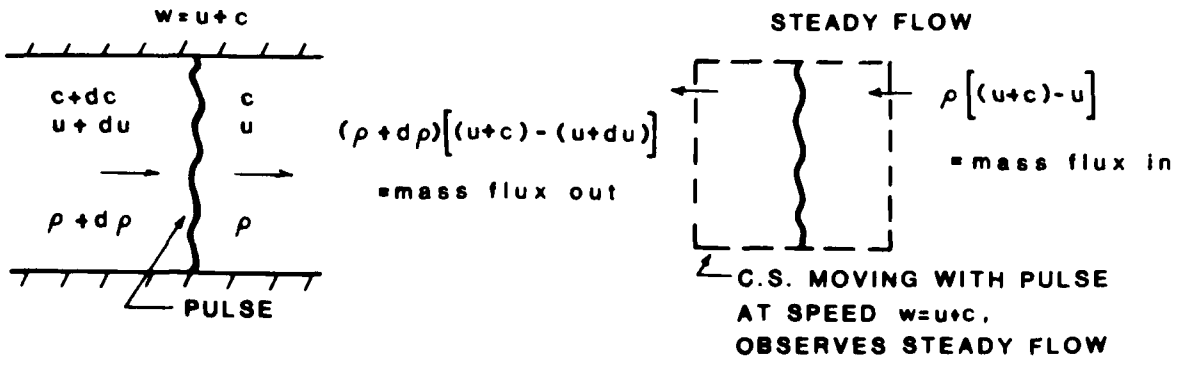

Figure 4. Mass Conservation Principle Applied to Control Surface Moving with Pulse

Eqn. 18 is similar to Eqn. (13), which we developed by applying linear theory (see Section II). The two equations are identical if Eqn. (13) is applied locally so that $\rho_1 = \rho$ and $c_1 = c$.

Since c is known in terms of ρ [from the isentropic relation given by Eqn. (17)], Eqn. (18) can be integrated to obtain u.

$$\int_0 du = \pm \int_{\rho_1}^{\rho} \frac{c_1}{(\rho_1)^{\frac{k-1}{2}}} (\rho)^{\frac{k-1}{2} - 1} d\rho = \pm \frac{c_1}{(\rho_1)^{\frac{k-1}{2}} (\frac{k-1}{2})} (\rho)^{\frac{k-1}{2}} \Bigg]_{\rho_1}^{\rho}$$

or

$$u = \pm \frac{2}{k-1} (c - c_1)$$

If we solve this equation for c and then substitute it into Eqn. (16), the wave speed at any point on the wave (in terms of the speed of sound in the undisturbed gas, c_1, and local gas velocity, u) becomes

$$w = c_1 \pm \frac{k+1}{2} u \qquad (19)$$

In the compression portion of a wave, u increases according to Eqn. (18), since the pressure and density increase as shown by Eqn. (3). Because of this, wave speed increases as the wave moves through the gas, and thus trailing parts of the wave will travel faster than leading parts. This causes the wave to steepen as the trailing parts overtake the leading parts. We hear this steepening as a sonic boom when an aircraft traveling faster than the speed of sound flies overhead. Conversely, the opposite effects arise in the rarefaction portion of a wave.

This article demonstrates how the equations governing non-linear, one-dimensional, unsteady, isentropic flow can be reduced, or linearized, when variations in properties of the gas are small. The governing equations have the same form as the classical wave equation.

Thus, disturbances in velocity, density, pressure, and temperature will propagate through a gas as waves with the properties described in Part I of this series.

SECTION V

Engineer's Bookshelf

THE ENGINEER'S BOOKSHELF: THE MYTH OF OBJECTIVITY IN THE WRITING OF ENGINEERS

Robert M. Hogge*

Picture in your mind a wind tunnel in an aeronautics laboratory. A scientist, dressed in a white lab jacket and wearing horn-rimmed glasses, enters the observation area. With a professional air, he scans the equipment, makes sure everything is ready for the test, jots down a few notes on a clipboard checklist, then flips a switch to begin the experiment. During the test, he looks at gauges and dials, observing exactly how his model (a forward-swept-wing aircraft) behaves in 0.8 Mach coinditions. Then when the test is over, he reviews his findings and writes up his report. He'd like to write his report completely in the language of math, but he knows he'll also have to use the English language to communicate his findings to some members of his target audience. So he picks his words carefully, striving for absolute objectivity, avoiding personal pronouns, using passive verbs, and writing in what he appropriately feels is the "scientific style." He then reads the paper to himself. It's based on empirical evidence; his reasoning is sound; and other scientists will be able to replicate his experiment. So his writing must be objective. Or is it?

Of course it is, you say. Scientists don't write about their feelings, opinions, and emotions. These "seekers after truth" focus on objective reality (the empirical evidence) and record simply and uniquely what they detect through the five senses. That's perfect objectivity, isn't it? But how well does the English language serve as a vehicle for that objectivity? Two scientists, Cox and Roland, have some grave concerns about the written language and what kinds of words scientists use to present their findings: "Since scientists agree that their observations and conclusions should be presented as objectively as

*Major, USAF, Associate Professor of English, USAF Academy

possible, rhetoric should be avoided assiduously in scientific writing." (Ref. 1, page 140) Here Cox and Roland imply that subjectivity exists in scientific writing, and one of the great culprits is "rhetoric," language designed to persuade or impress an audience. So, like Puritans, scientists attempt to strip rhetoric from their specialized use of language, usually ending up with a cold, lifeless, dreary, and boring set of verbal alternatives.

But where did we get this scientific penchant for objectivity in writing? Probably it originated in the Greek society with Plato who had no room in his Republic for men of literature (those who used words imaginatively and emotionally). Or maybe it came as a reaction against the Sophists who, by clever and intricate arguing, could make any set of facts seem true. Or perhaps it was from Aristotle, the patron saint of scientists, who argued that the mind is simply a passive receptor and recorder of external stimuli. Or maybe it originated later in France with Descartes (the Cartesian method of analysis) or Ramus (who separated rhetoric from dialectic and argued for an objective language free from emotion). Whatever its origins, "objective" writing became thoroughly entrenched in the minds of scientists, almost a sacred ritual they passed on from generation to generation. Today many scientists and engineers still firmly hold to this "objective" theory of writing.

But there is another (and more expansive) way to look at writing. To show you what I mean, let's look at a major philosophical debate between David Hume (1711-1766) and Immanuel Kant (1724-1804). Hume, an empiricist, argued that all thought comes to us through the five senses--that the mind is a passive observer and receptor. This is the philosophical position many engineers adhere to when they write. Kant too believes that all knowledge begins with sensory experience but that a separate phenomenon (what he calls a priori knowledge) exists already

in the mature mind and does not come from the senses. As examples of *a priori* knowledge, Kant specifies *space and time*, two aspects of reality the mind understands intuitively. Because of our awareness of space and time, the mind is able to interpret and arrange sensory data into meaningful patterns.

If Kant is correct in his theorizing, what does it mean for scientists and engineers today? Robert Pirsig provides an interesting explanation:

> If you presume that *a priori* concepts in our heads are independent of what we see and actually screen what we see, this means that you are taking the old Aristotelian concept of scientific man as a passive observer, a 'blank tablet,' and truly turning this concept inside out (Ref. 2, page 119).

Does this mean that the whole tradition of "objective" writing might be in error? Throughout the years, have scientists and engineers limited themselves unnecessarily by clinging to a seemingly passive, impartial, disinterested, or purely objective mode of writing? Can the human mind do more than passively record external stimuli? Yes! The mind not only receives, but it also creates.

To show how the mind creates, Robert Pirsig describes an analytical process you're already familiar with—The Scientific Method. First he lists the six steps:

1. statement of the problem,
2. hypotheses as to the cause of the problem,
3. experiments designed to test each hypothesis,
4. predicted results of the experiments,
5. observed results of the experiments,
6. conclusions from the results of the experiments.

(Ref. 2, page 93)

Using the Scientific Method is a logical and empirical way to arrive at truth. Or is it? How does the scientist formulate hypotheses? Where do they originate? Albert Einstein developed a law to answer these questions: "The number of rational hypotheses that can explain any given phenomenon is infinite." (Ref. 2, page 100) If Einstein's theory

is true, then do we ever arrive at one truth or one reality? Does the human mind have the awesome responsibility to respond to these infinite hypotheses, selecting those that are the most credible and prioritizing them? Yes, the mind is so much more than a passive receptor. Thomas S. Kuhn describes the almost mystical and often erratic workings of the mind as it develops hypotheses to solve scientific puzzles:

> Scientists then often speak of the 'scales falling from the eyes' or of the 'lightning flash' that 'inundates' a previously obscure puzzle, enabling its components to be seen in a new way that for the first time permits its solution (Ref. 3, page 122).

So science does not always move forward "objectively," by induction or deduction. Occasionally (and in the best of situations) the mind provides insights intuitively.

The mind, in other words, creates or shapes reality. To explain how the mind works, Kuhn discusses his concept of "paradigms." For him, a paradigm is a perception or a model for what's out there—reality. For example, he shows how astronomy first of all matured within a Ptolemaic paradigm, the philosophy that the universe is geocentric (earth centered). Ptolemy not only perceived it that way, but he also developed an extensive mathematical construct to support that perception. Throughout the years, different scientists suggested alternative world views. But it wasn't until scientists (with advanced mathematics and instrumentation) revealed a major flaw in Ptolemy's paradigm that the scientific world looked for another way to interpret reality. Thus, the Copernican Revolution. Then, Kepler, Newton, and Einstein—each with a different perception of what's out there.

How the mind perceives reality makes all the difference. And we don't always perceive stimuli in the same way. According to Kuhn, researchers in modern psychology have shown that "two men with the same retinal impressions can see different things." (Ref. 3, 126-127) Also, in 1938 Albert Einstein said: "Physical concepts are free creations of

the human mind, and are not, however it may seem, uniquely determined by the external world." (Ref. 4, page 8) In other words, Isaac Newton's mind created the Law of Gravity as it relates to interplanetary motion; that specific law or concept didn't exist before Newton. And it's the same with all other laws, hierarchies, and concepts in science—all are inventions of the human mind.

How "objective" is the human mind? When we move especially from the macromolecular (Newtonian) universe to the micromolecular (quantum mechanics), objectivity does not exist. John Wheeler, a physicist at Princeton, explains

> 'Participator' is the incontrovertible new concept given by quantum mechanics. It strikes down the term 'observer' of classical theory, the man who stands safely behind the thick glass wall and watches what goes on without taking part (Ref. 4, page 29).

But I submit to you that the "participator" mode is not just reserved for those studying quantum mechanics. It also applies to engineers working in aeronautics labs, with computers, on construction projects. As engineers, we are much more than passive observers and recorders of objective data. Our minds shape, mold, organize, and even create what's out there.

It's time now for a Copernican Revolution in scientific writing. Let's leave behind once and for all the Ptolemaic notion of "objective" writing. Instead let's use the English language fully, uniting rhetoric and dialectic, to create even more effective "paradigms" in engineering—new discoveries, new ways to see the world.

References

1. Cox, Barbara G. and Charles G. Roland. "How Rhetoric Confuses Scientific Issues," IEEE Transactions on Professional Communication, Vol. PC-16, No. 3, September 1973, pp. 140-142.

recorders of objective data. Our minds shape, mold, organize, and even create what's out there.

It's time now for a Copernican Revolution in scientific writing. Let's leave behind once and for all the Ptolemaic notion of "objective" writing. Instead let's use the English language fully, uniting rhetoric and dialectic, to create even more effective "paradigms" in engineering—new discoveries, new ways to see the world.

References

1. Cox, Barbara G. and Charles G. Roland. "How Rhetoric Confuses Scientific Issues," IEEE Transactions on Professional Communication, Vol. PC-16, No. 3, September 1973, pp. 140-142.

2. Pirsig, Robert M. Zen and the Art of Motorcycle Maintenance: An Inquiry into Values, Bantam Books, New York, 1975.

3. Kuhn, Thomas S. The Structure of Scientific Revolutions, University of Chicago Press, Chicago, 1970.

4. Zukav, Gary. The Dancing Wu Li Masters: An Overview of the New Physics, Bantam Books, New York, 1980.

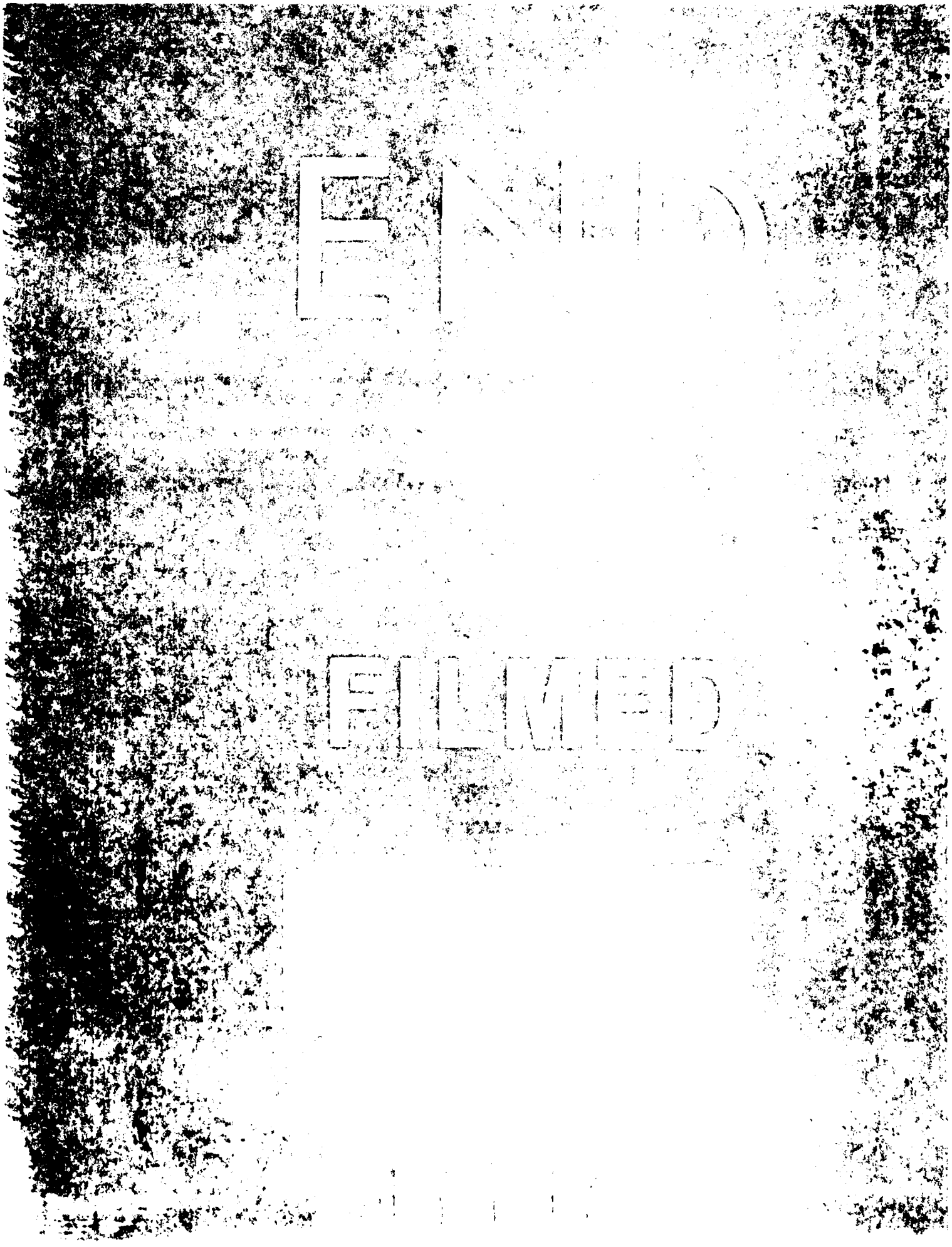
FILMED